Rare Fluctuations in One Dimensional Hydrodynamics

By

Michael Clark

A thesis submitted to
the University of Birmingham
for the degree of
DOCTOR OF PHILOSOPHY

Theoretical Physics Group
School of Physics and Astronomy
College of Engineering and Physical Sciences
University of Birmingham
July 2021

ABSTRACT

In this thesis we study the particular rare fluctuation of emptiness formation probability in a one dimensional harmonically trapped system, and the associated last particle distribution. Inspired by the Tracy-Widom distribution we present the last particle distribution in the weakly interacting regime. We then construct a hydrodynamic formalism which allows us to extend the region of study of these phenomena to include dynamical properties. Using this new formalism we show two key results. First, how to link the Gaussian unitary ensemble of random matrix theory to the Kardar–Parisi–Zhang equation using a hydrodynamic approach. In doing so we gain understanding of why the Tracy-Widom distribution appears in the edge fluctuations of an equilibrium system of fermions in a harmonic trap as well as the surface fluctuations of the non equilibrium surface growth with specific initial conditions. Second, using the now available dynamics of our formalism we calculate time dependent emptiness configurations. Analysis of these configurations shows that a good description of emptiness configurations is that of the algebraic curve and its associated topology. We use this to analyse known emptiness configurations and find new ones.

Dedicated to my friends and family.

ACKNOWLEDGMENTS

First and foremost I would like to thank my supervisor Dr. Dimitri M. Gangardt. It was only through many pleasant discussions and with much enlightening guidance from him that I was able to complete this work. He was also instrumental in me doing a PhD, for which I shall always be grateful. I acknowledge financial support from the University of Birmingham and the EPSRC. I would also like to thank the theoretical physics group for a collaborative and enjoyable atmosphere to research in. In order to complete a PhD, constructive conversation, jokes and board games are essential. For these I thank my fellow research students, it has been a pleasure to work alongside you for the past four years. I would also like to thank my housemates, for sanity preserving casual conversation and the many evenings of video/board games. Last but by no means least I thank family and friends who have always been there for me with words of advice and support throughout my PhD.

Arthur: *Have you got an answer?*

Ford: *No, but I've got a different name for the problem!*

'The Hitchhiker's Guide to the Galaxy', by Douglas Adams

Contents

List of Figures

Introduction

One dimensional systems differ greatly from their higher dimensional counterparts. Having greatly restricted degrees of freedom, particles in one dimension must interact in order to move past each other. Additionally, local excitations in one dimension are unique in the fact that they can be converted into collective excitations, which are the only type of excitations that exist in one dimension [1]. It is due to the reduced amount of freedom that one dimensional models often have exact solutions via analytical and computational techniques, some of which are designed for one dimension [2]. For example; the Fermi liquid theory breaks down in one dimension and is replaced by the Luttinger liquid model which was developed in the 1950s specifically for one dimensional systems. In contrast to Fermi liquid theory the Luttinger liquids asymptotic properties only depend on velocity and the Luttinger parameter [3]. More recently these models have been realised experimentally in the form of spin chains or ultra cold Bose gases [4, 5]. When created experimentally these systems are under very fine control. They can be made at very low temperatures in a variety of confining potentials and even be adjusted dynamically to induce quenches in, for example, potential trapping or interaction strength; allowing quenches to be studied. Due to the low temperatures these systems are in, thermal effects can be neglected and a ground state equilibrium can be achieved. This leaves the dominant fluctuations in the system to be due to quantum uncertainty and hence are an ideal system in which to study quantum effects.

Of all the phenomena available to study in this area, the ones that we will interest ourselves with in this thesis fall under the banner of rare fluctuations. It is well known that if you measure a system of quantum particles in the ground state at two different times they will have slightly different particle positions for each measurement. It is even possible, albeit with an exponentially low probability, that the second measurement would reveal particles that have moved substantially from the equilibrium configuration. This would be a rare fluctuation. Not confined purely to the weird world of quantum mechanics, rare fluctuations also appear from randomness when large enough sample sizes are used. This connection will be of fundamental importance in the following chapters, as it is the backbone of techniques in random matrix theory that we can use to analyse our quantum mechanical problem. Aside from the benefit this connection has for our calculations, the benefits of studying rare fluctuations span multiple real world applications. It is often of utmost importance to understand with what probability a system can be observed far from its intended mode of operation in some space of variables [6, 7]. This may either be to predict failure rates or to spot outliers in some set of data.

Returning to our focus for this thesis, we will mainly be interested in a type of rare fluctuation called emptiness formation probability or EFP. This is the probability of observing a lack of particles in a region of a system that would normally have a finite particle density in the ground state. Our interest in the probability of this particular fluctuation is due to its close link to the edge distribution of a trapped system, explained in detail in chapter 2. The edge distribution, the main target of our calculations, comes from considering a deceptively simple question: "Where is the edge of a trapped one dimensional system?" By simple logic we can deduce that for any trapped one dimensional system there must be a particle where all the other particles are to the left of it, the location of this particle is by definition the location of one edge of the system. By definition of being trapped a similar particle must exist where all the other particles are to the right hand side of it, this will be

the other edge of the system. If both locations are known we can say that all the particles in the system lie in in this region. At this point it may seem that our question has been answered and just the calculation of two points will suffice. The complications that arise with quantum particles, as stated above, are that the locations we seek to calculate can and will change slightly upon each measurement. Therefore instead of an edge point we in fact have an edge distribution.

One of the simplest confining potentials that is available is the harmonic trap. Not only is this a good choice as it is simple to generate experimentally and relatively easy to perform calculations on it also has the benefit of being the leading order behaviour for any confining potential at small distances from the traps centre. The edge distribution for fermions in a harmonic trap was first calculated by Tracy and Widom in 1994 [8] using the aforementioned link to emptiness formation probability. Since its discovery the Tracy-Widom distribution has been found in many areas of study, not confined to mathematics it appears in surface growth, stochastic processes and economics to name some examples [9, 10]. The reasons for its appearance in these areas is largely a mystery. Although we do not attempt to answer this question in this thesis, we will use the fact that methods from the wide variety of areas it appears in can be applied to our system. Deep links between areas of mathematics are surprisingly common and a huge benefit of working on one dimensional analytical problems.

We will begin by covering some background knowledge that will be useful for the rest of the thesis. This section will contain no new results and can safely be skipped by readers who already have a good understanding of the topics. It will cover the Lieb-Liniger model [11] which will be the main physical model of the thesis. We will then move onto relevant sections from random matrix theory, showing how to calculate relevant quantities and the equivalence to a trapped system of fermions where the free fermion description of random matrix theory will be shown as equivalent to one end of the interaction space of

Lieb-Liniger. The opposite regime, one of weak interaction, will then be considered in the form of Gross-Pitaevskii. The final background topic will be formulating a hydrodynamic description of Gross-Pitaevskii, our first hint that a hydrodynamic description of certain random matrix ensembles may be possible.

The following chapter, "Motivation"; starts with a detailed look at the Tracy-Widom distribution. Including an explicit calculation and how it relates to emptiness formation probability. One of the initial questions that we had at the beginning of this project is then considered: "How does the edge distribution depend on interaction strength?" This question is answered by presenting a new calculation: the edge distribution in the Gross-Pitaevskii regime. We finish off the chapter with some discussion of numerical techniques that can be used to calculate edge distributions as well as a summary on how best to proceed to more challenging questions.

In the penultimate chapter we formulate most of the techniques essential to show our main results. This chapter does not necessarily present any new techniques but the links between them are new results. This chapter is really a showcase of what can be achieved mathematically when working with integrable one dimensional systems. The techniques covered in this chapter come from hydrodynamics, electrostatics and stochastic methods. It is one of the most exciting features of the systems we discuss in this thesis that all these approaches from different areas of maths and physics are all applicable to our problem.

Finally we finish the thesis with a chapter on the main results. We build upon the work of the previous chapters and show two new results. The first is the ability to connect the Tracy-Widom distribution from random matrix theory to the Kardar–Parisi–Zhang (KPZ) equation. This equation traditionally comes from surface growth and has links to the Tracy-Widom distribution discovered before in [9], but here for the first time we show an analytical path from the base theory of random matrix theory through hydrodynamics to the KPZ

equation. The second new result is the study of the third order phase transition in emptiness formation probability, originally considered by Dean and Majumdar [12]. In this thesis however we study the third order phase transition from the dynamic perspective. Examining the action along the zero energy trajectory, the so called separatrix condition, leads us to the structure of emptiness in the complex space of a Riemann surface and how this structure evolves over time. In doing so we see how the emptiness region heals along the separatrix trajectory and provide interesting links to algebraic curves.

Chapter One

Background

Before we begin the main sections of work contained in this thesis, we will cover some background techniques in this chapter. This should not only help to make the thesis more self-contained but also show more of an explanation of these techniques and where they originate from. To be covered are the topics of the Lieb-Liniger model, considering the strong and weak limits of interaction, the Bethe ansatz solutions and experimental realisation. We will then move onto select topics in random matrix theory covering basic setup before continuing to show an exact correspondence to fermions with correlation functions and densities calculated. Finally we will discuss hydrodynamics starting from the Gross-Pitaevskii equation and showing scaling solutions. As stated in the introduction this chapter can be safely skipped by readers who are comfortable with the topics.

1.1 Lieb-Liniger Model

To begin to study any system we need a mathematical model to work with. The starting point in this thesis will be the famous Lieb-Liniger model [11]. Initially looking like a model with only theoretical interest, it has since been created experimentally in labs using dilute

alkali metal gases [13, 14]. These gases are used due to their energy level spacing making them highly controllable in a laboratory environment. Additionally they exhibit a contact interaction that is thousands of times stronger than the relevant longer range corrections, in this case Coulomb interaction. All this means that the Lieb-Liniger model is a good theoretical description to study; it is complicated enough to accurately describe real world experiments. In order to be useful a model must also be able to predict real world phenomena. This can only be achieved if calculations can be performed with the model. The Lieb-Liniger model can be solved analytically for various relevant quantities [15]. Additionally, it is robust enough to allow for the inclusion of some external potential and the relevant quantities remain solvable. So, for our model we will consider a one dimensional system of bosons with mass m. The system, of length L, is occupied by N bosons that obey the Lieb-Liniger model [11] of a contact interaction

$$H = -\frac{\hbar^2}{2m}\sum_{i=1}^{N}\frac{\partial^2}{\partial x_i^2} + g\sum_{i<j}^{N}\delta(x_i - x_j), \tag{1.1}$$

where g is the interaction strength. As we will work at zero temperature, g is only dependent on the scattering length of our particles [16, 17]. In equilibrium the particles will spread out uniformly and the probability of finding them will be the same at any location. Additionally we will often consider the thermodynamic limit when our system size and number of particles both tend to infinity but in such a way that their ratio is still finite i.e. $N, L \to \infty$ but $\frac{N}{L} = n$ is kept finite. In second quantised form our model becomes

$$\hat{H} = \int dx \left(-\frac{\hbar^2}{2m}\partial_x\hat{\psi}^\dagger(x)\partial_x\hat{\psi}(x) + \frac{g}{2}\hat{\psi}^\dagger(x)\hat{\psi}^\dagger(x)\hat{\psi}(x)\hat{\psi}(x)\right). \tag{1.2}$$

When the particles are free, the Bose fields are given by the sum over momentum states of the single particle free wave function

$$\hat{\psi}(x) = \sum_k \frac{1}{\sqrt{L}}e^{ikx}\hat{a}_k. \tag{1.3}$$

As stated above a key feature of one dimension is that particles must interact in order to move past each other. It is therefore useful to define a dimensionless interaction strength

$\gamma = \frac{\hbar^2 gm}{n}$ to allow investigation of different interaction regimes. When one dimensional systems are realised the particles are only free to move in the dimension with the weaker potential creating a one dimensional system in a harmonic trap. As there is still a potential in the one dimension of interest the particles are no longer uniform in space due to the extra energy cost required to move away from the origin. Therefore a potential term must be added to (1.1)

$$H = -\frac{\hbar^2}{2m}\sum_{i=1}^{N}\frac{\partial^2}{\partial x_i^2} + g\sum_{i<j}^{N}\delta(x_i - x_j) + \sum_{i=1}^{N}\frac{m\omega^2 x_i^2}{2}. \tag{1.4}$$

The potential we have chosen to add is a quadratic term called the harmonic trap, this is a good choice for a few reasons. Firstly, it is simple enough to solve analytically and second, it is a common potential used in experiments. Additionally in cases where a different confining potential is used near the local minimum of that potential the first order Taylor expansion in the potential will always give the harmonic trap, so for ground state systems the theory applies to other confining potentials as well. To get an estimate of where our gas is confined to with the introduction of a harmonic trap, we will assume that the kinetic energy term of our system is negligible in comparison to the potential and interaction terms. By comparing the magnitude of the kinetic, interaction and potential terms it can be shown that this approximation a valid in the centre of the trap, called the bulk, but less accurate in the edge region of the gas. This is called the Thomas-Fermi approximation (see appendix A.1). Even with this approximation we will initially only consider our system in the limits of strong and weak interactions.

1.1.1 Strong Interaction: Free Fermions

In the limit of strong interactions, defined as $\gamma \longrightarrow \infty$, particles can no longer occupy the same location, this prevents them passing each other. Therefore the particles behave like billiard balls and can be accurately described by non interacting, spinless fermions.

Interaction is accounted for by the fact that the fermions can't share the same location due to the Pauli exclusion principle. This case of strong interaction is known as an impenetrable, hardcore or Tonks-Girardeau gas. Under this assumption we can calculate the density profile for the Tonks-Girardeau gas in a harmonic trap using the formula $\mu + V(x) = \frac{\partial E_0^{(\infty)}}{\partial N}$ from statistical mechanics. The ground state energy in the thermodynamic limit, $E_0^{(\infty)} = \frac{\pi^2 L n^3}{2m}$, comes from the Bethe ansatz solution of the Lieb-Liniger model [11]. This can be seen from a later section (1.36) by restoring the $2m$. We get the density profile to be

$$\rho_{TG}(x) = \frac{\alpha}{\pi}\sqrt{R^2 - x^2}, \tag{1.5}$$

where we have defined $\alpha = \frac{m\omega}{\hbar}$. This is known as the Wigner semi circular law [18]. We find that the gas extends up to the Thomas-Fermi radius, given by $R = \sqrt{\frac{2\mu}{m\omega^2}}$ where the chemical potential μ can be found from the normalization condition $\int dx \rho_{TG} = N$. For a Tonks-Girardeau gas in a harmonic trap $\mu = N\omega\hbar$. Therefore the edge of the density profile is located at

$$R_{TG} = \sqrt{\frac{2N}{\alpha}}. \tag{1.6}$$

As our system is inhomogeneous a natural length scale, called the correlation length emerges, this is the typical distance over which effects in our system take place and is given by $\xi = \frac{\hbar}{\sqrt{gnm}}$. The correlation length ξ will depend on local density and has been calculated in [19] to be $\frac{1}{\sqrt{\alpha N}}$ in the bulk and $\frac{1}{\sqrt{2\alpha} N^{\frac{1}{6}}}$ in the edge region. This shows that effects in the edge region take place over larger distances than those in the bulk at large particle numbers, corresponding to the average distance between particles being larger in the edge region than the bulk.

1.1.2 Weak Interaction: Gross-Pitaevskii Regime

In the opposite case, where γ is very small, we cannot remove interactions via some limit so we must make approximations. If we use the Hartree approximation we can write the many

body wavefunction as a product of the single particle wavefunctions

$$\Psi(x_1, x_2, \ldots, x_N) = \prod_{k=1}^{N} \frac{1}{\sqrt{N}} \phi_k(x_k). \tag{1.7}$$

We must now find the equation that our single particle wavefunctions satisfy. To do this we add a potential to the second quantised Hamiltonian (1.2); we get

$$H = \int dx \left(\frac{\hbar^2}{2m} \partial_x \hat{\psi}^\dagger(x) \partial_x \hat{\psi}(x) + V(x) \hat{\psi}^\dagger(x) \hat{\psi}(x) + \frac{g}{2} \hat{\psi}^\dagger(x) \hat{\psi}^\dagger(x) \hat{\psi}(x) \hat{\psi}(x) \right). \tag{1.8}$$

We will now take a variational approach, treating the above Hamiltonian as an energy functional and letting the Bose field be the complex order parameter ϕ where $|\phi|^2 = n(x)$, which has become position dependent due to the external potential, we seek to optimise the Hamiltonian while conserving the number of particles $\int dx |\phi|^2 = N$. Using Lagrange multipliers we see that

$$\chi(\phi) = \int dx \left(\frac{\hbar^2}{2m} \partial_x \phi^* \partial_x \phi + V(x) |\phi|^2 + \frac{g}{2} |\phi|^4 \right) - \mu \left(\int dx |\phi|^2 - N \right). \tag{1.9}$$

For a general ϕ we need to minimise the functional under the variation of $\phi \to \phi + \delta\phi$ doing this we get

$$\delta\chi = \int dx \left(-\frac{\hbar^2}{2m} \partial_x^2 \phi \delta\phi^* + V(x) \phi \delta\phi^* + g |\phi|^2 \phi \delta\phi^* - \mu \phi \delta\phi^* \right) + \text{c.c.}, \tag{1.10}$$

where we have used integration by parts along with suitable boundary conditions on the kinetic energy term. As $\delta\phi$ and $\delta\phi^*$ are independent to minimise the functional we require $\delta\chi = 0$ we get the Gross-Pitaevskii equation

$$-\frac{\hbar^2}{2m} \partial_x^2 \phi + V(x)\phi + g|\phi|^2 \phi - \mu\phi = 0, \tag{1.11}$$

with chemical potential μ. In this case the particles can now move through each other but at a small cost. For a weakly interacting gas in a harmonic trap the density profile can be obtained simply from the Gross-Pitaevskii equation (1.11) under the Thomas-Fermi approximation

$$\rho_w(x) = \frac{\mu}{g} \left(1 - \frac{x^2}{R_w^2} \right). \tag{1.12}$$

The Thomas-Fermi radius for a weakly interacting Bose gas, R_w, is defined in the same way as above but the chemical potential is now $\mu^{\frac{3}{2}} = \frac{3g\omega N}{4}\sqrt{\frac{m}{2}}$, which means that R_w scales with particle number as $N^{\frac{1}{3}}$. The correlation length in this case becomes $\xi = \left(\frac{2m^2\omega^2 R_w}{\hbar^2}\right)^{-\frac{1}{3}}$ giving an edge region scaling proportional to $N^{-\frac{1}{9}}$. As the Gross-Pitaevskii equation will only hold for weak interaction we need to define the regime where this is true. We require the number of particles within a correlation length to be large due to $\gamma = \frac{\hbar^2 gm}{n}$. On rearranging the definition of ξ we find that

$$\xi n = \left(\frac{\frac{m\omega^2 R^2}{2}}{\frac{g}{R}}\right)^{\frac{1}{3}} \frac{\gamma^{\frac{1}{3}}}{2}, \tag{1.13}$$

here we have a ratio of the potential energy at the Thomas-Fermi radius and the interaction energy multiplied by the dimensionless coupling constant γ. This combination is generally less than 1. Comparing particle number scaling to the strongly interacting regime we see that the gas cloud does not expand as much for the weakly interacting case and has a correspondingly higher density in the centre than for the strongly interacting case (Fig. 1.1), this is to be expected as the weaker interactions allow particles to get closer together.

1.1.3 Bethe Ansatz

Having considered the limits of strong and weak interaction we now examine the regime of intermediate interaction. The method we will describe here is called Bethe ansatz and was first proposed by Hans Bethe in 1931 [20], but we will be basing this section on a particularly good set of notes from 2010 [21]. The method consists of an educated guess as to what the eigenfunctions of the Hamiltonian will be. This can be shown to satisfy the eigenvalue equation as well as all boundary conditions. From this, a set of integral equations can be found that give relevant quantities of the system. The Lieb-Liniger Hamiltonian is

$$H = -\sum_{i=1}^{N} \frac{\partial^2}{\partial x_i^2} + 2c\sum_{i<j}^{N} \delta(x_i - x_j), \tag{1.14}$$

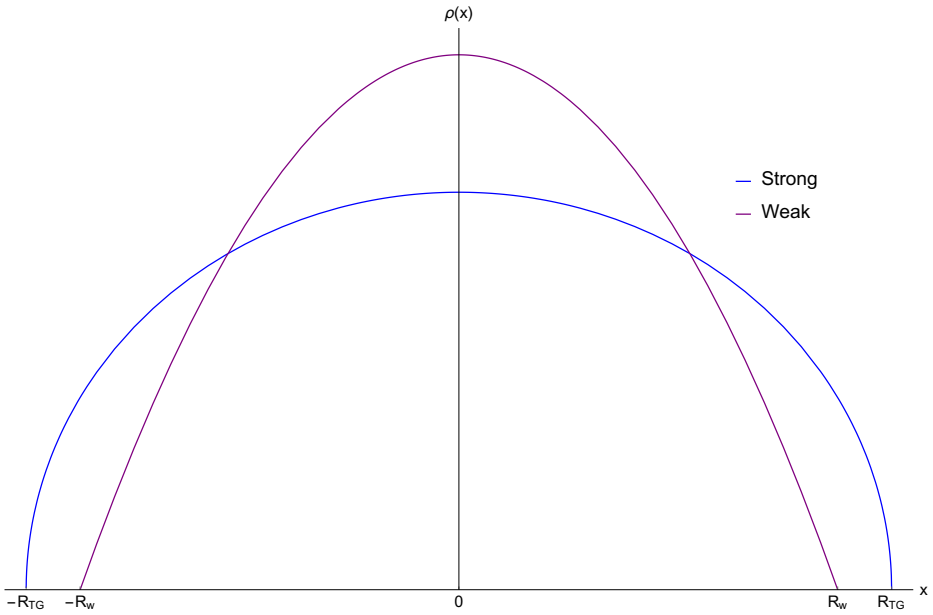

Figure 1.1: Comparison of ground state density profile in the strong and weakly interacting regimes with higher density at the origin for the weakly interacting case and wider support for the strongly interacting case.

where we have rescaled so that $c = \frac{mg}{\hbar}$. The corresponding eigenvalue equation is given by

$$H\chi = E(k_1, \ldots, k_N)\chi. \tag{1.15}$$

To find the boundary conditions for our system we will switch to the variables

$$z = x_{j+1} - x_j, \tag{1.16}$$

$$Z = \frac{1}{2}(x_{j+1} + x_j). \tag{1.17}$$

Which gives the derivatives

$$\frac{\partial}{\partial x_{j+1}} - \frac{\partial}{\partial x_j} = 2\frac{\partial}{\partial z}, \tag{1.18}$$

$$\frac{\partial^2}{\partial x_{j+1}^2} + \frac{\partial^2}{\partial x_j^2} = 2\frac{\partial^2}{\partial z^2} + \frac{1}{2}\frac{\partial^2}{\partial Z^2}. \tag{1.19}$$

Then integrating our eigenvalue equation over the small region $|z| < \epsilon \to 0$ we get the condition

$$\left(\frac{\partial}{\partial x_{j+1}} - \frac{\partial}{\partial x_j} - c\right)\chi = 0, \qquad \text{as} \qquad x_{j+1} \to x_j. \tag{1.20}$$

Here we make the leap of guessing a form for our eigenfunctions

$$\chi = \text{const} \left[\prod_{1 \leq l < i \leq N} \left(\frac{\partial}{\partial x_j} - \frac{\partial}{\partial x_l} + c \right) \right] \text{Det} \left(e^{ik_j x_l} \right). \tag{1.21}$$

We can see that the determinant is a Slater determinant of free particle wave functions and the derivatives will be enforcing the boundary conditions. It can be seen that this guess does indeed satisfy the boundary conditions (see appendix A.2). The derivatives can be evaluated by using the Leibniz form of the determinant to get

$$\chi = \text{const} \left[N! \prod_{l<j} ((k_j - k_l)^2 + c^2) \right]^{-\frac{1}{2}} \sum_P (-1)^P e^{i \sum_{n=1}^N x_n k_{P_n}} \prod_{l<j} (k_{P_j} - k_{p_l} - ic\text{sgn}(x_j - x_l)). \tag{1.22}$$

The typical energy and momentum operators still give the expected eigenvalues on our function of

$$E = \sum_{j=1}^N k_j^2, \tag{1.23}$$

$$P = \sum_{j=1}^N k_j. \tag{1.24}$$

Next we will impose periodic boundary conditions on our system of length L giving the equation

$$e^{ik_j L} = \prod_{j \neq l}^N \frac{k_j - k_l + ic}{k_j - k_l - ic}. \tag{1.25}$$

Together with the energy and momentum operators these are called the Bethe equations. For practical use we will take the logarithm of the equation, noting that the exponential is defined up to an integer multiple of 2π, to get

$$Lk_j + \sum_{m=1}^N i \ln \left(\frac{ic + k_j - k_m}{ic + k_m - k_j} \right) = 2\pi \left(n_j - \frac{N+1}{2} \right). \tag{1.26}$$

This equation shows that there is a one to one mapping between the set of integers n_j, which will be quantum numbers, and the set of momenta k_j. So these quantities can be used interchangeably. This can be made clearer by summing over all j's to remove the logarithmic

term due to antisymmetry. This gives

$$LP = L\sum_{j=1}^{N} k_j = 2\pi \sum_{j=1}^{N} \left(n_j - \frac{N+1}{2} \right). \tag{1.27}$$

We now wish to consider the ground state of our system, where $n_j = j$, in the thermodynamic limit. The thermodynamic limit is defined as taking the particle number N and length of the system L to infinity while keeping the ratio of the two quantities ρ constant. We define

$$\rho(k_j) = \frac{1}{L(k_{j+1} - k_j)}. \tag{1.28}$$

In the thermodynamic limit we can convert our sums to integrals in the following way

$$\sum_{j=1}^{N} f(k_j) \to \int_{-\Lambda}^{\Lambda} dk \rho(k) f(k). \tag{1.29}$$

The value of Λ is fixed by normalizing $\rho(k)$ to the constant ratio of particle number and system length. Examining the thermodynamic limit of the Bethe equations we note that the difference $k_{j+1} - k_j$ is small and can be used to get a derivative

$$L(k_{j+1} - k_j) + (k_{j+1} - k_j) \sum_{m=1}^{N} \Omega'(k_j - k_m) = 2\pi, \tag{1.30}$$

where

$$\Omega(k) = i \ln \left(\frac{ic + k}{ic - k} \right). \tag{1.31}$$

Now applying our rules (1.29) for converting sums to integrals we have

$$\rho(k) - \frac{1}{2\pi} \int_{-\Lambda}^{\Lambda} dq \rho(q) \frac{2c}{c^2 + (k-q)^2} = \frac{1}{2\pi}. \tag{1.32}$$

The ground state energy can be similarly converted to give

$$E = \sum_{j=1}^{N} k_j^2 \to L \int_{-\Lambda}^{\Lambda} dk \rho(k) k^2. \tag{1.33}$$

The equations we are interested in; the Bethe equation, ground state energy and normalization are now rescaled by Λ. $k = \Lambda z, \qquad c = \Lambda\alpha, \qquad \rho(\Lambda z) = g(z)$ to get

$$\gamma \int_{-1}^{1} dz g(z) = \alpha, \tag{1.34}$$

$$g(z) - \frac{1}{2\pi}\int_{-1}^{1} dy g(y) \frac{2\alpha}{\alpha^2 + (y-z)^2} = \frac{1}{2\pi}, \tag{1.35}$$

$$e(\gamma) = \frac{\gamma^3}{\alpha^3}\int_{-1}^{1} dy g(y) y^2 = \frac{E}{N\rho^2}, \tag{1.36}$$

where $\gamma = c/\rho$. A standard procedure exists to evaluate the above equations. First (1.35) can be solved for $g(z)$ in terms of α. On substitution into the nominalisation condition (1.34) a relation between γ and α can be found. Finally using both of the above (1.36) can be found as a function of γ only. These can then be used to calculate our object of interest for arbitrary interaction $\mu(\rho)$ as

$$\mu = \left(\frac{\partial E}{\partial N}\right)_L = \rho^2(3e(\gamma) - \gamma e'(\gamma)). \tag{1.37}$$

To show the procedure we will check it agrees with the results for strong interaction discussed earlier. In this limit the integral in (1.35) is lower order in the interaction parameter so at leading order $g(z) = 1/2\pi$ is a constant. This means that normalisation gives the relation $\gamma = \pi\alpha$. To finish (1.36) gives $e(\gamma) = \pi^2/3$ to leading order. The other limit we can check is the weak interaction limit $c \to 0$, this is a far harder limit to evaluate but has been done in [21] and references within resulting in

$$g(z) \approx \frac{\sqrt{1-z^2}}{2\pi\alpha}, \tag{1.38}$$

and consequently $e(\gamma) \approx \gamma$. Therefore our chemical potential in this case is given by $\mu(\rho) = 2c\rho$ which is linear in density.

1.1.4 Experiments

In order to study a Bose gas we must first contain it to be able to manipulate it [13, 14]. This can be achieved by using a magneto-optical trap (MOT), a wide variety of MOT's can be made depending on the temperatures, type and amount of atoms that are required. Here we will describe some general principles of a MOT used to trap and cool a Bose gas of alkali metal atoms such as ^{85}Rb or ^{40}K.

A typical MOT consists of a three dimensional quadrupole field and orthogonal laser beams along the three Cartesian axes in a vacuum chamber. The quadrupole field can be made, for example, via magnetic coils in anti-Helmholtz configuration. This creates Zeeman splitting in the energy levels of the atoms causing them to seek low magnetic fields. If the atoms come into the trap with an amount of energy that is large compared to the energy that the experiments require they need to be cooled. The laser beams achieve this by being tuned to a frequency slightly less than the resonant frequency of the targeted transition. Hence if the atom is moving towards the incoming beam, Doppler shift ensures that the light is at resonant frequency. When the atom absorbs the resonant light it is given a momentum kick towards the centre of the trap, spontaneous emission then occurs and the atom de-excites to a lower energy state. Spontaneous emission also produces a momentum kick but in a random direction, but as the absorption-emission cycles happen multiple times the random momentum kicks tend to cancel out and the atom remains in the centre of the trap. As the laser is targeting a specific transition, it is beneficial for the atom to have a closed optical loop, this is where the exited state can only decay back to the state it came from. If this is not the case or a small probability exists of it decaying to a lower energy level a pump beam can be used to force the atom to return to the desired state.

A final complication to discuss relates to the lack of magnetic field at the centre of the trap. As the atoms cool down they are more likely to be at the centre where, due to

zero magnetic field, they can flip into a non trapped state, known as Majorana losses [22]. Adding a constant field will prevent this from happening. With all this in place a typical MOT can capture relatively hot atoms and cool them to about 100mK.

The MOT is an excellent tool for trapping atoms, but in order to change the interaction strength it is useful to be able to exploit Feshbach resonance where a magnetic field can be used to change the scattering length, this in turn directly effects the interaction strength. It is impossible to do this in a MOT as it will disrupt the trapping magnetic fields. A solution is to transfer the system to an optical dipole trap which uses light only. When an atom is placed in the light a dipole moment is induced, the intensity gradient of the light is then seen as a potential and hence it can be trapped. As the energies involved are far less than in the MOT the optical dipole trap can reach temperatures of about 10mK [23]. An optical dipole trap can realize a wider variety of trapping potentials such as strong potentials in two dimensions and a much weaker one in the third. When this is the case we say that our system is effectively one dimensional.

1.2 Random Matrix Theory

Random matrix theory (RMT) is the study of eigenvalue statistics from defined matrix ensembles. Although this may seem to be of purely mathematical interest RMT has a wide range of applications starting with Wigner who used it to calculate energy level spacing in large atoms [18]. Since then techniques from RMT have been instrumental in many areas of applied maths, physics, chemistry and biology [24]. As random matrix theory is a vast area of study with many applications we will only discuss the points relevant to this thesis such as calculation of correlation functions, emptiness formation probabilities and its use as a description of one dimensional systems.

1.2.1 Setting up a Random Matrix

The first decision we have is what ensemble to choose for our random matrices. As our main goal is describing trapped particles we must choose our random variables from a distribution that has zero or vanishing probability at spacial infinity. In fact by consulting the literature [24] we see that choosing the distribution to be Gaussian will correspond to a harmonic confinement. The simplest ensemble with a Gaussian distribution is the Gaussian orthogonal ensemble (GOE). As stated before the selecting of our random variables from a Gaussian/normal distribution will give harmonic confinement. The two variables that define this distribution, mean and variance correspond to the location of the trap and its frequency respectively. The other defining characteristic of the GOE is that the matrices can by diagonalised by an orthogonal transformation. This tells us how many independent and identically distributed (iid) variables to generate from our distribution, in this case $N(N+1)/2$ where N is the size of our matrix. These values will be formed into a real hermitian matrix

$$M = \begin{pmatrix} \mathcal{N}(0,1) & \dots & \mathcal{N}(0,1) \\ \vdots & \ddots & \\ & & \mathcal{N}(0,1) \end{pmatrix}. \tag{1.39}$$

For each of the elements in the above matrix we can write a probability density function (PDF) as

$$1 = \frac{1}{Z}\int dM_{12} e^{-\frac{M_{12}^2}{2}}, \tag{1.40}$$

the factor of Z is just normalisation. Since our matrix has $N(N+1)/2$ iid entries we can multiply them all together to form the joint PDF

$$1 = \frac{1}{Z_N}\int \prod_{\substack{i,j \\ i\leq j}} dM_{ij} e^{-\sum_{i<j}\frac{M_{ij}^2}{2} - \sum_i \frac{M_{ii}^2}{4}}, \tag{1.41}$$

It is easy to see that the exponent is equal to the trace of the matrix squared

$$1 = \frac{1}{Z_N}\int \prod_{\substack{i,j \\ i\leq j}} dM_{ij} e^{-\frac{1}{4}\mathrm{Tr}(M^2)}. \tag{1.42}$$

We now wish to change basis to one where our matrix is diagonal, from the symmetry of the ensemble this can be done by using orthogonal matrices. The trace will transform simply into the sum of eigenvalues squared but the measure will need to be modified by the Jacobian as follows

$$dM = J(\Lambda, A)d\Lambda(\vec{x})dA(\alpha_1 \dots \alpha_{N(N-1)/2}), \tag{1.43}$$

where the Jacobian is given by

$$J = \begin{vmatrix} \frac{\partial M_{11}}{\partial x_1} & \cdots & \frac{\partial M_{11}}{\partial x_N} & \frac{\partial M_{11}}{\partial \alpha_1} & \cdots & \frac{\partial M_{11}}{\partial \alpha_{N(N-1)/2}} \\ \vdots & & \vdots & \vdots & & \vdots \\ \frac{\partial M_{NN}}{\partial x_1} & \cdots & \frac{\partial M_{NN}}{\partial x_N} & \frac{\partial M_{NN}}{\partial \alpha_1} & \cdots & \frac{\partial M_{NN}}{\partial \alpha_{N(N-1)/2}} \end{vmatrix}. \tag{1.44}$$

A derivative of any component of M with respect to an eigenvalue $\vec{x}$ will only depend on the components of the orthogonal matrix $\vec{\alpha}$ and any derivative with respect to a component of $\vec{\alpha}$ will give an eigenvalue times some function of orthogonal components. Using these facts we can see that if any two eigenvalues are the same the Jacobian will be zero, there are $N(N-1)/2$ factors like this due to the fermionic nature of the determinant. Furthermore as it can be seen that the Jacobian must be order $N(N-1)/2$ in the eigenvalues these factors are the entire contribution of the x's with the remaining contribution depending only on $\vec{\alpha}$

$$J = \prod_{\substack{i,j \\ i<j}} (x_j - x_i)h(\vec{\alpha}). \tag{1.45}$$

On completing the change of basis we see that the only dependence on $\vec{\alpha}$ is in the Jacobian and as such can be integrated over and moved into the normalisation factor

$$1 = \frac{1}{\tilde{Z}_N} \int d^N x \prod_{\substack{i,j \\ i<j}} (x_j - x_i)^\beta e^{-\frac{\beta}{4}\sum_i x_i^2}, \tag{1.46}$$

The calculation we have just done is for $\beta = 1$. In general beta can vary and corresponds to a particular ensemble of random matrices, equivalent to the type of interaction between particles.

1.2.2 Equivalence to Fermions

To see the relation to fermions we consider a system of N fermionic particles of mass m in a harmonic trap with frequency ω. In one dimension the particles behave like billiard balls and the many body wavefunction can be accurately described by the Slater determinant

$$\Psi(x_1, x_2, \ldots, x_N) = \frac{1}{\sqrt{N!}}\mathrm{Det}(\psi_j(x_i)), \tag{1.47}$$

defined as an $N \times N$ determinant of single particle wavefunctions where the ith particle is in the jth energy level. This naturally takes into account the fermionic statistics. In order to retain a hardcore or Tonks-Girardeau Gas description it is enough to multiply by an antisymmetric function to account for the sign change. The single particle wavefunction for a non interacting fermion is given by the Schrodinger equation

$$i\partial_t\psi_j = -\frac{\hbar^2}{2m}\partial_x^2\psi_j + \frac{m\omega^2x^2}{2}\psi_j. \tag{1.48}$$

The solutions of which are well known to be the Hermite polynomials times a Gaussian factor. By substituting this into the Slater determinant (1.47) we arrive at

$$\Psi(y_1, \ldots, y_N) = \frac{1}{\sqrt{N!}}\left(\frac{\alpha}{\pi}\right)^{\frac{N}{4}}\left(\prod_{j=0}^{N-1}\frac{1}{\sqrt{j!}}\right)e^{-\sum_i^N\frac{y_i^2}{4}}\mathrm{Det}\left(He_j(y_i)\right), \tag{1.49}$$

where we have rescaled our particle positions $y_i = x_i\sqrt{2\alpha}$ and, as before, set the combination $\alpha = \frac{m\omega}{\hbar}$. An important note here is that we are using the monic Hermite polynomials $He_n(x)$, as opposed to the Hermite polynomials with leading coefficient 2^n which we will denote by $H_n(x)$, this property that the coefficient of the highest power of x is one will be used straight away. As determinants are unchanged under row and column operations, the determinant of monic Hermite polynomials is equivalent to the Vandermonde determinant, defined as

$$\Delta(x_1, \ldots, x_N) \equiv \mathrm{Det}(x_i^j) = \prod_{i<j}^{N}(x_i - x_j). \tag{1.50}$$

Therefore the probability density is

$$1 = \int |\Psi(x_1, \ldots, x_N)|^2 d^Nx = \frac{1}{N!}\left(\prod_{j=0}^{N-1}\frac{1}{j!\sqrt{2\pi}}\right)\int d^Nye^{-\sum_i^N\frac{y_i^2}{2}}\prod_{i<j}^{N}(y_i - y_j)^2. \tag{1.51}$$

We now recognise this form as identical to the PDF for the GUE ensemble of random matrices, where the eigenvalues of the ensemble are equivalent to positions of the particles. The normalization constant from (1.46) can be easily identified. Fermionic statistics and interactions are encoded in the Vandermonde determinant where the randomness corresponds to the probabilistic nature of the particles.

1.2.3 Correlation Functions

In order to get some results from random matrix theory we must be able to calculate observables. To achieve this we will consider the 1-point correlation function, physically the average density, we see that our joint PDF for the GUE can be written

$$1 = \frac{1}{N!} \int \mathrm{Det}\left(K_N(x_i, x_j)\right) d^N x, \tag{1.52}$$

where the kernel is given by

$$K_N(x_i, x_j) = e^{-\frac{x_i^2}{4}} e^{-\frac{x_j^2}{4}} \sum_{k=0}^{N-1} \frac{He_k(x_i) He_k(x_j)}{k!\sqrt{2\pi}}. \tag{1.53}$$

We now look at the definition of the 1-point correlator where the sum over delta functions shows us the combinatorial factor of N as we can replace any of the x_i for x to find our average density.

$$\langle \rho(x) \rangle = \frac{1}{N!} \int \left(\frac{1}{N} \sum_{l}^{N} \delta(x - x_l) \right) \mathrm{Det}\left(K_N(x_i, x_j)\right) d^N x, \tag{1.54}$$

We can see that each factor of density will effectively remove one of the integrals and give

$$\langle \rho(x) \rangle = \frac{1}{N!} \int \mathrm{Det}\left(K_N(x_i, x_j)\right) d^{N-1} x, \tag{1.55}$$

To evaluate these integrals we will need the determinant integration formula (see appendix A.3) which states that

$$\int \mathrm{Det}\left(K_N(x_i, x_j)_{1 \le i,j \le k+1}\right) dx_{k+1} = (N-k) \mathrm{Det}\left(K_N(x_i, x_j)_{1 \le i,j \le k}\right), \tag{1.56}$$

Therefore to calculate the expected density, the 1-point correlation function, we will integrate out all but one of the x's to get

$$\langle \rho(x) \rangle = \frac{1}{N} e^{-\frac{x^2}{2}} \sum_{k=0}^{N-1} \frac{He_k(x) He_k(x)}{k! \sqrt{2\pi}}. \tag{1.57}$$

This density is the average over all possible measurements of our microscopic density and is therefore normalised to one. It can also be shown [25] that in the thermodynamic limit it converges to the Wigner semi circle (1.5) as expected.

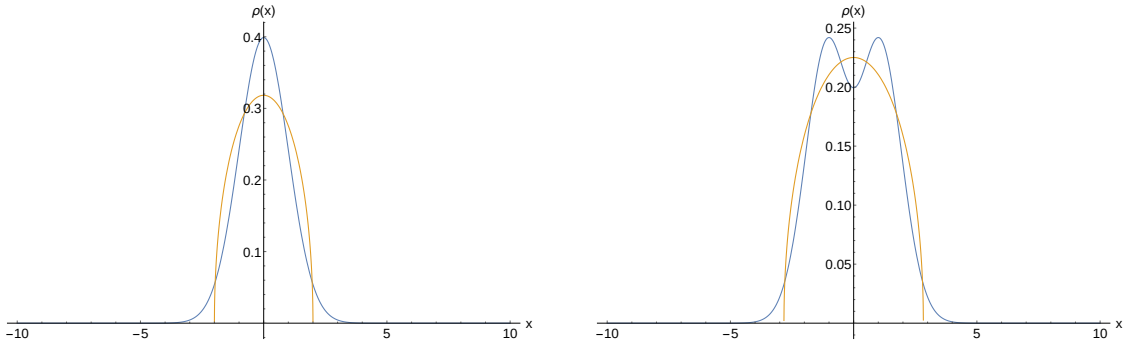

(a) $N = 1$

(b) $N = 2$

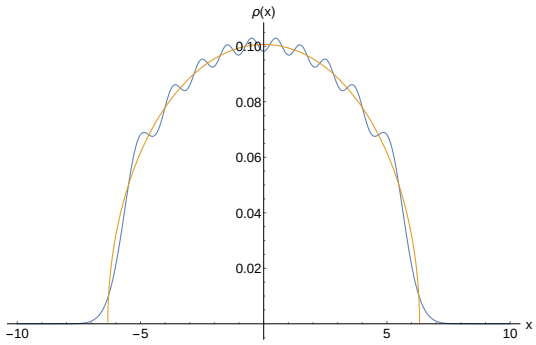

(c) $N = 10$

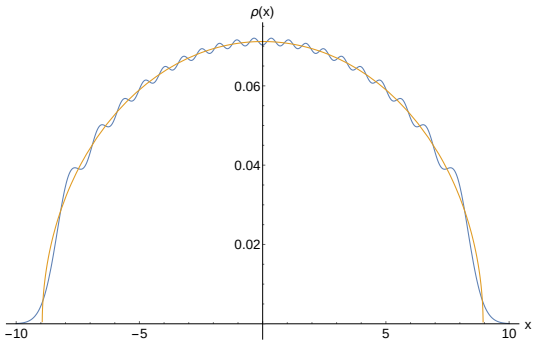

(d) $N = 20$

Figure 1.2: Comparison of exact density from random matrix theory in blue with the Wigner semi circle for $\alpha = 0.5$ in orange. The Wigner semi circle is a better approximation closer to the centre and for higher particle numbers.

1.2.4 Exact Density

Although the Wigner semi circle is a simple function that holds well at large particle numbers for Gaussian random matrix ensembles it will never be the exact density for any finite number of particles. Starting with one particle we see that the exact density is just the Gaussian distribution itself (Fig. 1.2), centred around zero the variance of the distribution is in some way analogous to the uncertainty in the position of our one particle at equilibrium. Moving to two particles we see that the most likely position is no longer at the origin but in fact at two symmetric points either side of it. Here we see the repulsive contact interactions come into play the symmetry being kept by the harmonic trap. As we increase particle number past two and into the tens of particles we see the bumps in the distribution reduce in size and the distinctive semi circle shape begins to emerge. We can also observe the increasing full width half maximum of the density also in accordance with the semi circle. The largest difference between the exact distribution and the semi circle can be seen in the way they decrease to zero at large position. The semi circle has a square root zero at both ends of the density and therefore finite support. In contrast the exact density goes exponentially to zero at larger positions maintaining a small but finite chance of a particle being observed past the end of the support for the semi circle. This is also the most pronounced difference in the plots, we can see that near the origin the bumps converge to the semi circle repetitively fast but even when the particle number rises into the tens of particles an exponential tail can still be seen defying the finite support. This is not surprising as we are working with the Thomas-Fermi approximation (See appendix A.1) we expect our density to be a better approximation the closer we get to the origin but less accurate near the Thomas-Fermi radius.

1.3 Hydrodynamics

In previous sections we saw how the strongly and weakly interacting regimes of the Lieb-Liniger model differ greatly in their behaviour. We have also already seen how random matrix theory can be used to describe the limit of strong interactions in the same model via the equivalence of free fermions. However in doing this we completely remove the interaction strength as a parameter in our calculations when we use the random matrix theory approach. It is clear then that the same technique can't be used in the weakly interacting limit as interaction strength must remain in the calculation. To investigate the weakly interacting region we will be using a hydrodynamic approach. This is a very different way of thinking to random matrix theory where our calculations gave us the microscopic details like positions of every particle in our system at equilibrium. In contrast hydrodynamics is a macroscopic approach, we forgo the ability to find individual particles in favour of a macroscopic density. It may seem that this is a bad move as we could also gain density from our random matrix theory approach using correlation functions. So at first glance it seems although we have just lost access to the microscopic variables for no gain. Hydrodynamics does however present some advantages over random matrix theory. First in addition to the density field we also get information about the velocity field and associated dynamics, this allows us to examine an entirely new space of time dependent solutions that were previously unavailable. Second and probably most importantly for describing a weakly interacting gas, the interaction parameter remains in the calculation. This in principle allows us to perform calculations on any interaction strength when combined with results from Bethe ansatz. We can even take our interaction parameter to infinity to recover the strong interaction limit and reconnect with random matrix theory, which will be shown in detail in later chapters.

1.3.1 Euler Equations from Gross-Pitaevskii

In this section we will derive the hydrodynamic equations from the time dependent Gross-Pitaevskii equation

$$\frac{-\hbar^2}{2m}\partial_x^2\psi + g|\psi|^2\psi + V(x)\psi = i\hbar\partial_t\psi. \tag{1.58}$$

We then separate ψ into aptitude and phase $\psi = \sqrt{\rho(x,t)}e^{i\phi(x,t)}$ and examine the real and imaginary parts of the resulting equation. Additionally we identify superfluid velocity as $v = \frac{\hbar}{m}\partial_x\phi$, this is because in one dimension the fluid is irrotational ($\nabla \wedge v = 0$ holds trivially when $v = \nabla\phi$). From the imaginary part we get

$$\partial_t\rho + \partial_x(\rho v) = 0, \tag{1.59}$$

which is just conservation of mass. The real part gives

$$\frac{1}{2}mv^2 - \frac{\hbar^2}{4m}\frac{\partial_x^2\rho}{\rho} + \frac{\hbar^2}{2m}\frac{(\partial_x\rho)^2}{4\rho} + g\rho + V(x) + \hbar\partial_t\phi = 0. \tag{1.60}$$

Considering the terms in the equation we neglect the two terms with the highest derivatives as they are due to quantum pressure and identify $g\rho$ as the chemical potential, which has this form due to the fact that we started with the Gross-Pitaevskii equation, in general this term would be $\mu(\rho)$. Finally, we differentiate with respect to x to get

$$m\partial_t v + \partial_x\left(\mu(\rho) + V(x) + \frac{1}{2}mv^2\right) = 0, \tag{1.61}$$

which is conservation of momentum. We have obtained the hydrodynamic equations (1.59,1.61). These equations correspond, in the Tonks-Girardeau gas, to the action

$$S = N^2\int_{-\frac{\beta}{2}}^{\frac{\beta}{2}} dt \int dx \left(\phi\partial_t\rho + \frac{\rho}{2}\left(\frac{\pi^2}{3}\rho^2 + (\omega x)^2 - (\partial_x\phi)^2\right)\right), \tag{1.62}$$

where $\hbar$ and m have been set to one and the external potential has been chosen as the harmonic trap. This action will be derived in detail in later chapters and will turn out to be a critical point in this thesis.

1.3.2 Scaling Solutions

In this section we will seek scaling solutions to the hydrodynamic equations. These types of solutions are formed, as the name suggests, by scaling a function and its independent variables by a new parameter [26]. In our case we will use them to solve dynamic problems so our new parameter will be dependent on time. These types of solutions are always spherically symmetric and constructed to be normalised. We will find that this is particularly effective for poly-tropic gases. Explicitly we seek a form

$$\rho(x,t) = \frac{1}{b(t)}\rho\left(\frac{x}{b(t)}, 0\right). \tag{1.63}$$

Substituting the above into (1.59) we find that the scaling form of the velocity is

$$v_{eff}(x,t) = \frac{x\dot{b}}{b}. \tag{1.64}$$

This is equivalent to the following scaling of the wavefunction [26]

$$\psi_j(x,t) = \frac{1}{\sqrt{b(t)}}\psi_j\left(\frac{x}{b(t)}, 0\right) e^{\frac{imx^2\dot{b}}{2\hbar b} - iE_j\tau(t)}, \tag{1.65}$$

where $\dot{\tau} = 1/b^2$. Initial conditions on our scaling function can be obtained by considering the initial conditions of the wavefunction or equivalent density and velocity fields. They are $b(0) = 0$ and $\dot{b}(0) = 0$. When dealing with a strongly interacting Bose gas we have that the chemical potential depends on the square of the density $\mu(\rho) \approx \pi^2\rho^2/2$ found in section 1.1.3. With this expression, the previous scaling forms of the density and velocity as well as the ground state density of the Wigner semi circle (1.5) we consider the other hydrodynamic equation (1.61). This gives an equation in the scaling variable only

$$\ddot{b} - \frac{\alpha^2}{b^3} + \omega^2 b = 0. \tag{1.66}$$

This is called the Ermakov equation and can be linearised to

$$\ddot{\xi}(t) + \omega^2(t)\xi(t) = 0, \tag{1.67}$$

by the simple transformation $\xi(t) = b(t)e^{i\alpha\tau(t)}$ and the initial conditions have become $\xi(0) = 1$ and $\dot{\xi}(0) = i\alpha$. This process has transformed the non-linear equation (1.66) into the linear equation (1.67). When dealing with a weakly interacting Bose gas we now have a chemical potential that only depends on the density in a linear way $\mu(\rho) \approx g\rho$. We use the same scaling forms of the density and velocity as before but must adjust the ground state density to (1.12) the other hydrodynamic equation (1.61) then gives

$$\ddot{b} - \frac{m\omega^2}{b^2 g} + \omega^2 b = 0. \tag{1.68}$$

When generalising to a poly-tropic gas the chemical potential scales like a power of density $\mu(\rho) \approx \rho^\gamma$, this power encodes the interaction strength of the Bose gas. The previous scaling still applies but as before the ground state density changes but can still be found from the hydrodynamic equations of motion (1.59,1.61). The result is the equation

$$\ddot{b} - \frac{m\omega^2}{b^{\gamma+1}} + \omega^2 b = 0. \tag{1.69}$$

The previous cases corresponded to $\gamma = 2$ and $\gamma = 1$ respectively.

1.3.3 Arbitrary Interaction Procedure

Combining the hydrodynamic action (1.62) and the Bethe ansatz equations (1.34,1.35,1.36) we have, in principle, a method to calculate the left tail asymptotics of the last particle distribution. This would allow us to see how the transition between Tracy-Widom at infinite interaction and our solution for weak interaction occurs. In particular an interesting property is whether this is a smooth transition or if a phase transition occurs at some interaction strength. Although the method is clear it is not viable analytically and anyone attempting it must resort to numerical calculation.

To begin we would use the Bethe ansaetze to find our chemical potential as a function of density. We note here that although the Bethe ansaetze were derived in the unconfined

case we can use the Thomas-Fermi approximation as shown in the section on Lieb-Liniger and apply this locally where the density can be considered constant. Our chemical potential can then be substituted into the hydrodynamic action, which when minimised will give the equations of motion. We must then find solutions to these equations of motion that have an emptiness boundary condition. Previously we have started with the most likely density to provide an emptiness but in this case it is not known. However, we do know the equilibrium solution and as our initial density must relax to equilibrium at long times we can employ the shooting method in order to find it. This is where a guess is made as to the initial density then after evolving in time according to the equations of motion we see how far from the desired equilibrium our final configuration is. This information can be used to modify the initial guess and make it more accurate in an iterative process. After many iterations of this process a full time dependent solution to our equations of motion is achieved. The hydrodynamic action can then be evaluated on the solution to the equations of motion in the same way as in [12] in order to get the left tail asymptotics.

Chapter Two

Motivation

The background covered in the first chapter shows the application of random matrix theory to the Lieb-Liniger model and most intriguingly allows us to 'perform a measurement' of the system, in a theoretical sense, to find the location of every single particle at some time. This level of resolution is rarely available in theoretical work and even more unusual in experiment. We will see in this chapter how this can be used to ask incredibly precise questions about the edge of the support in a gas and prompt questions that fall well outside the realm of random matrix theory. We start with the original 1994 calculation by Tracy and Widom [8] and include a more recent viewpoint in connection with polynomials. We then show how to use the scaling solution from the previous chapter the find a time dependent version of Tracy-Widom to the authors knowledge the first time this has been done. Next we cover the significant new result of the equivalent edge distribution in the weakly interacting regime before ending the chapter with some numerical simulation of edge distributions.

2.1 Tracy-Widom Distribution

When a one dimensional system is confined by an external potential the particles will come to rest at the minima in equilibrium. This creates a particle density with a large amount of particles in the minima, called the bulk, and as we look closer and closer to infinity no particles are detected. Thus, upon performing a microscopic measurement, there will exist a point on either side of the system (Fig. 2.1) where the last particle is detected. This

Figure 2.1: Sketch of a harmonically trapped system with the last particle on either side shown in red. The bulk is between the last particles and the emptiness regions are on the outside.

point may fluctuate even under equilibrium conditions due to quantum uncertainty. Two possibilities exist; the first is that the external potential exhibits a discontinuity from a low value to a high value, in fact if this value is infinite, for example an infinite box trap, then the wave function will drop to precisely zero at that point. Often no fluctuations occur and the edge is defined by a single point. This is known as a hard edge. The other possibility is far more common. It is where the external potential will increase in a smooth monotonic way in some region up to infinity, this means it is energetically unfavourable for the particles to be found higher up in the external potential but it is still possible under quantum fluctuations for this to happen. This is called a soft edge. The position of the last particle in a system with a soft edge is not a single point, as it can move under fluctuations, however, its fluctuations to different points in space can be measured and a probability distribution of its expected location calculated. One of the most common external potentials studied is the harmonic trap. Not only is it a particularly easy external potential to apply but any smooth potential with a local minima may be approximated by a harmonic trap in a sufficiently small region near that minima. At equilibrium a gas of fermions under harmonic confinement will have

symmetric soft edges. This was originally calculated using the equivalence between random matrix theory and free fermions and its edge distribution worked out by Tracy and Widom [8] whose names it bears. In this section we will show this remarkable work from the viewpoint of a condensed matter physicist.

2.1.1 Emptiness Formation Probability in Random Matrix Theory

Although the question of finding the last particle distribution is straightforward we must be able to write down a mathematical procedure to calculate it. One thing that is very accessible in quantum mechanics is the calculation of various probabilities. From a simple probability argument it has been shown that the emptiness formation probability is directly related to the last particle distribution. As mentioned before, the emptiness formation probability is the probability of measuring a system and finding a total absence of particles where under normal conditions they would be expected. This occurs in our system due to the exponentially small chance of quantum fluctuations allowing particles to be measured far from their expected location.

We will now show a nice probability argument from [24] to see how this relates to the last particle distribution. The emptiness formation probability $E(0;s)$ is the probability that no particles exist in the region (s,∞), formally given by the probability to find all particles in the region $(-\infty,s)$

$$E(0;s) = \langle\Psi|\,\hat{\chi}\,|\Psi\rangle = \int \Psi(x_1,\ldots,x_N)\prod_{i=1}^{N}\chi_{(-\infty,s)}(x_i)\Psi^*(x_1,\ldots,x_N)d^Nx, \qquad (2.1)$$

where $\chi_{(-\infty,s)}(x)$ is the indicator function, which has value 1 when x is in the set $(-\infty,s)$ and 0 otherwise, this ensures that the integral (2.1) will only be one when the region (s,∞) contains no particles. Therefore the quantity $E(0;s-\delta s)$ is the probability that no particles exist in the region $(s-\delta s,\infty)$. If we subtract these two we get $E(0;s)-E(0;s-\delta s)$, the

probability for no particles in (s, ∞) but at least one in $(s - \delta s, s)$ (Fig. 2.2). If we take δs

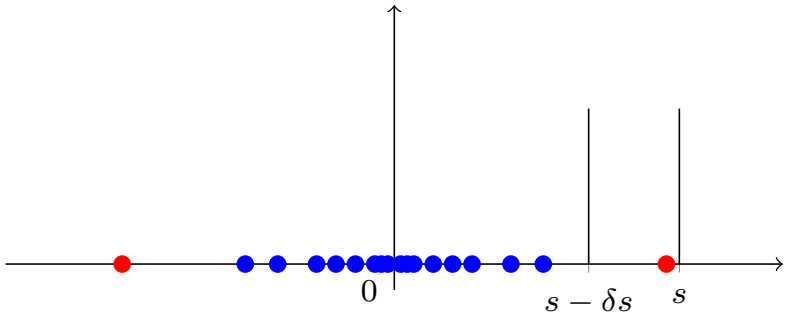

Figure 2.2: Typical configuration of particles in relation to required emptiness region, if δs is very small s can be varied. The probability of exactly one particle in the region $(s - \delta s, s)$ with none in the region (s, ∞) can then be measured.

to be small we can expand to get

$$E(0; s - \delta s) = E(0; s) - \delta s \frac{d}{ds} E(0; s) + O(\delta s^2). \tag{2.2}$$

From this we see that the most likely outcome is one particle anywhere in the region (s, ∞), the next term proportional to δs is the next most probable outcome which is one particle in the region $(s - \delta s, s)$. As the probability of higher numbers of particles will be higher order in δs we ignore them. A simple rearrangement in the limit $\delta s \to 0$ gives us the last particle distribution as

$$F(0; s) = \frac{d}{ds} E(0; s). \tag{2.3}$$

This argument can be performed for particles other than the last one [8, 24] to give the probability distribution of the n^{th} particle in from the edge $F(n; s)$. This is given in terms of the corresponding $E(n; s)$, the probability that n particles exist in the region (s, ∞)

$$F(n; s) = \sum_{k=0}^{n} \frac{dE(k; s)}{ds}. \tag{2.4}$$

Now we know that the quantity required is the emptiness formation probability we can calculate it starting with the probability density (1.51)

$$1 = \int |\Psi(x_1, \ldots, x_N)|^2 d^N x = \frac{1}{N!} \left(\prod_{j=0}^{N-1} \frac{1}{j!\sqrt{2\pi}} \right) \int d^N y e^{-\sum_i^N \frac{y_i^2}{2}} \prod_{i<j}^{N} (y_i - y_j)^2. \tag{2.5}$$

We now can calculate the EFP for the Tonks-Girardeau gas by looking at the probability of finding all the particles in a region $J' = (-\infty, s)$, given by

$$E_{TG}(0;s) = \frac{1}{N!}\left(\prod_{j=0}^{N-1}\frac{1}{j!\sqrt{2\pi}}\right)\int d^N x e^{-\sum_i^N \frac{x_i^2}{2}} \prod_{k=0}^{N-1}\chi_{J'}(x_k)\prod_{i<j}^{N}(x_i - x_j)^2, \tag{2.6}$$

with the indicator function $\chi_{J'}(x)$ enforcing the EFP condition. We can rewrite the expectation value of an operator by using the fact that the Vandermonde determinant can be written as a determinant of Hermite polynomials and then move everything else inside the determinant with the help of the determinant integration formula (see appendix B.1) to get

$$E_{TG}(0;s) = \frac{1}{N!}\mathrm{Det}\left(\int \frac{He_j(x)He_k(x)}{\sqrt{j!k!2\pi}}\chi_{J'}(x)e^{-\frac{x^2}{2}}dx\right). \tag{2.7}$$

We note that this step is still valid if $\chi_{J'}(x)$ was replaced by an arbitrary function of x. By splitting the range of integration and using the Hermite orthogonality relation we get the EFP for a system of N particles to be the $N \times N$ determinant

$$E_{TG}(0;s) = \frac{1}{N!}\mathrm{Det}\left(\delta_{ij} - \int_s^\infty \frac{He_j(x)He_k(x)}{\sqrt{j!k!2\pi}}e^{-\frac{x^2}{2}}dx\right). \tag{2.8}$$

The above function is the probability of having no particles in the region $J = (s, \infty)$, we see that this function tends to 0 and 1 as s tends to $-\infty$ and ∞ respectively as expected. To evaluate this determinant we will use Sylvester's determinant identity ($\mathrm{Det}(I_{n\times n} - A_{n\times m}B_{m\times n}) = \mathrm{Det}(I_{m\times m} - B_{m\times n}A_{n\times m})$). We will define two kernels

$$A(j,x) = \psi_j(x)f(x), \tag{2.9}$$

$$B(x,j) = \psi_j(x), \tag{2.10}$$

where $\psi_j(x)$ and $f(x)$ are arbitrary. It is instructive here to think of these kernels like matrices that have one discrete index and one continuous index. In this way we see that they don't commute and that the combination of them is either

$$AB(j,k) = \int \psi_j(x)\psi_k(x)f(x)dx, \tag{2.11}$$

or

$$BA(x,y) = \sum_{k=0}^{N-1} \psi_k(x)\psi_k(y)f(y). \tag{2.12}$$

For the EFP $f(x) = \chi_J$ and $\psi_k(x) = e^{-\frac{x^2}{4}} He_k(x)/\sqrt{k!\sqrt{2\pi}}$, we find that BA is the 1-Point correlator $K_N(x,y)$ valid in the region (s,∞). This can be seen by beginning with the definition from before

$$K_N(x,y) = e^{-\frac{1}{4}(x^2+y^2)} \sum_{i=0}^{N-1} \frac{He_n(x)He_n(y)}{n!\sqrt{2\pi}} \chi_J. \tag{2.13}$$

A useful formula to evaluate this correlator is the Christoffel Darboux formula (see appendix B.2) So we can write the emptiness formation probability as

$$E_{TG}(0;s) = \mathrm{Det}\left(I - K_N(x,y)\right). \tag{2.14}$$

We note that this process has transformed the determinant (2.8) with discrete indices into one with continuous indices called a Fredholm determinant. In general these types of determinants can be evaluated by

$$\mathrm{Det}\left(I - K_N(x,y)\right) = \sum_{n=0}^{\infty} (-1)^n \int_s^\infty \cdots \int_s^\infty \mathrm{Det}(K_N(x_i,x_j))|_{1\geq i,j\geq n} dx_1 \ldots dx_n. \tag{2.15}$$

Now that we have an expression for the EFP we take the thermodynamic limit and consider the edge region. In the thermodynamic limit the last particle distribution will move off to infinity and become infinitely thin but still normalised to 1, in accordance with the scaling shown in section 1.1.1. So we need to expand around $\sqrt{2N}$ with a characteristic length scale proportional to $\sqrt{2}N^{-\frac{1}{6}}$. On applying the appropriate scaling, while simultaneously taking the thermodynamic limit we find the 1-point correlator in the edge region (see appendix B.3)

$$K_N(x,y) = \frac{Ai(x)Ai'(y) - Ai'(x)Ai(y)}{x-y} \chi_J \equiv \mathcal{A}_{(s,\infty)}, \tag{2.16}$$

is a quantity known as the Airy kernel. The Airy functions, $Ai(x)$ and their derivatives $Ai'(x)$, have come from the asymptotics in the thermodynamic limit of the Hermite polynomials [27]. Finally we have a formula for the EFP in the thermodynamic limit, given by

$$E_{TG}(0;s) = \mathrm{Det}\left(I - \mathcal{A}_{(s,\infty)}\right). \tag{2.17}$$

Several useful expressions exist for the emptiness formation probability in the thermodynamic limit. The first is shown above but it can also be written using the Fredholm determinant formula or in terms of the Hastings McLeod solution to the Painleve II equation $q(x)$ (Appendix B.4) as in [8]

$$E_{TG}(0;s) = \text{Det}\left(I - \mathcal{A}_{(s,\infty)}\right) = e^{-\sum_{k=1}^{\infty} \frac{Tr(\mathcal{A}^k)}{k}} = e^{-\int_s^{\infty}(x-s)q(x)^2 dx}. \tag{2.18}$$

To find the probability density of the last particle in the trap we simply differentiate the above expression

$$F_{TG}(0;s) = \frac{dE_{TG}(0;s)}{ds}. \tag{2.19}$$

The quantity $F_{TG}(0;s)$ is known as the Tracy Widom distribution and has applications to a wide variety of problems [24]. If we plot these two expressions for different particle numbers (Fig. 2.3) we can see that the distribution does indeed move further out and becomes

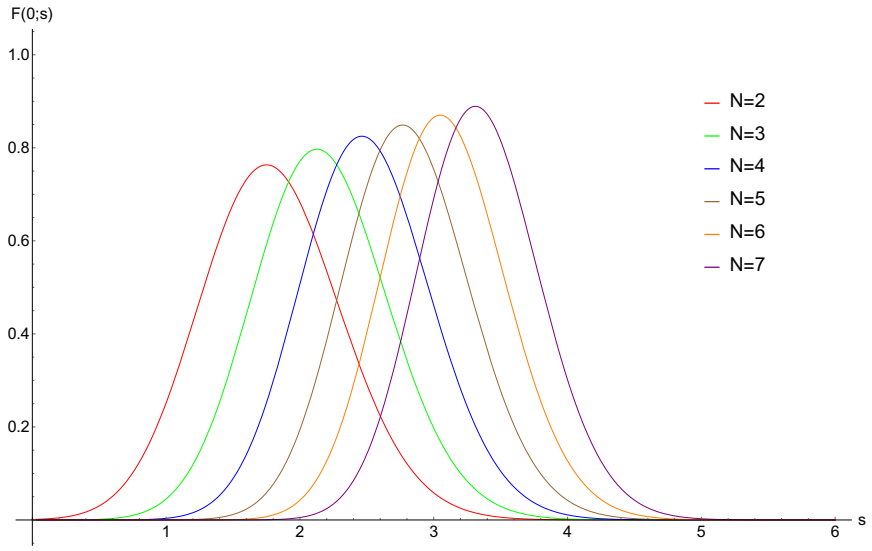

Figure 2.3: The last particle distribution for $2, 3, 4, 5, 6$ and 7 particles calculated from (2.8). The last particle distribution becomes narrower and further from the origin with increasing particle number.

narrower as particle number increases, as expected from section 1.1.1. This corresponds to the last particle being pushed further out by the increasing number being added to the gas.

Furthermore we see that the EFP goes from 0 to 1 as expected (Fig. 2.4) and the probability

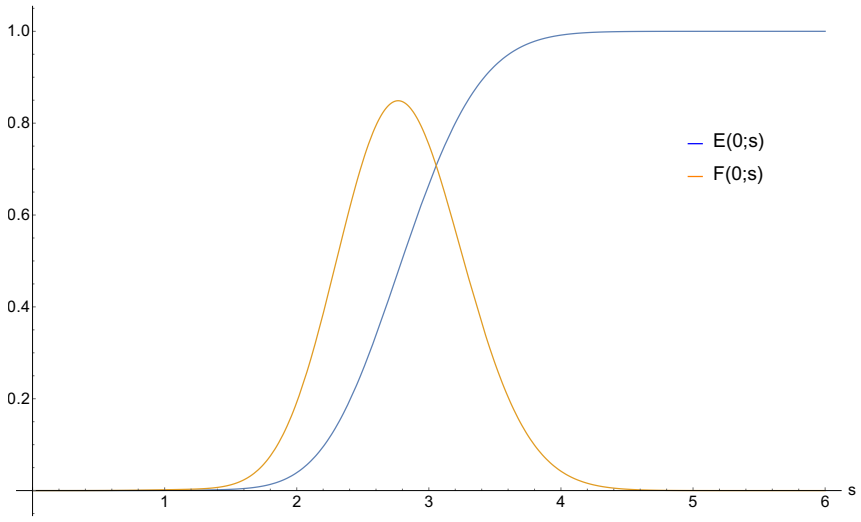

Figure 2.4: The last particle distribution in orange is the derivative of emptiness formation probability in blue plotted for 5 particles calculated from (2.8).

distribution is asymmetric as it decays faster into the bulk than into the emptiness region. The explanation is that the particle will be prevented from moving out of the gas by the gradually increasing potential, whereas upon moving into the gas it will be stopped by the sudden contact interaction with another particle.

This method can be extended to find $E(n;s)$ for other values of n. Originally found by Tracy and Widom [8], it is related to bosons in [28] and is given by

$$E(n;s) = \frac{(-1)^n}{n!}\frac{d^n}{dz^n}\mathrm{Det}\left(I - z\mathcal{A}_{(s,\infty)}\right)\Big|_{z=1}. \tag{2.20}$$

From this relation we can also find $F(n;s)$, the probability density of the particle labelled by n in the gas (where 0 is the last particle in the trap, 1 is the penultimate particle, etc.) given by (2.4). To evaluate the decay of the distribution into the bulk and the emptiness regions we wish to examine the asymptomatic behaviour of the tails. We will look at the form of the distribution in terms of the Painleve II transcendent (2.18) as the asymptotics of Painleve II are well known. In the $s \longrightarrow \infty$ limit our integration variable x is restricted to large values

only; where the Painleve II transcendent behaves as an Airy function $q(x) \approx Ai(x)$, we can therefore expand (2.18) in s to get

$$E_{TG}(0;s) = e^{\int_s^\infty (x-s)Ai(x)^2 dx} = e^{Ai(s)Ai'(s)+s^2Ai^2(s)-sAi^2(s)}, \tag{2.21}$$

and

$$F_{TG}(0;s) = \frac{d}{ds}E_{TG}(0;s) = (Ai'^2(s) - sAi^2(s))e^{Ai(s)Ai'(s)+s^2Ai^2(s)-sAi^2(s)}. \tag{2.22}$$

As we wish to examine the asymptotics of $F_{TG}(0;s)$ into the emptiness region we take the limit $s \longrightarrow \infty$ to get

$$F_{TG}(0; s \longrightarrow \infty) \approx \frac{e^{-\frac{4}{3}s^{\frac{3}{2}}}}{s}. \tag{2.23}$$

The power of s in the exponent has come from the asymptotic expansion of the Airy function [27]. This is the same asymptotic behaviour as the many body probability distribution calculated by setting $y \longrightarrow x$ in (2.16). This is expected as the last particle should provide the largest contribution to the asymptotic behaviour of the many body probability distribution. In the $s \longrightarrow -\infty$ limit the integration variable x can take on a wide range of values; so the previous method will not work. Instead we seek to evaluate the integral using the same method as in [8] by writing

$$R(s) = \frac{d}{ds}\ln\left(E_{TG}(0;s)\right), \tag{2.24}$$

where

$$R'(s) = -q(s)^2. \tag{2.25}$$

Now we can insert the form of the Painleve II transcendent for large negative argument $q(x) \approx \sqrt{-\frac{x}{2}}$ and rearrange to get the bulk asymptotics as

$$F_{TG}(0; s \longrightarrow -\infty) \approx \frac{e^{\frac{s^3}{12}}}{(-s)^{\frac{1}{8}}}. \tag{2.26}$$

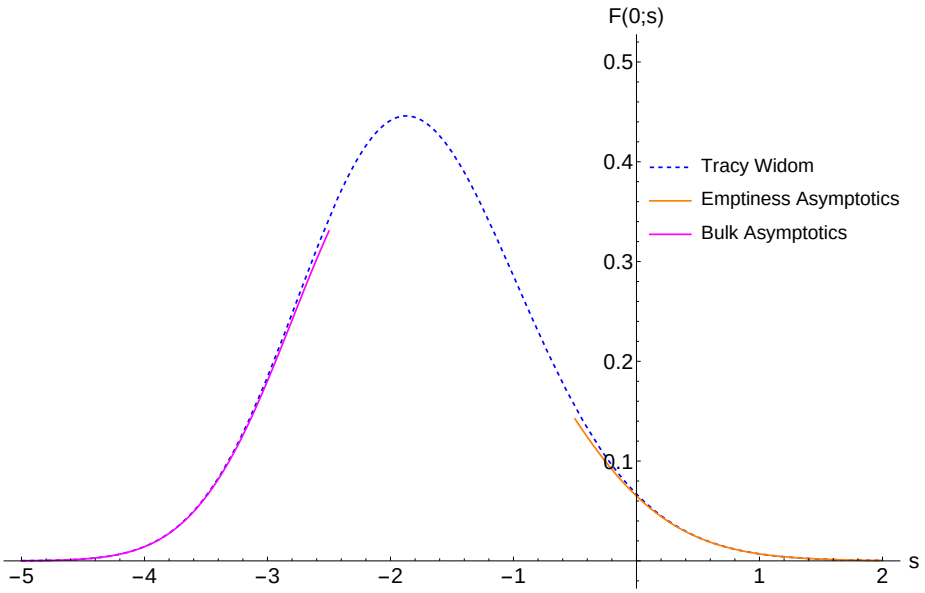

Figure 2.5: Asymptotics of the Tracy-Widom distribution from equations (2.23,2.26) plotted with Mathematica's 'TracyWidomDistribution' function have good agreement.

The asymptotic analysis has confirmed what we found graphically, that the asymptotic decay into the bulk is greater than the decay into the emptiness region. We now know that in fact both sides of the last particle distribution exhibit exponential decay (Fig. 2.5). Our hypothesis at this point is that the left tail of the edge distribution depends mainly on interaction strength as the last particle will be repelled by the remaining particles in the system, in contrast the right tail is dominated by the external trapping potential. This hypothesis makes sense physically and, as we have shown in this chapter, is true in the Tonks-Girardeau gas but in order to investigate it in general we must see if it holds in different interaction regimes. As we have seen in the random matrix theory approach all dependence on interaction strength is removed and so a different formalism must be used. Finally we note that in order to check this hypothesis we only need to find the asymptotics of the last particle distribution.

2.1.2 Connection to Polynomials

An alternative derivation of the Tracy-Widom distribution exists that only requires good knowledge of polynomials and careful study of asymptotics. It was done by Nadal and Majumdar [29] then generalised further by Akemann [30]. Although it is already known we will outline the method in this section as it gives a great appreciation for the connection to polynomials that the emptiness problem has. As was used in previous sections the Vandermonde determinant can be written as the determinant of a set of monic polynomials. In the main derivation we used this to change the Hermite polynomials into the Vandermonde determinant; the key insight of the method presented in this section is that we can define any family of monic polynomials that we wish. We begin with the EFP integral

$$E_{TG}(0;s) = \frac{1}{ZN!}\int d^N x e^{-\sum_i^N \alpha x_i^2} \prod_{k=1}^{N} \chi_{J'}(x_k) \prod_{i<j}^{N} (x_i - x_j)^2. \tag{2.27}$$

We note here that we have left the scaling of $\alpha = \frac{m\omega}{\hbar}$ in our integral, this will be used later. Following the method of [29] we can again move the integral under the determinant (See appendix B.1) to get

$$E_{TG}(0;s) = \mathrm{Det}\left(\int_{-\infty}^{s} dx e^{-x^2\alpha} p_m(x) p_n(x)\right). \tag{2.28}$$

Here we employ the main insight of this method and define a family of orthogonal monic polynomials in such a way as to make the emptiness formation probability easier to calculate

$$\int_{-\infty}^{s} dx e^{-x^2\alpha} p_m(x) p_n(x) = \delta_{n,m} h_n. \tag{2.29}$$

This allows us, if we wish, to calculate said polynomials, the first few are found in [29], they are relativity complicated but as we will only be interested in their asymptotic properties the full forms are not required. We also note that in the case of no emptiness ($s \to \infty$) they become the Hermite polynomials as expected. The advantage of defining this seemingly complicated set of polynomials is that our integral now simplifies greatly to

$$E_{TG}(0;s) = \prod_{n=0}^{N-1} h_n, \tag{2.30}$$

So we can see that the problem has been changed from one of integration to one of polynomial analysis. We now must find the values of the h_n. First, any reasonable set of orthogonal polynomials obey a recurrence relation of the form

$$\lambda p_n(\lambda) = p_{n+1}(\lambda) + S_n p_n(\lambda) + R_n p_{n-1}(\lambda), \tag{2.31}$$

where S_n and R_n are to be determined. This can be done by taking inner products of (2.31) and using integration by parts to find

$$R_n(s,\alpha) = \frac{h_n}{h_{n-1}}, \tag{2.32}$$

and

$$S_n(s,\alpha) = -\frac{1}{2\alpha}\frac{\partial \ln(h_n)}{\partial s}. \tag{2.33}$$

Using these we can relate S_n and R_n via the coupled pair of recurrence relations

$$R_{n+1} = -\frac{\partial \ln(R_n)}{\partial \alpha} + R_{n-1} - S_n^2 + S_{n-1}^2, \tag{2.34}$$

$$S_n = S_{n-1} - \frac{1}{2\alpha}\frac{\partial \ln(R_n)}{\partial s}. \tag{2.35}$$

We want to examine the asymptotics of the partition function that can be related to R_n via (2.30). As we will be considering the edge region the partition function depends only on one variable which has the scaling found from physical principles in section 1.1.1

$$\mathcal{Z}_{\mathcal{N}}(s,\alpha) = f\left(x = \sqrt{2\alpha}N^{\frac{1}{6}}\left(s - \sqrt{\frac{2N}{\alpha}}\right)\right). \tag{2.36}$$

By Taylor expanding and comparing terms it can be shown [29] that as $N \longrightarrow \infty$

$$E_{TG}(0;s) = e^{-\int_s^\infty (x-s)q(x)^2 dx}. \tag{2.37}$$

Hence the Tracy-Widom distribution can be derived from properties of orthogonal polynomials and careful use of asymptotics. Although this method was different from random matrix theory both calculations relied on fermionic statistics in order to define determinants, and hence are only valid for infinite interaction strength. For this reason neither method can be generalised to arbitrary interaction and our best course of action is still hydrodynamics.

2.1.3 Time dependent Tracy-Widom

In this section we will combine two topics that have been discussed previously. The topics in question are the Tracy-Widom distribution for the position of the last particle and the scaling solutions that describe time evolution of the gas after an quench in trap strength. Combining these two we will see how the edge distribution changes over time as the trap frequency is changed. Although this is a simple combination of two known results it is not discussed in the literature. We begin by considering the scaling solutions as applied to the wavefunction, not the hydrodynamics as was previously mentioned. An exact solution to the Schrödinger equation with time dependent potential can be found using a scaling transformation as shown in [26]. The solution has the form

$$\psi_j(x,t) = \frac{1}{\sqrt{b(t)}}\psi_j\left(\frac{x}{b(t)},0\right)e^{\frac{imx^2\dot{b}}{2\hbar b}-iE_j\tau(t)}, \tag{2.38}$$

with conditions on $b(t)$ and $\tau(t)$. In order to have a consistent description we examine $\psi_j(x,0)$ and get the initial conditions $b(0)=1$ and $\dot{b}(0)=0$. Next, on substitution of this scaling solution into the Schrödinger equation we must impose the conditions

$$\ddot{b}+\omega^2 b = \frac{\omega_0^2}{b^3}, \tag{2.39}$$

and

$$\tau(t) = \int_0^t \frac{dt'}{b^2(t')}. \tag{2.40}$$

We find that $\psi_j(x,0)$ is the solution to the Schrödinger equation where the frequency of the harmonic potential is its initial value $\omega_0=\omega(0)$ and hence can be expressed in terms of Hermite polynomials. We now examine (2.39) and as in [31] we note that it can be written as

$$\ddot{\xi}(t)+\omega^2(t)\xi(t)=0, \tag{2.41}$$

where $\xi(t)=b(t)e^{i\omega_0\tau(t)}$ and the initial conditions have become $\xi(0)=1$ and $\dot{\xi}(0)=i\omega_0$. This process has transformed the non-linear equation (2.39) into the linear equation (2.41).

Now following the normal procedure for calculating Tracy-Widom we get the many body wavefunction amplitude squared as

$$1 = \int |\Psi(x_1, \ldots, x_N)|^2 d^N x = \frac{1}{b^N N!} \left(\prod_{j=0}^{N-1} \frac{1}{j!\sqrt{2\pi}} \right) \int d^N y e^{-\sum_i^N \frac{y_i^2}{2b^2}} \prod_{i<j}^{N} \left(\frac{y_i}{b} - \frac{y_j}{b} \right)^2. \quad (2.42)$$

We now can calculate the EFP for the Tonks-Girardeau gas by looking at the probability of finding all the particles in a region $J' = (-\infty, s)$, given by

$$E_{TG}(0; s) = \frac{1}{b^N N!} \left(\prod_{j=0}^{N-1} \frac{1}{j!\sqrt{2\pi}} \right) \int d^N y e^{-\sum_i^N \frac{y_i^2}{2b^2}} \prod_{k=1}^{N} \chi_{J'}(x_k) \prod_{i<j}^{N} \left(\frac{y_i}{b} - \frac{y_j}{b} \right)^2. \quad (2.43)$$

$\chi_{J'}(x)$ is the indicator function, which has value 1 when x is in the set J' and 0 otherwise, this enforces the EFP condition. Changing integration variables to y/b we use the same rearrangement as before to write the integral as a determinant (see appendix B.1).

$$E_{TG}(0; s) = \frac{1}{N!} \mathrm{Det} \left(\int \frac{He_j(x) He_k(x)}{\sqrt{j!k!2\pi}} \chi_{J'}(xb) e^{-\frac{x^2}{2}} dx \right). \quad (2.44)$$

Continuing with this line of reasoning we see that

$$E_{TG}(0; s) = \mathrm{Det} \left(\delta_{ij} - \int_{\frac{s}{b}}^{\infty} \frac{He_j(x) He_k(x)}{\sqrt{j!k!2\pi}} e^{-\frac{x^2}{2}} dx \right). \quad (2.45)$$

Therefore the time dependence of the edge distribution after a quench in trap strength is simply $E_{TG}(0; s(t)) = E_{TG}(0; s/b)$. From this the last particle distribution can be calculated in the normal way (see 2.3). The density is given by

$$\langle \rho(x, t) \rangle = \frac{1}{b} \left\langle \rho\left(\frac{x}{b}\right) \right\rangle. \quad (2.46)$$

We can see that both density and the last particle distribution spread out over time but remain normalised.

2.2 Edge Distribution in the Weakly Interacting Regime

We have just seen how to derive the last particle distribution for free fermions or equivalently for the Tonks-Girardeau gas. This distribution is called the Tracy-Widom distribution and

we noted some of its distinguishing features. It is centred around the edge of the Wigner semi circle so will slowly move away from the origin as more particles are added. We also found that the typical width scales with particle number as $N^{-1/6}$ giving us a sharper, but still normalised distribution at larger particle numbers. This fact is in agreement with the convergence of the density to a finite support in the thermodynamic limit. Probably the most striking feature of the Tracy-Widom distribution is its asymmetry: the right tail, out of the gas, has a much slower decay than the left tail, into the gas. Our hypothesis here is that these two tails are dominated by very different effects. For the right tail the effect forcing the distribution to zero will be predominantly the external confining potential. However on the left side the major effect causing the distribution to drop to zero are the interactions from the other particles.

For weak interactions we find that our many body wavefunction is given by the Hartree product (1.7) of single particle wavefunctions that obey the Gross-Pitaevskii equation

$$-\frac{\hbar^2}{2m}\partial_x^2\phi + \frac{m\omega^2 x^2}{2}\phi + g|\phi|^2\phi - \mu\phi = 0. \tag{2.47}$$

The system is only in the weakly interacting regime when the number of particles within a correlation length is large enough as explained in section 1.1.2. Again we use the idea of looking at the probability of finding all the particles in a given region to get an expression for the EFP. In general we can write the expectation value of an operator as

$$\langle\Psi|\,\hat{\chi}\,|\Psi\rangle = \int \prod_{k=1}^{N}\frac{1}{\sqrt{N}}\phi^*(x_k)\prod_{i=1}^{N}\chi_{J'}(x_i)\prod_{j=1}^{N}\frac{1}{\sqrt{N}}\phi(x_j)d^Nx = \left(\frac{1}{N}\int\phi^*(x)\chi_{J'}(x)\phi(x)dx\right)^N, \tag{2.48}$$

in order to get the EFP. It is noteworthy that in the bulk region where ϕ is approximately a constant we find that the EFP scales like e^{-nl} where l is the length of the set J. This is consistent with a hypothesis made by Abanov in [32]. We are more interested in the edge region around the Thomas-Fermi radius, $R = \sqrt{\frac{2\mu}{m\omega^2}}$. After approximating the potential as linear near the edge $V - \mu = (x - R_w)m\omega^2 R_w$, we seek the relevant scales in this region by

introducing the dimensionless variables

$$y = \frac{x - R_w}{\xi}, \tag{2.49}$$

and

$$\phi = af(y). \tag{2.50}$$

Physically we see that ξ is the correlation length defined in section 1.1.2 and a^2 has the dimensions of density. As $\xi = \left(\frac{2m^2\omega^2 R_w}{\hbar^2}\right)^{-\frac{1}{3}}$ we can make $a = \sqrt{\frac{\hbar^2}{2mg\xi^2}}$ to get the dimensionless equation

$$\partial_y^2 f - yf - 2f^3 = 0. \tag{2.51}$$

This has the same form of the Painleve II equation (Appendix B.33), so we identify $f(y) = q(y)$. Compared to the $N^{-\frac{1}{6}}$ particle number scaling of the edge region in the Tonks-Girardeau gas, we can see from the correlation length that the weakly interacting gas has an edge region with a smaller typical width of $N^{-\frac{1}{9}}$. The scaling equation (2.49) is the counterpart to that used to calculate (2.16) and ensures that we are using the correct length scales. After splitting the range of integration in (2.48) and using the normalisation condition, in a similar vein to the Tonks-Girardeau gas, the EFP for a weakly interacting system can be written as

$$E_w(0; s) = \left(1 - \frac{a^2\xi}{N}\int_{s'}^{\infty} q(x')^2 dx'\right)^N, \tag{2.52}$$

where s' is s after scaling by (2.49). We can see that as we take the thermodynamic limit the EFP will diverge. In order to prevent this we must make the quantity $a^2\xi$ independent of particle number. To achieve this we let the trap frequency, ω, scale with particle number as $N^{-\frac{1}{4}}$. In the thermodynamic limit the EFP can now be written as an exponential

$$E_w(0; s) = e^{-a^2\xi\int_{s'}^{\infty} q(x')^2 dx'}. \tag{2.53}$$

This is remarkably similar to (2.18). Another effect this has on the system is to change the dependence on particle number in the Thomas-Fermi radius from $N^{\frac{1}{3}}$ to $\sqrt{N}$ i.e. the

same as the strongly interacting case. Physically this corresponds to changing the strength of the trap as particle number increases so that the lower trap frequency allows the gas to expand at approximately the same rate as the Tonks-Girardeau gas. The quantity $a^2\xi$ can be thought of as the number of particles that are expected to be in the region (s, ∞) as a^2 has the meaning of density and ξ has the meaning of correlation length.

We can do the same asymptotic analysis as we did for the Tonks-Girardeau gas for a weakly interacting gas in a trap. When $s \longrightarrow \infty$ we use (2.53) with fact that the Painleve II transendent behaves as an Airy function $q(x) \approx Ai(x)$, to obtain

$$E_w(0;s) = e^{a^2\xi \int_{s'}^{\infty} Ai(x)^2 dx} = e^{a^2\xi(s' Ai^2(s') - Ai'^2(s'))}, \tag{2.54}$$

and

$$F_w(0;s) = \xi \frac{d}{ds'} E_w(0;s) = a^2\xi^2 Ai(s')^2 e^{a^2\xi(s' Ai^2(s') - Ai'^2(s'))}. \tag{2.55}$$

To examine the decay of $F_w(0;s)$ at the edge of the gas we expand the Airy functions for large values of s to get

$$F_w(0; s \longrightarrow \infty) \approx \frac{a^2\xi^{\frac{3}{2}}}{4\pi\sqrt{s}} e^{-\frac{4}{3}(\xi s)^{\frac{3}{2}}}. \tag{2.56}$$

Similar to the Tonks-Girardeau gas we find that this is the same asymptotic behaviour as the many body probability distribution found by taking the limit $y \longrightarrow \infty$ in (2.51). However, in contrast to the Tonks-Girardeau gas, the many body probability distribution in the thermodynamic limit was obtained only in the edge region whereas in the Tonks-Girardeau gas it was valid everywhere. In the $s \longrightarrow -\infty$ limit the Painleve II transcendent behaves as $q(x) \approx \sqrt{-\frac{x}{2}}$ and we use the same method as before [8] by noticing that

$$-a^2\xi q(s)^2 = \frac{d}{ds} \ln\left(E_w(0;s)\right). \tag{2.57}$$

Inserting the expansion of $q(x)$ and rearranging we find the asymptotic behaviour into the bulk to be

$$F_w(0; s \longrightarrow -\infty) \approx a^2\xi s e^{\frac{-a^2\xi s^2}{4}}. \tag{2.58}$$

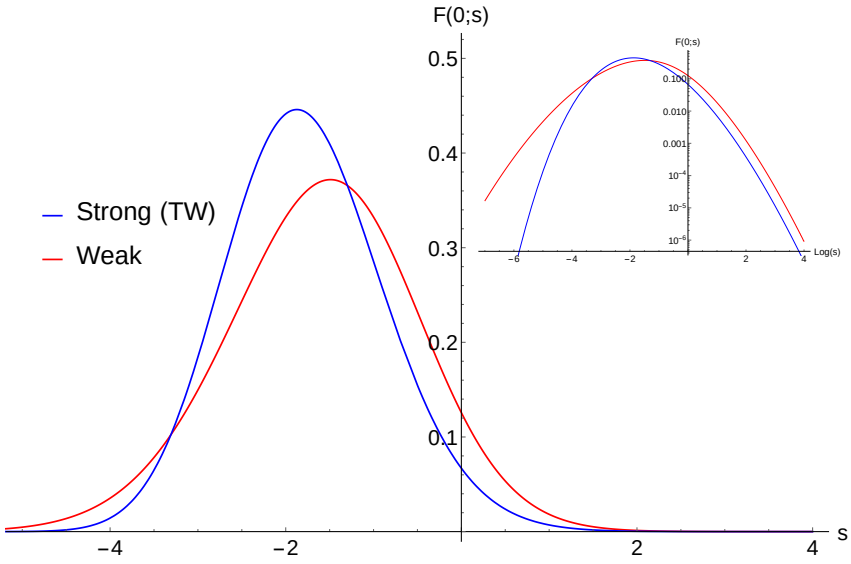

Figure 2.6: Comparison of last particle distributions for both the strong and weak interaction regimes with zero being the corresponding Thomas-Fermi radius. Log scale inset showing the similarity of the decay on the right hand side of the distribution and the difference in the decay on the left hand side.

Again we find that the asymptotic behaviour into the bulk and emptiness regions are both given by exponentials with the decay into the emptiness region being the same to leading order as the Tonks-Girardeau gas. The asymptotic behaviour into the bulk is noticeably weaker due to correspondingly weak interactions, this can be easily seen by plotting the asymptotics in both cases (Fig. 2.6). Thus our hypothesis from section 2.1.1 is confirmed. However, some consequences were not expected such as the need to scale the harmonic trap frequency with particle number (2.52). Interestingly this makes the Thomas-Fermi radius in the weakly interacting case have the same particle number scaling, $\sqrt{N}$, as the Tonks-Girardeau gas.

2.3 Numerics

In order to test a theory properly it must be compared with experiments and as discussed experiments on emptiness are few and far between. The nearest alternative is to simulate the experiment on a computer. The numerics of these systems is a vast area of study in itself and as this thesis is primarily an analytical investigation we will only touch on numerics in this section. Even though we do not perform any original calculations in this section an appreciation of numerical methods is important to complement our analytical knowledge. We will cover the discretization of the Lieb-Liniger model in order to make in numerically tractable and discuss the algorithms used and how the results compare to theory. Through this we will see how some discrete one dimensional models link together and understand how some of the algorithms needed here are vastly different in flavour to our analytical approach.

2.3.1 Discrete System

In order to simulate the Lieb-Liniger model on a computer it is easier to transform it from a continuous model to a discrete one. In this section we will see how this can be done, examine how the interaction term presents itself in the discrete formalism and take the infinite interaction limit to simplify further to the case of free fermions. We begin with the Hamiltonian

$$H = \int dx \psi^\dagger \left[-\frac{1}{2}\partial_x^2 + V(x) + \frac{g}{2}\psi^\dagger\psi \right] \psi. \tag{2.59}$$

The terms here have the same meaning as normal, g is the interaction strength and $V(x)$ is an external potential. The mass and Planks constant have been absorbed by rescaling. The principle of moving to a discrete system is simple, we will take a continuous dimension with points denoted by x_i and divide it up into L sites that are evenly spaced at intervals of Δx. In this way the position will become $x_i \to i\Delta x$, where i has now become a site index that

runs from 1 to L. The total length of the dimension is given by the last site $L\Delta x$, in order to model longer distances we can either increase the number of sites or the spacing. In practice increasing the number of sites increases computational time and increasing spacing reduces the accuracy. This can be seen if we try to take a continuous position between two discrete sites and place it on the discrete system, the maximum error in this process is half the lattice spacing. To reduce these errors we can decrease Δx, but to maintain a constant system size while doing this we must increase particle number. This in turn will incur a computational performance hit as described above. This balancing act is an important part of numerics. So our discreteising procedure for the continuous Hamiltonian is as follows

$$x_i \to i\Delta x, \tag{2.60}$$

$$\partial_x^2 \psi \to \frac{\psi(x_{i+1}) + \psi(x_{i-1}) - 2\psi(x_i)}{(\Delta x)^2}, \tag{2.61}$$

$$\psi(x_i) \to \frac{\hat{a}_i}{\sqrt{\Delta x}}, \tag{2.62}$$

$$\int dx \to \sum_i \Delta x. \tag{2.63}$$

On applying these transformations to the Hamiltonian we have

$$\hat{H} = \sum_i \left[-J\left(\hat{a}_i^\dagger \hat{a}_{i+1} + \hat{a}_i^\dagger \hat{a}_{i-1}\right) + D_i \hat{a}_i^\dagger \hat{a}_i + U \hat{a}_i^{\dagger 2} \hat{a}_i^2 \right]. \tag{2.64}$$

The new parameters are related to the old one by

$$J = \frac{1}{2(\Delta x)^2}, \tag{2.65}$$

$$D_i = \frac{1}{(\Delta x)^2} + V(i\Delta x) - \mu, \tag{2.66}$$

$$U = \frac{g}{2\Delta x}. \tag{2.67}$$

The discrete model we have derived is the Bose Hubbard model and as we have seen is the same as the Lieb-Liniger model in the limit of very small spacing between sites. The first term J is a hopping term allowing movement of bosons in the one dimensional lattice. This came from the kinetic energy term in the continuous Hamiltonian. The next term

is the external potential and will differ in strength depending on the site, it also contains some contribution from the kinetic energy term. The final term is on-site interaction and as expected only comes from the interaction term. This term will only come into play if more than one boson is present on a site. If we wish to examine the strong interaction limit we can let $g \to \infty$ thus removing the on site interaction term and allowing it to be replaced by fermionic statistics. The only remaining terms will be the hopping term and the external potential.

$$\hat{H} = \sum_i \left[-J\hat{\sigma}_i\hat{\sigma}_{i+1} + D_i\hat{\sigma}_i \right]. \tag{2.68}$$

This is the Heisenberg model. Even though it looks very similar to the Bose Hubbard model the physical interpretation is worth stating. Our hard core bosons are now thought of as spin half particles where a spin up can be interpreted as the presence of a boson and a spin down the absence of a boson. The external potential now has the interpretation of a position dependent magnetic field which will cause the particles to have regions of up spin and regions of down spin. The transition between these regions is what corresponds to the last particle distribution.

2.3.2 Random Matrix Theory

To simulate a one dimensional Bose gas we wrote a C++ program that generated a $N \times N$ matrix, where N was the number of particles in the system. The matrix had real values along the diagonal that were generated from a normal distribution with a mean of 0, variance of 1 and complex numbers on the off diagonal where the real and complex parts of the matrix entries came from independent normal distributions both with a mean of 0, variance of $\frac{1}{2}$. As the matrix was constructed to be hermitian, in total N^2 numbers were generated (N from the diagonal and $N(N-1)$ from the off diagonal). The eigenvalues, λ, of the matrix were then found using the GSL library [33]. It was possible to get both the Wigner semicircular law and

the Tracy-Widom distribution from this data. For the Wigner semi circle all the eigenvalues were stored, bin packed and the corresponding histogram plotted. It can be seen from the

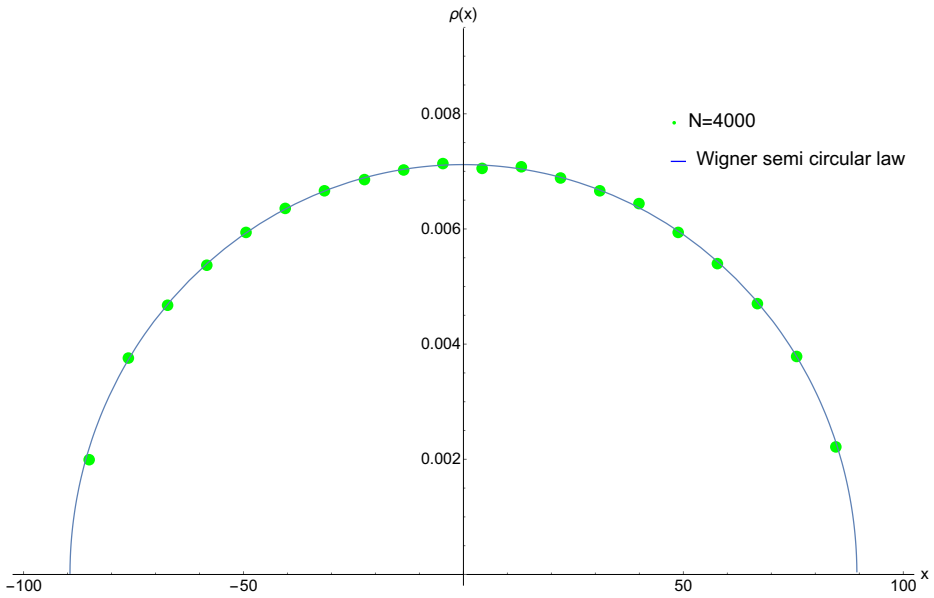

Figure 2.7: The Wigner semicircular distribution (1.5) with good agreement to data produced from random matrix theory numerics for 4000 particles packed into 20 bins.

graph (Fig. 2.7) that the Thomas-Fermi radius is indeed $\sqrt{2N}$. To get the Tracy-Widom distribution only the largest and the smallest eigenvalues are kept and as we are interested in the thermodynamic limit they are scaled appropriately: $\sqrt{2}N^{\frac{1}{6}}(\lambda-\sqrt{2N})$. This process must be repeated multiple times to collect enough data as in each iteration only two eigenvalues are recorded. After multiple iterations the eigenvalues are bin packed and a histogram is plotted. Due to the fact that each iteration is completely independent we could run the program in parallel multiple times in place of multiple iterations. The results of the program were then plotted in Mathematica along with Mathematica's own 'TracyWidomDistribution' function. As the Tracy-Widom distribution is only valid in the thermodynamic limit, we would require infinite particles and therefore infinite computing time to calculate it in this way. Therefore we restricted ourselves to the last particle distribution for $10, 100$ and 1000 particles. As expected we find that the simulation approaches the Tracy Widom distribution as particle

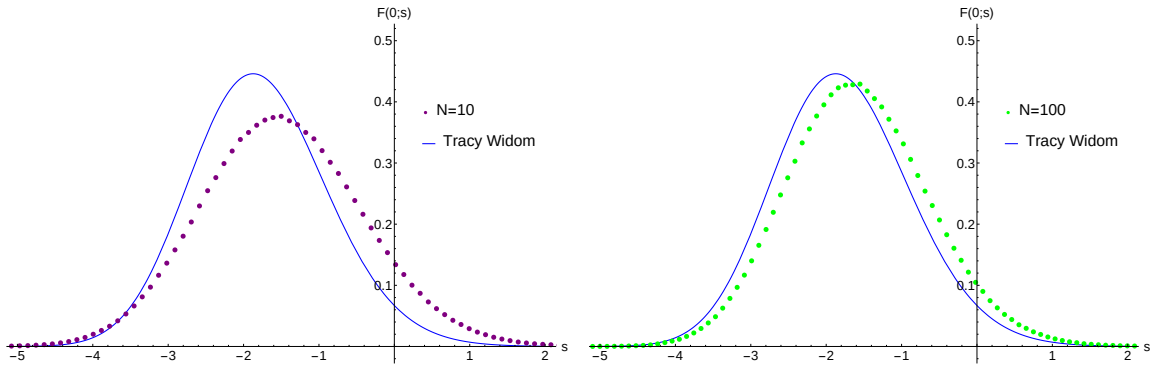

(a) $N = 10$

(b) $N = 100$

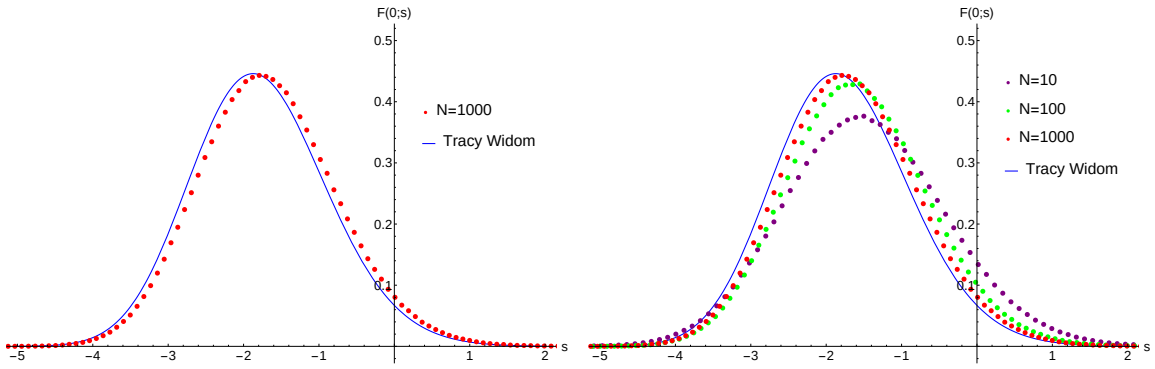

(c) $N = 1000$

(d) $N = 10, 100, 1000$

Figure 2.8: The last particle distribution calculated numerically for 10,100 and 1000 particles with increasing agreement at higher particle number. Each set of data has 3×10^6 data points packed into 100 bins.

number increases but will only reach it in the thermodynamic limit (Fig. 2.8).

2.3.3 DMRG

Density Matrix Renormalisation Group (DMRG) is a numerical technique that is commonly used in one dimensional systems to find the ground state. This is ideal for our system. In order to use this technique we first need to map our model to a discrete lattice, this has been done above and for the strong interacting regime we have our discrete system given by the Heisenberg model (2.68). We will aim to reproduce results from [34]. Luckily some python code exists [35] that performs DMRG on this model already. To adjust it for our purposes all that is needed is the addition of the harmonic trapping potential. This actually removes the need to specify open or closed boundary conditions as the particles are confined and never come into contact with the edge of the system. We can see from figure 2.9 that

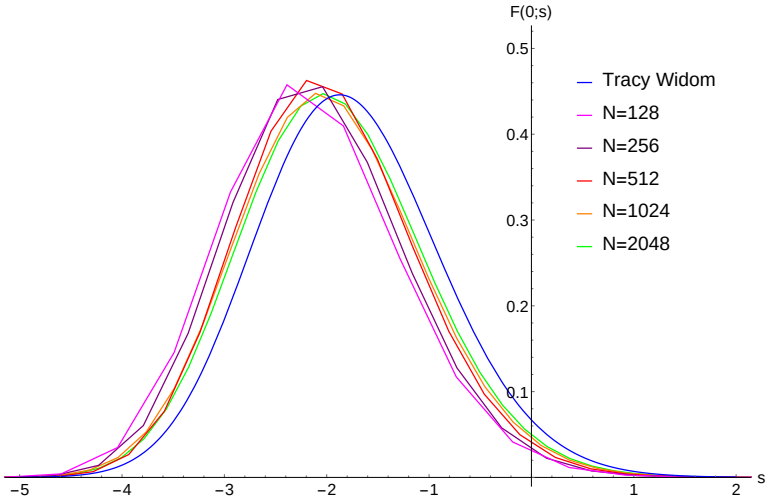

Figure 2.9: Calculation of Tracy-Widom distribution using DMRG for different particle numbers with better agreement at higher particle number.

as particle number increases we slowly converge to the Tracy-Widom distribution. As with random matrix theory the accuracy gains from doubling the number of particles are smaller

the larger the system is, in other words going from 5 to 10 particles gives far larger accuracy increase than going from 50 to 100 particles. Therefore the system converges very fast in particle number. Unlike random matrix theory for finite particle number the distribution is displaced to the left as opposed to random matrix theory where it is displaced to the right. From this we can conclude that random matrix theory over estimates the support of the system while DMRG underestimates it.

2.4 Motivation Summary

We have seen in this chapter how random matrix theory can be used to find edge distributions of a trapped hardcore Bose gas. We then saw how the opposite interaction regime could be analysed by a completely different approach and only the inner tail was affected significantly. The question of intermediate interaction regimes has not been addressed in this chapter, but we have a place to start. It was clear from the beginning that in order to examine any other interaction regimes in the Lieb-Liniger model a different approach would be needed. We have already seen hints that a hydrodynamic approach may be useful due to the fact that the interaction, and the chemical potential as a function of density and interaction, can be calculated from Bethe ansatz. While this is possible, it has not been until recently [34] that information about Tracy-Widom has been extracted from hydrodynamics. The hidden blessing/curse was that the mapping from random matrices to hydrodynamics is only possible due to the integrable nature of these one dimensional systems. However, these are not the only two powerful descriptions of our system as we will see in the next chapter.

Chapter Three

Theoretical Backbone

In the last chapter we looked at the emptiness formation probability and edge distribution of harmonically trapped gases. We explained how in the fermion case the connection covered in the first chapter with random matrix theory allows this calculation to be possible. We also showed how an equivalent expression can be found in the weakly interacting regime, seemingly unrelated to random matrix theory. Comments on the edge distributions in the two different regimes were made and the hypothesis that interaction strength only effects the tail on the outside of the gas was formulated. Further, we noted that a possible connection between the two interaction regimes was the theory of hydrodynamics and it is in that direction which we now wish to move. This chapter will be a discussion of the various different frameworks that can be used to describe harmonically trapped one dimensional particles. Starting with the classic one dimensional log gas we move onto the main derivation of a hydrodynamic action from a stochastic process. We then cover some other models and extensions of the hydrodynamic description before showing how it can be useful to view the system in more than one dimension with electrostatics and considering other variable changes that allow us to connect with some work by Gross and Witten [36]. To finish the chapter we discuss some new questions that arise as a result of viewing our system in these interesting ways.

3.1 1D Log Gas

The one dimensional log gas is the first approach we will formulate. It is provides a large amount of intuition and will act as a bridge to other techniques while being interesting in its own right. We will start with the joint probability density function of the Gaussian beta ensemble

$$1 = \frac{1}{\tilde{Z}_N} \int d^N x \prod_{\substack{i,j \\ i<j}} (x_j - x_i)^\beta e^{-\frac{\beta}{4}\sum_i x_i^2}. \tag{3.1}$$

We will follow the work of Dean Majumdar [12] and as we will be considering the thermodynamic limit it makes sense to rescale our position by a factor $\sqrt{2N}$ in accordance with the Wigner semi circle law. The first step is to move the Vandermonde determinant into the exponent as a logarithm

$$1 = \frac{1}{\tilde{Z}_N} \int d^N x e^{-\frac{\beta}{2}\left(\sum_i N x_i^2 - \sum_{i\neq j}^N \ln|x_i - x_j|\right)}. \tag{3.2}$$

The name 1D log gas is clear from the fact that our exponent is a description on a one dimensional line where the particles have a logarithmic interaction. The fact that the logarithm is the Green function of the 2D Laplacian gives hints to its connection with electrostatics and complex fields, but these will be covered later in this chapter. Next we wish to move from a microscopic description of particle positions to a macroscopic one in terms of particle density. We can introduce the density $\rho(x) = \frac{1}{N}\sum_i^N \delta(x - x_i)$, which is normalised, to write the exponent as

$$1 = \frac{1}{\tilde{Z}_N} \int D\rho J[\rho, x_i] e^{\frac{-N^2\beta}{2}\left(\int \rho(x)x^2 dx - \int\int \rho(x)\rho(x')\ln|x-x'|dxdx' - \frac{1}{N}\int \rho(x)\ln\rho(x)dx\right)}. \tag{3.3}$$

The last term in the exponent is required to regularise the expression by removing the term in the sum where particle positions are the same, in this way it can be interpreted physically as a self interaction term. This makes it of order particle number N whereas the interaction between particles is of order N^2 as expected, meaning that the self interaction will be negligible in the thermodynamic limit. Our last job is to evaluate the Jacobian between

the particle positions and the macroscopic density, this is almost a purely mathematical task beginning with the Jacobian by definition

$$J = \int d^N x \delta \left(N\rho(x) - \sum_{i=1}^{N} \delta(x - x_i) \right). \tag{3.4}$$

Introducing a new function to write the delta function as an exponential we find

$$J = \int d^N x Dg(x) e^{\int N g(x)\rho(x)dx - \sum_i g(x_i)}. \tag{3.5}$$

We can now match up each dx_i with its corresponding $g(x_i)$ to get

$$J = \int Dg(x) e^{N\int g(x)\rho(x)dx + N\ln\left(\int dx' e^{-g(x')}\right)}. \tag{3.6}$$

Stationary phase can be used to evaluate this integral with the saddle point condition

$$g(x) = -\ln\left(\rho(x)\int dx' e^{-g(x')}\right). \tag{3.7}$$

Hence

$$J = \int Dg(x) e^{-N\int \rho(x)\ln\rho(x)dx}, \tag{3.8}$$

and giving the action to be

$$S[\rho] = \frac{-N^2\beta}{2}\left(\int \rho(x)x^2 dx - \int \rho(x)\rho(x')\ln|x-x'|dx + \frac{1}{N}\left(\frac{2}{\beta} - 1\right)\int \rho(x)\ln\rho(x)dx \right). \tag{3.9}$$

We have shown that the joint probability distribution of the Gaussian beta ensemble can be transformed from an integral over the microscopic particle positions into one with an action given in terms of macroscopic particle densities. The final term in the action arose from two contributions; one from the removal of the self interaction of the particles and the other from the Jacobian. These two terms are both lower order in N than the main two and as discussed before can be neglected in the thermodynamic limit. We also note that if $\beta = 2$, equivalently we are in the Gaussian unitary ensemble describing free fermions, then the two terms will cancel for any particle number.

3.2 Hydrodynamic Action from Stochastics

In this section we will show how the log gas shown earlier can be extended to include dynamics. In this description the log gas is the boundary terms of a time dependent hydrodynamic action. This can be seen from a connection to stochastic processes that allows a hydrodynamic action to describe a Langevin process after the noise has been averaged over. This technique has been studied in [37] in relation to the HCIZ integral. Following [37] we will start by forming a continuity equation from a Langevin process. Converting this into a Martin-Siggia-Rose (MSR) path integral we will remove the noise by averaging over it. This will allow us to recover the standard hydrodynamic equations of motion by defining a new effective velocity. This new velocity will have the additional side effect of showing that the boundary conditions are the 1D log gas at the initial time. Finally we formulate a specific trajectory, on which the 1D log gas and the hydrodynamic action are equivalent. It is important to note that although the randomness of the stochastic approach is not our main goal here, and is therefore averaged out to give way for the hydrodynamic description, its equivalence is very interesting. As hinted before we know that distributions such as Tracy-Widom appear both in equilibrium conditions in random matrix ensembles as well as non-equilibrium conditions of the KPZ equation and surface growth. It is in this section that we begin to see the link between these two occurrences of this famous distribution that will be fully developed in the final chapter. We will start, as in [37], with the Langevin equation for N interacting Brownian particles and, following standard techniques that are well explained in a paper by Dean [38], we get an equivalent continuity equation. The Langevin equation to be considered is

$$dx_i = -\partial_x u(x_i)dt - \frac{1}{N}\sum_{j\neq i}^{N}\frac{1}{x_i - x_j}dt + \sqrt{\frac{2}{\beta N}}dW_i. \tag{3.10}$$

The terms on the RHS are the contribution from an external potential, which we will leave as a general term for now to be specified later, and the interaction term. We also have a

Weiner process describing some thermal noise. The coefficient depending on β will specify how important the noise is and will transpire to be the same β from the random matrix theory section. Defining a microscopic density

$$\rho(x,t) = \frac{1}{N}\sum_{i=1}^{N}\delta(x - x_i(t)), \tag{3.11}$$

and a trial function

$$\frac{1}{N}\sum_{i=1}^{N} f(x_i(t)) = \int f(x)\rho(x,t)dx, \tag{3.12}$$

we seek a hydrodynamic description. It can already be seen that this approach, in contrast to the one dimensional log gas in section 3.1, involves time dependence in the microscopic description. This will still be the case in the macroscopic variables where $t = 0$ will recover the log gas quantities. To this end we take the differential of the trial function and use the Ito formula to get

$$d\left[\frac{1}{N}\sum_{i=1}^{N} f(x_i(t))\right] = \frac{1}{N}\sum_{i=1}^{N}\partial_x f(x_i(t))dx_i + \frac{1}{\beta N^2}\sum_{i=1}^{N}\partial_x^2 f(x_i(t))dt. \tag{3.13}$$

The definition of dx_i can be substituted in from equation (3.10) and the microscopic density can be used to turn the sums into integrals containing a macroscopic density in all but the noise term

$$d\left[\int f(x)\rho(x,t)dx\right] = \left[-\int \partial_x f(x,t)\partial_x u(x)\rho(x,t)dx + \int \frac{1}{\beta N}\partial_x^2 f(x,t)\rho(x,t)dx\right.$$
$$\left. -P\int\int \partial_x f(x,t)\frac{\rho(x,t)\rho(y,t)}{x-y}dxdy\right]dt + \frac{1}{N}\int \partial_x f(x,t)\sqrt{\frac{2}{\beta N}}\sum_{i=1}^{N}\delta(x - x_i(t))dxdW_i. \tag{3.14}$$

The noise term will require special treatment as all other terms only contained dependence on the particle index i in the particle position x_i's but the noise also depends on the particle index. Further we note that the principle value is required for the interaction term. As $f(x)$ is a trial function we can form the following equation

$$\partial_t\rho = \partial_x\left[\rho\partial_x u + P\int\frac{\rho(x,t)\rho(y,t)}{x-y}dy + \frac{1}{\beta N}\partial_x\rho\right] - \sqrt{\frac{2}{\beta N^3}}\partial_x\left(\sum_{i=1}^{N}\delta(x - x_i(t))\xi_i(t)\right). \tag{3.15}$$

The special treatment of converting the noise term into a macroscopic density is done by considering its statistical properties to show that it can be reformulated in an equivalent way, see [38], as $\frac{2}{\beta N}\partial_x(\sqrt{\rho}\xi(t))$. This allows us to see that the original Langevin equation (3.10) has been transformed into an equivalent functional continuity equation

$$\partial_t \rho + \partial_x J(\rho(x,t)) = 0, \tag{3.16}$$

where

$$J(x,t) = -\rho\partial_x u - \int \frac{\rho(x,t)\rho(y,t)}{x-y}dy - \frac{1}{\beta N}\partial_x \rho + \frac{2}{\beta N}\sqrt{\rho}\xi(t). \tag{3.17}$$

Now that we have the continuity form of the Langevin equation we will use the Martin-Siggia-Rose path integral formulation to construct a hydrodynamic action from it. We see that our interaction term is just a Hilbert transform (See appendix C.1)

$$\rho^H(x,t) = P\int \frac{\rho(y,t)}{x-y}dy, \tag{3.18}$$

to make notation easier. We write a delta function enforcing our continuity equation as

$$1 = \int D\rho J_1[\rho]J_2[\rho, x_i]\delta(\partial_t\rho + \partial_x J(\rho)), \tag{3.19}$$

where the Jacobian J_1 is equal to one using the correct Ito regularisation, as shown in [39], and the other Jacobian J_2 enforces the definition of macroscopic density in terms of microscopic particle position at initial time. The Jacobian J_2 has already been evaluated as (3.8). Using the integral form of the delta function by introducing a new field we have

$$1 = \int D\rho D\psi e^{\int_0^1 dt \int dx N^2 \psi(\partial_t\rho + \partial_x J)}. \tag{3.20}$$

We can now average over the noise term $\langle \ldots \rangle_\xi$ to find that the action is

$$S = N^2 \int_0^1 dt \int dx \left(\psi\partial_t\rho + \rho^H\rho\partial_x\psi + \rho\partial_x u\partial_x\psi - \frac{\psi}{\beta N}\partial_x^2\rho + \frac{2}{\beta^2}\rho(\partial_x\psi)^2\right). \tag{3.21}$$

If we had formed an action starting from (3.10) we would not have got the viscosity term that depends on β, as this term comes from the Ito analysis. For a good comparison of these

different starting points see [37]. Functional derivatives with respect to ψ and ρ can now be taken to get the following equations of motion

$$\partial_t \rho = \partial_x(\rho^H \rho) + \partial_x(\rho \partial_x u) - \frac{1}{\beta N}\partial_x^2 \rho + \frac{4}{\beta^2}\partial_x(\rho \partial_x \psi), \tag{3.22}$$

$$\partial_t \psi - \frac{2}{\beta^2}(\partial_x \psi)^2 = \rho^H \partial_x \psi + \partial_x u \partial_x \psi - \frac{1}{\beta N}\partial_x^2 \psi - \int \frac{\rho(y,t)}{x-y}\partial_y \psi(y,t) dy. \tag{3.23}$$

We wish to define a hydrodynamic velocity as

$$v(x,t) = -\rho^H(x,t) - \frac{4}{\beta^2}\partial_x \psi(x,t) - \partial_x u(x), \tag{3.24}$$

the contributions to the velocity have clear physical meaning as they come from the other $N-1$ particles the temperature through the thermal noise and the external potential respectively. The normal conservation of mass equation is then recovered

$$\partial_t \rho + \partial_x(\rho v) = \frac{1}{\beta N}\partial_x^2 \rho. \tag{3.25}$$

Now we will define a new effective velocity that incorporates the dissipation term

$$-v_{eff}(x,t) = -\partial_x \phi = \rho^H(x,t) + \frac{4}{\beta^2}\partial_x \psi(x,t) + \partial_x u(x) - \frac{1}{\beta N}\frac{\partial_x \rho}{\rho}. \tag{3.26}$$

substituting this into the action (3.21), we temporally leave the time derivative alone and get

$$S = \frac{\beta^2 N^2}{4}\int_0^1 dt \int dx \Big(\frac{4}{\beta^2}\psi \partial_t \rho + \frac{\rho}{2}\Big(-\left(\rho^H\right)^2 - (\partial_x u)^2 + (\partial_x \phi)^2 \Big) - \rho^H \partial_x u \rho + \frac{\partial_x u}{\beta N}\partial_x \rho + \frac{\rho^H}{\beta N}\partial_x \rho - \frac{1}{2\beta^2 N^2}\frac{(\partial_x \rho)^2}{\rho} \Big). \tag{3.27}$$

Up until this point the derivation holds for any reasonable interaction potential but from now on we will be using properties of the Hilbert Transform in our calculations so are restricted to our specific case of the harmonic trap $u = \frac{\omega x^2}{2} + const$. We will now consider each of the terms in turn. The term that scales like $O(N^{-2})$ is quantum pressure. The term $\frac{\partial_x u}{\beta N}\partial_x \rho$ can be combined with the existing potential $-\rho(\partial_x u)^2$ to give a pseudo-potential of

$W(x) = (\partial_x u)^2 + \frac{2\partial_x^2 u}{\beta N}$. This has the form of the Riccati equation and has links to supersymmetry. We note that in the case of the harmonic trap the double derivative gives a constant and the single derivative squared returns the x^2 form, this is the only case where the pseudo-potential is a vertical shift of the original.

The next term we shall consider is $-\rho^H \partial_x u \rho$ in the case of the harmonic trap, using the definition of our microscopic density we write the integral over x as a sum

$$-\int dx dt \rho^H \partial_x u \rho = -\frac{\omega}{N^2} \int dt \sum_{i \neq j}^{N} \frac{x_i}{x_i - x_j}. \tag{3.28}$$

We see that we can match the i, jth term with the j, ith term which when added together gives one, after doing this process for every term in the sum we find that this term in the action is nothing more than a constant

$$-\int dx dt \rho^H \partial_x u \rho = -\frac{\omega(N-1)}{2N} \int dt. \tag{3.29}$$

The next term we shall consider is $-\frac{\left(\rho^H\right)^2 \rho}{2}$, again we write this as a sum

$$-\int dx dt \frac{\left(\rho^H\right)^2 \rho}{2} = -\frac{1}{2N^3} \int dt \sum_{\substack{i \neq j \\ i \neq k}}^{N} \frac{1}{x_i - x_j} \frac{1}{x_i - x_k}. \tag{3.30}$$

Considering the first sum we see that it can be separated into the part when $j = k$ and when $j \neq k$. These off diagonal terms combine to give zero. To see this we look at cyclic permutations of terms in the sum e.g the i, j, kth term when added to the j, k, ith term cancels with the k, i, jth term. This means that this term in the action gives

$$-\int dx dt \frac{\left(\rho^H\right)^2 \rho}{2} = -\frac{1}{2N^3} \int dt \sum_{i \neq j}^{N} \frac{1}{(x_i - x_j)^2}. \tag{3.31}$$

We recognise this as the integral from Matytsin's paper [40]

$$\frac{1}{N^3} \sum_{i \neq j}^{N} \frac{1}{(x_i - x_j)^2} \approx \int dx \frac{\pi^2}{3} \rho^3. \tag{3.32}$$

The final term is $\frac{\rho^H}{\beta N}\partial_x\rho$ which by integration by parts we can write as a Hilbert transform (See appendix C.1) bringing the the action to the form

$$S = \frac{\beta^2 N^2}{4}\int_0^1 dt \int dx \left(\frac{4}{\beta^2}\psi\partial_t\rho + \frac{\rho}{2}\left(-\frac{\pi^2}{3}\rho^2 - \frac{2}{\beta N}(\partial_x\rho^H) - (\partial_x u)^2 - \frac{2}{\beta N}\partial_x^2 u + (\partial_x\phi)^2 \right) - \frac{1}{2\beta^2 N^2}\frac{(\partial_x\rho)^2}{\rho} \right) - \frac{\omega N(N-1)}{2}\int dt. \tag{3.33}$$

The time derivative under the same velocity shift (3.26) gives us boundary terms of the same form as Dean and Majumdar [12]

$$N^2\int_0^1 dt\int dx\psi\partial_t\rho = \frac{\beta^2 N^2}{4}\int_0^1 dt\int dx\partial_t\rho\left(-\int \ln(x-y)\rho(y,t)dy - u - \phi + \frac{1}{\beta N}\ln\rho \right), \tag{3.34}$$

where we see that the last term coming from dissipation is the same one that is used to regularise the self interaction in section 3.1. Applying integration by parts to move the time derivative over we see that the first two terms are full time derivatives and therefore are functions of the density at the initial and final times $\rho_A(x) = \rho(x,0), \rho_B(x) = \rho(x,1)$. The next term will be kept as it is and the final one can be rewritten using the chain rule $\partial_t(\rho\ln\rho) = \partial_t\rho\ln\rho + \partial_t\rho$ as

$$\int_0^1 dt\int dx\partial_t\rho\ln\rho = \int \rho_A(x)\ln\rho_A(x)dx - \int_0^1 dt\int dx\partial_t\rho, \tag{3.35}$$

where the last term is the difference in particle number between the initial and final times

$$N^2\int_0^1 dt\int dx\psi\partial_t\rho = \frac{\beta^2 N^2}{4}\left[\int \rho_A(x)x^2dx - \int \rho_A(x)\rho_A(x')\ln|x-x'|dxdx' + \frac{1}{\beta N}\int \rho_A(x)\ln\rho_A(x)dx\right]. \tag{3.36}$$

If the action is evaluated along a zero energy trajectory, as will be discussed in detail in the next section, we will find that the time dependent part is just another copy of the same boundary term we already have. These are formally a forward in time and backwards in time contribution to the action but due to the symmetry of the problem they give the same

contribution.

$$\int_0^1 dt \int dx \left(-\phi\partial_t\rho + \frac{\rho}{2}\left(-\frac{\pi^2}{3}\rho^2 - \frac{2}{\beta N}(\partial_x\rho^H) - (\partial_x u)^2 - \frac{2}{\beta N}\partial_x^2 u + (\partial_x\phi)^2 \right) - \frac{1}{2\beta^2N^2}\frac{(\partial_x\rho)^2}{\rho} \right) - \frac{\omega N(N-1)}{2}\int dt$$
$$= \int \rho_A(x)x^2dx - \int \rho_A(x)\rho_A(x')\ln|x-x'|dxdx' + \frac{1}{\beta N}\int \rho_A(x)\ln\rho_A(x)dx + \frac{1}{\beta N}\int dx\rho_A(x) - (A \to B). \tag{3.37}$$

We have obtained a form of the 1D log gas action written in hydrodynamic variables. The form of u in the harmonic trap is $u = \frac{\omega x^2}{2} + const$, this agrees with [12] and has the correct dimensions for the original Langevin equation (3.10).

3.2.1 Separatrix Condition

In order for our hydrodynamic description to be equivalent to the one dimensional log gas we must have be on a specific zero energy trajectory of the path integral

$$S = \int_0^1 dt \int dx \left(\phi\partial_t\rho + \frac{\rho}{2}\left(\frac{\pi^2}{3}\rho^2 + \frac{2}{\beta N}(\partial_x\rho^H) + (\partial_x u)^2 + \frac{2}{\beta N}\partial_x^2 u - (\partial_x\phi)^2 \right) + \frac{1}{2\beta^2N^2}\frac{(\partial_x\rho)^2}{\rho} \right). \tag{3.38}$$

Shifting the effective velocity by a factor $\pm\frac{\partial_x\rho}{N\beta\rho}$ we see that the quantum pressure term will be removed in favour of a term giving diffusion in the equations of motion. In the full time derivatives the $\rho\ln(\rho)$ term will also be affected, consequently the continuity equation will no longer allow conservation of particles due to the extra term. This ability to swap between quantum pressure and diffusive terms is very useful here and we first discussed this in section 3.4 and equation (3.24). With our new velocity we have

$$S = N^2\int_0^1 dt \int dx \left(\phi\partial_t\rho + \frac{\rho}{2}\left(\frac{\pi^2}{3}\rho^2 + (\partial_x u)^2 - (\partial_x\phi)^2 \right) + \frac{1}{\beta N}\left(\rho\partial_x^2 u \pm \partial_x\phi\partial_x\rho - \partial_x\rho\rho^H \right) \right). \tag{3.39}$$

We have removed some constant factors in the action that can be incorporated into the normalisation. We have also grouped together the action as it would be in the thermodynamic limit and them the terms of lower order which will cause particle loss or gain in the equations of motion. The N^2 is important as it provides us with a large parameter to use for stationary phase to evaluate our integral, its origins are examined in papers like [40]. In order to see how our action can be zero we will note that the ρ^3 term can also be written as the square of a Hilbert transform

$$\int_{-\infty}^{\infty} dx\, \rho(x) \left(\rho^H(x)\right)^2 = \frac{1}{3}\int_{-\infty}^{\infty} dx\, \rho^3(x)\,, \tag{3.40}$$

and using this our thermodynamic limit action, with the potential set to the harmonic trap, becomes

$$S = N^2 \int_{-\frac{\beta}{2}}^{\frac{\beta}{2}} dt \int dx \left[\phi\partial_t\rho - \frac{\rho}{2}\left((\partial_x\phi)^2 - \left(\omega x - \pi\rho^H\right)^2\right)\right]. \tag{3.41}$$

We must now consider which trajectory we wish to be on in our path integral. In general field theory calculations use the ground state density as the weight. Under equilibrium conditions this is a time independent quantity, but can be generalised to arbitrary times by considering it as the long time limit of a dynamic quantity

$$|\,\langle 0|\rho(x)\rangle\,|^2 \underset{\beta\to\infty}{=} \langle\rho(x)|\, e^{-\beta(H-E_0)}\,|\rho(x)\rangle\,. \tag{3.42}$$

We will write out the ground state probability distribution as an integral

$$\langle\rho(x)|\, e^{-\beta H}\,|\rho(x)\rangle = \int D\rho D\phi e^{-S[\rho,\phi]}, \tag{3.43}$$

where the action is that of (1.62). To evaluate (3.43) we will integrate over all fields ρ and ϕ that have the fixed value at $t = \pm\beta/2$ of $\rho(x,-\beta/2) = \rho_0(x) = \rho(x,\beta/2)$ as shown in figure 3.1. In the thermodynamic limit we wish to use stationary phase approach in evaluating (3.43). On minimising the action we find that the equations of motion for fermions in a harmonic trap are

$$\partial_t\rho + \partial_x(\rho v) = 0, \tag{3.44}$$

$$\partial_t v + v\partial_x v = \pi^2\rho\partial_x\rho + \omega^2 x, \tag{3.45}$$

where $v = \partial_x \phi$ and the boundary condition $\rho_0(x)$ is given. We note that this hydrodynamic theory has links to the HCIZ equations as shown by Matytsin [40]. In equilibrium it is easy to solve the equations of motion for a time independent solution. We get zero velocity and $\pi\rho = \sqrt{\omega(2 - \omega x^2)}$, the Wigner semi circle is recovered. As we are interested in the ground state probability distribution we will examine the limit as $\beta \to \infty$. From (3.42) we see that this will recover the boundary density up to a constant. Therefore as β increases the density tends towards a distribution that is time independent. Our equilibrium configuration is exactly this solution as it will not change over time. However the space of densities we are integrating over is restricted to be the ones that have the corresponding boundary conditions. As $\beta \to \infty$ the equilibrium configuration will be preferred so the dominant solution will be the one that approaches equilibrium as fast as possible from its initial disturbed state. We will call this the separatrix condition and it corresponds to a particular initial gradient in figure 3.1.

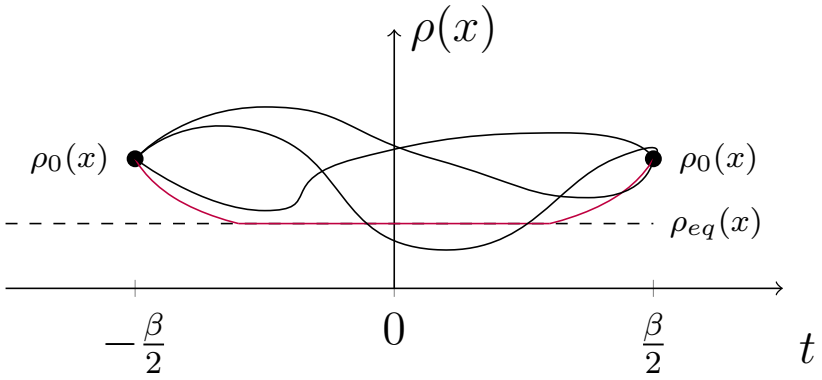

Figure 3.1: Sketch of all possible path integral trajectories with dominant trajectory on separatrix condition in purple that begins and ends at the boundary condition density spending as much time in-between as close to equilibrium as possible.

We can see that this path must be symmetric by splitting the range of integration

$$\int D\rho D\phi e^{-\int_{-\beta/2}^{0} \ldots dt - \int_{0}^{\beta/2} \ldots dt}, \tag{3.46}$$

and performing a shift by $\beta/2$ to reveal the symmetry. The solution must be as close to equilibrium as possible while still meeting the boundary conditions at $t = \pm\beta/2$. The separatrix condition, that the dominant trajectory goes to equilibrium as fast as possible, can be used to give mathematical constraints on the field ϕ. This can be seen from figure 3.2.

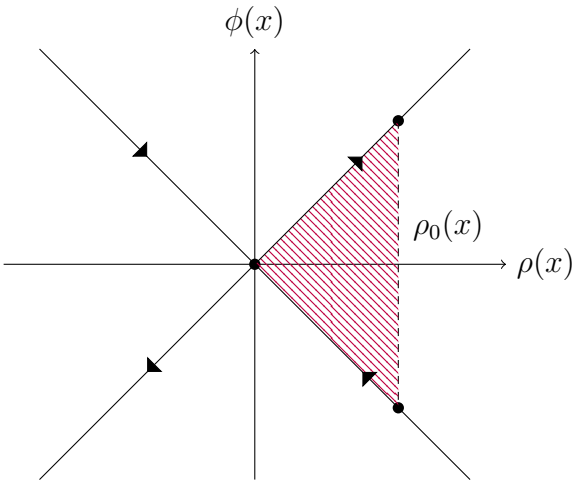

Figure 3.2: Sketch of area enclosed in the ρ, ϕ between conditions for zero energy, forward and reverse time contributions are in the upper and lower half plane respectively. Additionally the separatrix condition trajectory with equilibrium at the origin.

Using the fact that the Hamiltonian part of the action corresponding to this trajectory must be zero we formulate a mathematical separatrix condition that can be found from the action. A zero energy trajectory can by achieved trivially be having zero density $\rho = 0$, in which case the entire action is also zero. Alternatively and far more interestingly, we can have the following relation between density and velocity.

$$v(x,t) = \partial_x \phi(x,t) = \omega x - \pi \rho^H(x,t) = \omega x - P \int_{-\infty}^{\infty} \frac{\rho(y,t)}{x-y} dy \,. \tag{3.47}$$

We wish to evaluate our action (1.62) on the separatrix condition. The squared terms will cancel with other parts of the action using (3.40). Additionally we find the cross term will

just give a constant that is exactly the ground state energy E_0 from (3.42)

$$\int dx\, x\rho(x,t)\pi\rho^H(x,t) = \int dx\rho(x,t)P\int dy\,\rho(y,t)\frac{x}{x-y} = \frac{1}{2}\left(\int dx\rho(x,t)\right)^2 = \frac{1}{2}\,. \quad (3.48)$$

Thus giving us the zero energy we expect on the separatrix. To see the value of the action at this point we note that the remaining term is a full time derivative

$$S = N^2\left[\int dx\frac{\omega x^2}{2}\int dt\,\partial_t\rho(x,t) - \frac{1}{2}\int dxdy\log|x-y|\int dt\,\partial_t[\rho(x,t)\rho(y,t)]\right]. \quad (3.49)$$

This means that our action can be projected onto its values at the initial and final times

$$e^{-N^2S} = \exp\left[-\frac{N^2}{2}\int dx\,\omega x^2\rho_0(x) + \frac{N^2}{2}\int dxdy\,\rho_0(x)\log|x-y|\rho_0(y)\right] = \prod_{i<j}(x_j-x_i)^2e^{-\frac{1}{2}\sum_i\omega x_i^2}, \quad (3.50)$$

where the last equality holds using $N\rho = \sum_i\delta(x-x_i)$. It is well known that the many body wave function of N free fermions under harmonic confinement is the probability density function of eigenvalues in a $N\times N$ GUE matrix [24]. In the aforementioned paper by Dean and Majumdar [12] this is shown in more detail. The fact that we recover their action explicitly here shows the equivalence of the hydrodynamic action to the stationary one on the separatrix condition (3.47).

3.2.2 Closely Related Actions

We will now consider other useful rescaling of our hydrodynamic action (3.33), these will be in order to show that our hydrodynamic action can be related to other known systems that are of particular physical interest and/or solvable either numerically or analytically. If we set $\beta = 2$ and substitute in $Q(x,t) = \sqrt{\rho}e^{-\theta}, P(x,t) = \sqrt{\rho}e^{\theta}, t = -i\tau$ into our action (3.33) following [41] we bring it to the form

$$S = iN^2\int d\tau\int dx\left[P\partial_\tau Q + \frac{1}{2}\partial_x P\partial_x Q + \frac{\pi^2}{6}P^3Q^3 + \frac{(\partial_x u)^2}{2}PQ + const\right], \quad (3.51)$$

where the constant is known from the above calculations. This action is interesting as its corresponding equations of motion are a system of equations named after Mark J. Ablowitz, David J. Kaup, Alan C. Newell and Harvey Segur known as the AKNS equations [42]. A set of coupled equations that admit many solutions either exactly [43] or by numerical methods [44]. Another rescaling that is of interest is the one that leads to the hydrodynamic action for the Gaussian beta ensemble. The rescaling needed is then $\rho^H \to \lambda\rho^H, u \to \lambda u$ and $N \to \frac{N}{\lambda^2}$. The new dimensionless parameter $\lambda = \frac{\beta}{2}$ is an interaction strength in the Calogero-Sutherland model related by a factor of two with the Dyson index of random matrix theory. Under this scaling the action has become

$$\begin{aligned}\int_0^1 dt \int dx \Bigg(&- \phi\partial_t\rho + \frac{\rho}{2}\left(-\frac{\lambda^2\pi^2}{3}\rho^2 + \frac{\lambda^2}{2N}\pi(\partial_x\rho)^H - (\lambda\partial_x u)^2 - \frac{\lambda^2}{2N}\partial_x^2 u + (\partial_x\phi)^2\right) \\ &- \frac{\lambda^2}{8N^2}\frac{(\partial_x\rho)^2}{\rho}\Bigg) \\ = \lambda\Bigg(&\int \rho_A(x)x^2dx - \int \rho_A(x)\rho_A(x')\ln|x-x'|dxdx' + \frac{1}{2N}\int \rho_A(x)\ln\rho_A(x)dx \\ &+ \frac{1}{2N}\int dx\rho_A(x) - (A \to B)\Bigg).\end{aligned} \tag{3.52}$$

We now have the action of [45] in imaginary time with a harmonic trap. To complete the relation to the one dimensional log gas action used by Dean and Majumdar [12] we simply need to include the Jacobian between the macroscopic density and microscopic particle positions as stated in (3.19). Fortunately the Jacobian has been previously calculated (3.8), with its inclusion we have a hydrodynamic action for any β including terms of all orders in particle number. These both the AKNS system and the Gaussian beta ensemble system are interesting in their own right but we will not discuss them much further here.

3.3 Calogero Sutherland

Until now we have been restricting the values of beta to $\beta = 1, 2, 4$ in order to stay in the orthogonal, unitary or symplectic ensemble respectively. However, when we write the joint

pdf this choice seems needlessly restrictive as we could make beta any value and the integral still makes sense. In this section we will show the known result that other values of beta can be used and do, in fact, have physical meaning. To do this we will study the Calogero Sutherland model.

$$H = -\frac{1}{2}\sum_{i=1}^{N}\frac{\partial^2}{\partial x_i^2} + \frac{1}{2}\sum_{i<j}^{N}\frac{\lambda(\lambda-1)}{(x_i-x_j)^2} + \frac{\lambda^2\alpha^2}{2}\sum_{i=1}^{N}x_i^2. \tag{3.53}$$

Like the Lieb-Liniger model this model is prolific in the area of integrable one dimensional systems. Where the difference occurs is that unlike the Lieb-Liniger model Calogero Sutherland has a long range interaction. Additionally the strength of that interaction does not have a fixed sign this allows it to describe both fermions and bosons. As a final note when $\lambda = 1$ we recover the Hamiltonian of free fermions. One of the reasons Calogero Sutherland is popular is due to the simplicity of the many body wave function, this can be seen by considering solutions to the equation of motion

$$N\frac{\partial\phi}{\partial t} = -\frac{1}{2}\sum_{i=1}^{N}\frac{\partial^2\phi}{\partial x_i^2} + \frac{1}{2}\sum_{i<j}^{N}\frac{\lambda(\lambda-1)}{(x_i-x_j)^2}\phi + \frac{\lambda^2\alpha^2}{2}\sum_{i=1}^{N}x_i^2\phi. \tag{3.54}$$

We look for a stationary solution in the form $\phi = e^{N^2W}$

$$0 = -\sum_{i=1}^{N}\left(N^4\left(\frac{\partial W}{\partial x_i}\right)^2 + N^2\frac{\partial^2 W}{\partial x_i^2}\right) + \sum_{i<j}^{N}\frac{\lambda(\lambda-1)}{(x_i-x_j)^2} + \lambda^2\alpha^2\sum_{i=1}^{N}x_i^2. \tag{3.55}$$

Inserting an educated guess for our solution

$$W = -\frac{\lambda}{2N^2}\sum_{i<j}^{N}\ln|x_i-x_j| + \frac{\lambda\alpha}{N}\sum_{i=1}^{N}x_i^2. \tag{3.56}$$

We find that the majority of terms cancel the only remaining terms transpire to be constants

$$\frac{2\alpha\lambda^2}{N^2}\sum_{i\neq j}^{N}\frac{x_i}{x_i-x_j} + \frac{\lambda\alpha}{N^2}\sum_{i=1}^{N}1 = \frac{2\alpha\lambda^2N(N-1)}{N^2} + \frac{\lambda\alpha}{N}. \tag{3.57}$$

This means our educated guess was only out by a constant which can be included and will only contribute to the normalisation. Substituting W back into the form for ϕ we see that the integral for the normalised wave function looks like

$$1 = \frac{1}{\tilde{Z}_N}\int d^Nx\prod_{\substack{i,j\\i<j}}(x_j-x_i)^{2\lambda}e^{-\frac{\lambda\alpha}{2}\sum_i x_i^2}. \tag{3.58}$$

Finally we make the identification $\beta = 2\lambda$ to recover the integral for the Gaussian beta ensemble of random matrix theory, it can be clearly seen that $\lambda = 1$ does indeed correspond to the GUE. In this section we have seen that the joint pdf can have a physical interpretation for all real values of β and not just the three that correspond to the usual random matrix ensembles. Furthermore we have shown that this interpretation is in fact the Calogero Sutherland model, an interesting model in its own right.

3.4 Alternative Derivation from Fokker–Planck Equation

The derivation of a hydrodynamic action from stochastic processes above is a crucial point in this thesis but alternative derivations are possible. Here we will show a derivation based a the Fokker–Planck equation, we could use the Fokker–Planck equation corresponding to the Langevin equation (3.10), and this would reproduce the calculation in section 3.2. So we will perform a the calculation in a slightly different way to showcase the usefulness of the effective velocity in this system. This calculation has already been done in the homogenous case by Matytsin [40], where it is equivalent to the heat equation, we will only modify it slightly with the addition of a harmonic trap and the inclusion of diffusive terms. We will start from the Fokker–Planck equation without a trap

$$2N\frac{\partial I(x,t)}{\partial t} = \frac{1}{\Delta(x)}\sum_{i=1}^{N}\frac{\partial^2}{\partial x_i^2}\Delta(x)I(x,t). \tag{3.59}$$

where Δ is the Vandermonde determinant. Seeking the form of an action we will set $I = e^{N^2 W}$

$$2\frac{\partial W}{\partial t} = \frac{1}{N}\sum_{i=1}^{N}\frac{\partial^2}{\partial x_i^2}W + N\sum_{i=1}^{N}\left(\frac{\partial W}{\partial x_i}\right)^2 + 2\sum_{i=1}^{N}V(x_i)\frac{\partial W}{\partial x_i} - \frac{\omega^2}{2N}\sum_{i=1}^{N}x_i^2, \tag{3.60}$$

where $NV(x_i) = \sum_{j\neq i}(x_i - x_j)^{-1}$. At this point a difference from the derivation used in [40] is the treatment of the second derivative. As the second derivative is lower order in N it could be neglected but we will keep it in our calculation as it is the source of diffusion. Another

difference is the external potential term which will make our system inhomogeneous, this has been added here as we are about to incorporate the harmonic trap by specifying a form for W and the inclusion of this term is needed to recover the Langevin equation for (3.10). From the previous section we know the appropriate form of W is

$$W = S - \frac{1}{2N^2}\sum_{i\neq j}\ln|x_i - x_j| + \frac{\omega}{2N}\sum_{i=1}^{N}x_i^2 + \frac{1}{N^2}\sum_{i=1}^{N}\ln(\rho(x_i)). \tag{3.61}$$

These are the terms on the boundary that we have found in previous sections. They correspond to interaction, external potential and a diffusive term. On substitution into our equation we have

$$\begin{aligned} 2\frac{\partial S}{\partial t} = \sum_{i=1}^{N}\Bigg[\left(\sqrt{N}\frac{\partial S}{\partial x_i} + \frac{\omega}{\sqrt{N}}x_i + \frac{1}{N^{\frac{3}{2}}\rho}\frac{\partial \rho}{\partial x_i}\right)^2 + \frac{1}{N^2}\frac{\partial}{\partial x_i}\left(N\frac{\partial S}{\partial x_i} + \omega x_i + \frac{1}{N\rho}\frac{\partial \rho}{\partial x_i}\right) \\ -\frac{\omega^2}{N}x_i^2 - \frac{1}{N}V^2(x_i) - \frac{1}{N^2}V'(x_i)\Bigg]. \end{aligned} \tag{3.62}$$

The next logical step is to define the effective velocity in the same way as previous sections

$$v_{eff}(x_i) = N\frac{\partial S}{\partial x_i} + \omega x_i + \frac{1}{N\rho}\frac{\partial \rho}{\partial x_i}, \tag{3.63}$$

it contains the same physical terms as before, the contribution from the other particles is not present due to its existence in the definition of W but the contribution from the trap and a diffusion term still persist. We note that if we had chosen to have our potential in the original Fokker–Planck equation then the potential term would also be absent in the effective velocity but the resulting hydrodynamic Hamiltonian would remain unchanged. Then using our density to convert the sum into an integral we have a hydrodynamic Hamiltonian

$$H = \frac{\partial S}{\partial t} = \int dx\left[\frac{\rho}{2}\left(-\frac{\pi^2}{3}\rho^2 - (\partial_x u)^2 + (v_{eff})^2\right) - \frac{v_{eff}\partial_x\rho}{2N} + \frac{\rho^H\partial_x\rho}{2N}\right]. \tag{3.64}$$

To achieve the above equation we have identified the terms in the action dependent on $V(x_i)$ and its derivative as the same ones in (3.30). In doing so we can see that this action is identical to (3.33) with the choice of effective velocity (3.24). We have just shown an alternative method to derive a hydrodynamic action for the one dimensional log gas, this

procedure is slightly simpler as it does not use stochastic methods. It has also shown us that we have significant freedom in how we define our effective velocity. This will be used to great effect in the last chapter.

3.5 Electrostatic Analogy

In this section we will consider an analogous system of interacting charged particles, we will use this analogy to go from the action that Dean and Majumdar consider in [12] that comes from the Coulomb gas to the linearised action Abanov uses [32] that comes from hydrodynamics. We begin with Gauss's law for N charges on the real line

$$\vec{\nabla} \cdot \vec{E} = \rho\delta(y) = \frac{1}{N}\sum_{i=1}^{N} \delta(x - x_i)\delta(y). \tag{3.65}$$

Rewriting our field as the gradient of a potential ($\vec{E} = \vec{\nabla}\phi$) we see that the potential must satisfy Poisson's equation

$$\nabla^2\phi = \rho\delta(y). \tag{3.66}$$

This can be solved by the Greens function for the 2D Laplacian

$$\phi = \frac{1}{N}\sum_{i=1}^{N} \ln|\vec{x} - \vec{x_i}| = \int d^2x'\rho(\vec{x'}) \ln|x - \vec{x'}|. \tag{3.67}$$

With this electrostatic analogy in mind we now take a look at the action from Dean and Majumdar [12]

$$S = \int dxdx'\rho(x)\rho(x') \ln|x - x'|. \tag{3.68}$$

Including extra integrals over delta function we can write this in a way with extra dimensions where the charges are confined on some lines

$$S = \int d^2xd^2x'\rho(\vec{x})\rho(\vec{x'}) \ln|\vec{x} - \vec{x'}|. \tag{3.69}$$

We now substitute in expressions for the potential given above

$$S = \int dxdy\phi\nabla^2\phi, \tag{3.70}$$

and apply integration by parts requiring that the boundary term vanishes

$$S = \int dxdy(\vec{\nabla}\phi)^2. \tag{3.71}$$

We obtain the linearised action from Abanov [32]. This interpretation of our system in terms of electrical charges can be an effective tool to understand our system in more detail. For example we can interpret our system as some charges on a rod which when the charges are confined into a region, when the emptiness condition is applied, gather at one end of the rod. This charge build up could also be another way of experimentally verifying our theoretical calculations. The other advantage of the electrostatic analogy is that even though the charges are confined to a one dimensional line the field lines extend out into higher dimensions, we therefore see that an effective description maybe to work in a complex space using cuts through the real axis for measurement, this will be used in the final chapter of this thesis.

3.5.1 Extra Charges as the Trap

In this section we introduce m extra particles at positions $y_1 \dots y_m$ instead of a harmonic trap, we show how these particles can make an effective trap when positioned correctly and how this allows the system to be written as a Gaussian integral. Consider the quantity

$$S = \left| \frac{\Delta(x_1 \dots x_n, y_1 \dots y_m)}{\Delta(y_1 \dots y_m)} \right|^2, \tag{3.72}$$

where we have divided by the vandermonde of the $y_1 \dots y_m$ in order to remove the interactions between then, leaving only the interactions with the $x_1 \dots x_n$. factorising out the vandermonde determinate of x's we have

$$S = |\Delta(x)|^2 \prod_{i=1}^{n} \prod_{j=1}^{m} (x_i - y_j)^2. \tag{3.73}$$

We must now choose the position of the y's carefully in order to trap our system. We let half of the y's be at position y_+ and the other half at position $y_- = -y_+$. This gives

$$S = |\Delta(x)|^2 \prod_{i=1}^{n} (x_i^2 - y_+^2)^m. \tag{3.74}$$

Which can be converted into exponentials as

$$S = |\Delta(x)|^2 e^{m\sum_{i=1}^{n} \ln\left(1-\frac{x_i^2}{y_+^2}\right) + nm\ln\left(y_+^2\right)}. \tag{3.75}$$

Finally letting $y_+ = \sqrt{m}$ and allowing $m \longrightarrow \infty$ we recover the many body wave function of particles in a harmonic trap

$$S = |\Delta(x)|^2 e^{-\sum_{i=1}^{n} x_i^2}. \tag{3.76}$$

We now wish to consider these extra particles from the viewpoint of electrostatics. To include the y's into this picture we simply let $\rho \longrightarrow \rho_{tot} = \rho_1 + \rho_2 = \frac{1}{N}\sum_{i=1}^{N} \delta(x - x_i) + \frac{m}{2}\sum_{i=1}^{m} \delta(x - y_i)$, where the locations of the y_i's have been worked out above. We see that the extra particles can be thought of as charges in the same way as before

$$\vec{\nabla} \cdot \vec{E} = (\rho_1 + \rho_2) = \frac{1}{N}\sum_{i=1}^{N} \delta(x - x_i) + \frac{m}{2}\sum_{i=1}^{m} \delta(x - y_i). \tag{3.77}$$

Rewriting our field as the gradient of a potential ($\vec{E} = \vec{\nabla}(\phi_1 + \phi_2)$) we see that the potential must satisfy Poisson's equation

$$\nabla^2\phi_1 + \nabla^2\phi_2 = \rho_1 + \rho_2. \tag{3.78}$$

With this electrostatic analogy in mind we now consider the action

$$S = \int dxdx' \rho_1(x)\rho_1(x') \ln|x - x'| + \int dxdx' \rho_1(x)\rho_2(x') \ln|x - x'| + \int dxdx' \rho_2(x)\rho_2(x') \ln|x - x'|. \tag{3.79}$$

The final term between the extra charges will cancel exactly with the Vandermonde determinant in the extra variables as shown earlier. We now substitute in expressions for the potential given above

$$S = \int dxdy(\phi_1\nabla^2\phi_1 + \phi_1\nabla^2\phi_2). \tag{3.80}$$

The above form of the action makes it clear that under the transformation $\phi_1 \to \phi_1 + const$ charge neutrality is required to allow the action to remain invariant this is of great importance in other applications of these methods [46] and will be briefly touched on here in the next section. Applying integration by parts and requiring that the boundary term vanishes we have

$$S = \int dxdy((\vec{\nabla}\phi_1)^2 + \nabla\phi_1 \cdot \nabla\phi_2). \tag{3.81}$$

In comparison to the free case we can see that the presence of extra charges forming a trapping potential appears as a source term in the equations of motion.

3.5.2 Charge Neutrality

The addition of extra particles of opposite charge to create a trapping potential will have a large effect on the total charge of the system. In this section we will consider how the system appears from a large distance examining quantities such as charge neutrality and large x asymptotics. Starting from the identity

$$\phi = \int \rho(x') \ln|x - x'| dx'. \tag{3.82}$$

We note here that if we wish to consider the extra charges to create the trap we just identify $\phi = \phi_1 + \phi_2$ and $\rho = \rho_1 + \rho_2$. Expanding for large x we have

$$\phi \approx \int \rho(x') \ln|x| dx' + \frac{1}{x}\int x'\rho(x')dx'. \tag{3.83}$$

This is the monopole expansion with the first term being the monopole followed by the dipole term and so on. If we have charge neutrality then ϕ will decay at large x. The greens function is given by

$$G = \ln|x - x'|, \tag{3.84}$$

using this we can rewrite the identity as

$$\int \phi\nabla^2 G d^2x' = \int G\nabla^2\phi d^2x'. \tag{3.85}$$

From greens second identity we must have

$$\oint (\phi \nabla G - G \nabla \phi) \cdot dS = 0, \tag{3.86}$$

if we have charge neutrality both terms will decay at infinity and this is true. The other option is that $N\rho = \sum_{i=1}^{N} \delta(x - x_i)$. The former is used by Abanov in [47], the latter used by Dean and Majumdar [12].

3.6 Action Angle Variables

In this thesis we have only used standard Cartesian coordinates in describing our systems but it is a well known fact that action angle variables are very useful in studying harmonic oscillators. In this section we will see what effect this variable change has on our system. It will transpire that this is equivalent to adding periodic boundary conditions to our system and therefore moving from the GUE to the CUE ensembles in random matrix theory. We will see that this connects to some work done by Gross and Witten many years before the Tracy-Widom distribution was discovered [36]. We begin with some general theory, the Hamiltonian of a harmonic oscillator in imaginary time can be written in angular variables

$$H = \frac{p^2}{2} - \frac{\omega^2 x^2}{2} = \omega I, \tag{3.87}$$

where ω is the frequency of the harmonic trap and (α, I) are the action angle variables defined by

$$p = i\sqrt{2I\omega}\sin\alpha, \tag{3.88}$$

$$x = \sqrt{\frac{2I}{\omega}}\cos\alpha. \tag{3.89}$$

In phase space (x, p) this becomes the hyperbola

$$p = i\omega\sqrt{\frac{2I}{\omega} - x^2}. \tag{3.90}$$

To make the solution time dependent we make the transformation $\alpha \to \alpha + i\omega t$ so we get

$$p(t) = p_0 \cosh(\omega t) + \omega x_0 \sinh(\omega t), \tag{3.91}$$

$$x(t) = \frac{p_0}{\omega} \sinh(\omega t) + x_0 \cosh(\omega t). \tag{3.92}$$

We will now investigate what happens if we remove the trap and recover breathing modes. Upon taking the limit $\omega \to 0$ we have

$$p(t) = p_0, \tag{3.93}$$

$$x(t) = x_0 + t p_0. \tag{3.94}$$

This has the same form as the time dependence in [40]. If we choose $x(0) = \cos\alpha$ and $p(0)e^{-i\alpha}$ we can eliminate α to find

$$p(x,t) = \frac{1}{b}\left[\frac{x}{b} \pm \sqrt{\frac{x^2}{b^2} - 1}\right] = \frac{1}{b} p\left(\frac{x}{b}\right), \tag{3.95}$$

where $b(t) = \sqrt{1+2t}$. This is the same as a scaling solution in the absence of the trap. We will now examine how this formalism works in the case of emptiness formation probability. As our example we will use critical emptiness densities from [12]. The quantity analogous to momentum in the Dean and Majumdar solution for symmetric emptiness [12] is

$$p = \frac{2 + s^2 + 2z^2\left[-1 + \sqrt{1 - \frac{s^2}{z^2}}\right]}{2z\sqrt{1 - \frac{s^2}{z^2}}} - z, \tag{3.96}$$

where s is the location of the hard wall and z is the complex version of x. Under the transformation $z = s\cos\alpha$ we get

$$p = -i\left(s\cos\alpha + \frac{2 - s^2}{2s\sin\alpha}\right). \tag{3.97}$$

We note that if time dependence is introduced in the same way $\alpha \to \alpha + i\omega t$ the second term will be negligible at large times and the system will look like a harmonic oscillator. The transformation must also be applied to the separatrix condition that we enforced earlier (see

section 3.2.1) therefore we consider the effect of angular variables on the Hilbert transform

$$x = \mathrm{P}\int \frac{\rho(y)}{x-y}dy. \tag{3.98}$$

For the Wigner semi circle we have

$$x = \cos\alpha, \tag{3.99}$$

$$\rho = \sin\alpha. \tag{3.100}$$

This makes the Hilbert transform

$$\cos\alpha = \mathrm{P}\int \frac{\rho(\cos\beta)\sin\beta}{2\sin\left(\frac{\alpha+\beta}{2}\right)\sin\left(\frac{\alpha-\beta}{2}\right)}d\beta. \tag{3.101}$$

This is the description of interacting charges on a unit circle. From the density we can see

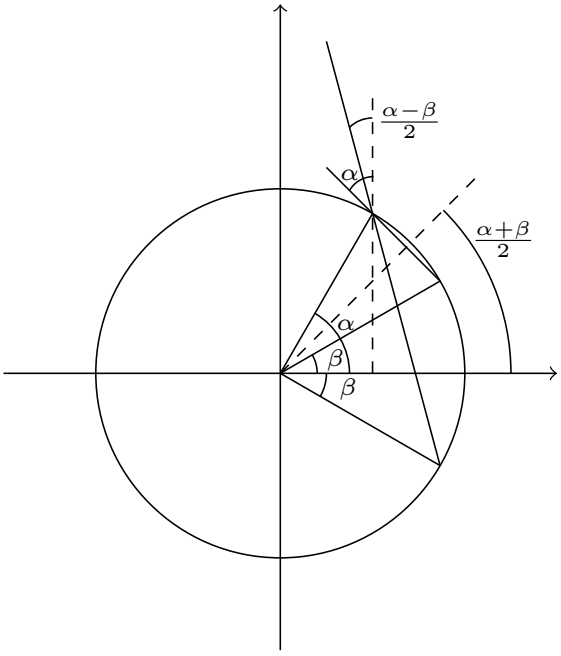

Figure 3.3: Diagram of forces on a test charge placed at α from the existing positive charges in the top half of the circle and the corresponding negative charges in the bottom half of the circle.

that all the positive charges are in the top half of the circle with all the negative charges in

the bottom half. If a unit test charge is placed at α then the forces felt from the charge at β and $-\beta$ are

$$F_\beta = 2\sin\left(\frac{\alpha+\beta}{2}\right)\cos\left(\frac{\alpha-\beta}{2}\right), \tag{3.102}$$

$$F_{-\beta} = -2\sin\left(\frac{\alpha-\beta}{2}\right)\cos\left(\frac{\alpha+\beta}{2}\right), \tag{3.103}$$

respectively giving a total force $2\sin\beta$ and making the Hilbert transform

$$\cos\alpha = \frac{1}{2}\,\mathrm{P}\int \rho(\cos\beta)\cot\left(\frac{\alpha-\beta}{2}\right)d\beta - \frac{1}{2}\,\mathrm{P}\int \rho(\cos\beta)\cot\left(\frac{\alpha+\beta}{2}\right)d\beta. \tag{3.104}$$

Combining this with the electrostatic analogy we have developed in previous section we can understand the problem of emptiness in a trap in the CUE. We can think of the system as charged particles on a circle with an external potential such that the equilibrium configuration has all the particles of negative charge in the bottom half of the circle with a semi circular charge density. Correspondingly an identical number of positive charges, conserving charge neutrality, are present in the top half of the circle also with a semi circle density distribution. The case of an emptiness configuration is where some parts of the circle are no longer allowed to hold charges, this breaks the boundary conditions where particles could move between halve of the circle and causes charge build-up at the emptiness boundary.

3.7 New Questions

We began this chapter searching for a way to describe emptiness formation probabilities in the arbitrary interaction case. We had already concluded that a promising approach would be to form some kind of hydrodynamic action in combination with Bethe ansatz. In this chapter we achieved this but in doing so saw many interesting links between different descriptions of one dimensional physics. We saw how the one dimensional log gas description can be viewed as the boundary term of a hydrodynamic action when evaluated on the separatrix condition.

This was shown by considering another description, that of stochastic process, forming a path integral from it and averaging over the noise. We also showed how other systems, for example, Calogero Sutherland can be described very well by random matrix theory. Additionally the interpretation on terms of electrostatics was discussed and showed some intuitive incites into the system. These alternative ways of describing our system open up new and interesting questions that we did not have at the beginning of this chapter. Namely, we know that the Tracy-Widom distribution appears in the equilibrium configuration of the GUE from random matrix theory, we also know that it is found via completely separate methods in the surface growth of the KPZ equation [9], a non-equilibrium stochastic process. Can we find the link between these two occurrences of this infamous distribution, using hints from our hydrodynamic derivation that relied on stochastics? Also now that we have access to time in out hydrodynamic action, what are the dynamic properties of emptiness once it has been observed? It is with these questions in mind that we proceed into the next chapter.

Chapter Four

Results

This final chapter is comprised of almost entirely new results that arose from studying the hydrodynamic description of our system. As seen in the previous chapter it is possible to derive a hydrodynamic action using a stochastic approach by averaging over the noise. This raises the possibility of performing this process in reverse to study the appearance of the Tracy-Widom distribution in the surface growth models of KPZ as well as the ground state equilibrium fluctuations of non interacting fermions. This shall be addressed first in this chapter, we shall see how this process can indeed be achieved with the introduction of noise into our hydrodynamic description followed by a hodograph transform (See appendix D.2) and identifying the relevant height function. The second question that arose from the last chapter was more open ended. It concerned studying time dependent solutions to the equations of motion due to our hydrodynamic description involving a time variable. We will finish the chapter with this investigation, showing that a time dependent emptiness formation density can indeed be found. Furthermore we form a new description in terms of algebraic curves. Using this description we show how to find emptiness configurations that were not apparent before as well as examine the topology of these solutions at all times.

4.1 Connection to Kardar–Parisi–Zhang Equation

The Kardar–Parisi–Zhang (KPZ) equation is a famous model of stochastic surface growth which has applications to systems such as the asymmetric simple exclusion process (ASEP) [48]. The equation can be formulated from physical arguments by starting with the diffusion equation for the height of a surface at a given time $h(x,t)$.

$$2\partial_t h = \partial_x^2 h. \tag{4.1}$$

We then wish to add a Gaussian noise of the form $\langle \xi(x,t) \rangle = 0$ and $\langle \xi(x,t)\xi(x',t') \rangle = D\delta(x-x')\delta(t-t')$. Due to the fluctuation dissipation theorem the second moment of the noise D must depend on the dissipation term. The insight by Kardar–Parisi–Zhang in [49] was to argue that this term would depend on the gradient of the height field only. Therefore for a small gradient the leading order term to include would be a constant, which could be removed by a shift in time. The next largest term, a linear one could also be removed, this time with a velocity shift. Therefore the first non trivial term that can be added is a non linear one.

$$\partial_t h = \nu \partial_x^2 h + \lambda(\partial_x h)^2 + \xi. \tag{4.2}$$

To see that we do indeed have dissipation we can make the useful transformation $g = \partial_u h$ to turn the KPZ equation into the stochastic Burgers equation. Another useful transform is the Cole-Hopf transform given by $Z(x,t) = e^{\frac{\lambda h(x,t)}{\nu}}$ which removes the non linear term in the KPZ equation. When solving the KPZ equation we can expect the solution to be made up of two parts. The first part will be the continual growth, this is the largest contribution but not stochastic and equivalent to a time shift. The second and more interesting part of the solution is fluctuations about this height, these are small in comparison but have a characteristic scale and distribution that is dependent on the initial conditions (Fig. 4.1). Luckily the initial conditions we are interested in are also some of the simplest ones and both have fluctuations that scale as $t^{\frac{1}{3}}$ [9]. The initial conditions, in terms of the Cole-Hopf

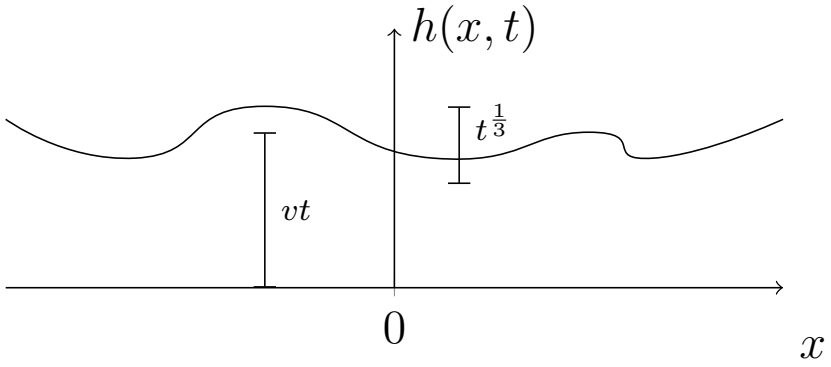

Figure 4.1: Sketch of a typical KPZ surface with the dominant linear growth in time with the additional surface fluctuations of lower order in time.

transformed variable are $Z(x,0) = c$ and $Z(x,0) = \delta(x)$ the corresponding distribution of fluctuations is given by the Tracy-Widom distribution for the GOE and GUE respectively [9].

4.1.1 Density Shift

We begin with the hydrodynamic action (3.33) with the aim of reintroducing noise in order to see a connection to the KPZ equation. We have performed a velocity shift in order to swap between quantum pressure and diffusive terms in the same way as we first discussed in section 3.4 and (3.24). The difference here is that we have chosen the sign of the separatrix condition (3.47) in such a way that the terms of order N^{-1} combine into one term. With this sign of the separatrix condition our action is still equivalent to the one dimensional log gas in the thermodynamic limit. Although as previously discussed corrections of order N^{-1} are present with this particular sign choice. With our new velocity we have

$$S = N^2 \int_0^1 dt \int dx \left(\phi \partial_t \rho + \frac{\rho}{2} \left(\frac{\pi^2}{3} \rho^2 + (\partial_x u)^2 - (\partial_x \phi)^2 \right) + \frac{\partial_x \phi \partial_x \rho}{N} \right). \tag{4.3}$$

We will now shift the density field by a constant $\rho \to \rho + c$ this will generate extra terms in the action that we can use to introduce the new noise

$$N^2 \int_0^1 dt \int dx \left(\frac{cv^2}{2} - \frac{c\pi^2\rho^2}{2} + \frac{c^2\rho}{2} - \frac{c\omega^2 x^2}{4} \right). \tag{4.4}$$

The last two terms will not contribute to the equations of motion. In order to find the value of the constant we see that the quadratic terms should give the standard Luttinger liquid action (See appendix D.1) [50] this sets $c = 1$. We will now introduce noise through a Hubbard Stratonovich transformation on these terms

$$\int D\xi_1 e^{-\xi_1^2 + vN\sqrt{2c}\xi_1} = \sqrt{\pi} e^{\frac{cN^2v^2}{2}}. \tag{4.5}$$

These new noise terms are not the same as the ones used in the stochastic derivation, they are in fact associated with the density and velocity fields. The equations of motion have now become

$$\partial_t \rho + \partial_x(\rho v) = \frac{1}{N}\partial_x^2 \rho - \frac{\sqrt{2}}{N}\partial_x \xi_1, \tag{4.6}$$

$$\partial_t v + v\partial_x v = \pi^2 \rho \partial_x \rho - \frac{1}{N}\partial_x^2 v + \omega^2 x - \pi\frac{\sqrt{2}}{N}\partial_x \xi_2, \tag{4.7}$$

where ξ_1, ξ_2 is the noise associated with v, ρ respectively. We can see that the fluctuation dissipation theorem is obeyed with the particle number N appearing in both the dissipative term as well as the coefficient of the noise. In the complex variable $p = v + i\pi\rho$ these equations are

$$\partial_t p + p\partial_x p = \frac{1}{N}\partial_x^2 p + \omega^2 x - \frac{\sqrt{2}}{N}\partial_x \xi, \tag{4.8}$$

with $\xi = \xi_1 + i\pi\xi_2$. This is the stochastic Burgers equation and by a simple substitution $p = \partial_x h$ can be turned into KPZ. We now wish to change variables in such a way as to remove N from the equation, therefore we perform the transformations $x \to \sqrt{N}x, p \to \frac{p}{\sqrt{N}}$ and $\omega \to \frac{\omega}{\sqrt{N}}$. The hydrodynamic theory described above takes an equilibrium distribution at $t = -\infty$ and evolves it to a distribution under some condition (e.g emptiness) at $t = 0$. For this method to work we must have equilibrium at $t = -\infty$. We now wish to investigate

fluctuations of the last particle, to do this we will introduce noise through the transformation above and consider evolution from no particles at $t = -\infty$ to the thermodynamic limit $N \to \infty$ at $t = 0$. Allowing noise to be proportional to some positive power of particle number will ensure that at $t = -\infty$, and only then are the noise and dissipation terms exactly zero. Hence we can have equilibrium and therefore zero velocity. As the KPZ

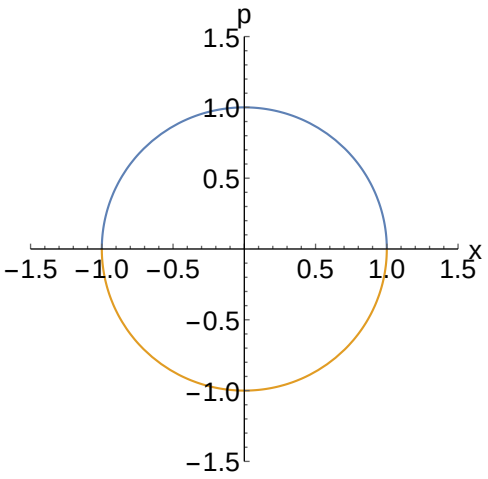

Figure 4.2: Equilibrium phase space plot for a harmonic oscillator with positive and negative branches of the momentum in blue and orange respectively.

equation deals with surface fluctuations it will be much more convenient if the position of the last particle was the height of something as opposed to the edge of the support. Inspired by [41] we apply the following hodograph transform (See appendix D.2) to the above Burgers equation

$$p(x,t) = u, \quad t = t', \quad x = g(u,t'), \tag{4.9}$$

where the partial derivatives transform as

$$\partial_x p = (\partial_u g)^{-1}, \quad \partial_t p = -\partial_{t'} g (\partial_u g)^{-1}, \tag{4.10}$$

$$\partial_x^2 p = -(\partial_u g)^{-3} \partial_u^2 g, \quad \partial_x = (\partial_u g)^{-1} \partial_u. \tag{4.11}$$

Our equation is now

$$\partial_{t'} g + \omega^2 g \partial_u g - (\partial_u g)^{-2} \partial_u^2 g - \sqrt{2} \partial_u \xi = u. \tag{4.12}$$

We now have a function g where the last particle position is given by it's value at the origin and we wish to investigate the fluctuations around this point. The natural object of study is the height field given by the standard substitution of $g = \partial_u h$. This object is monotonic increasing from zero to total particle number over the support of the gas, see (Fig. 4.3). It will not have the same value as g at the origin but will have the same fluctuations.

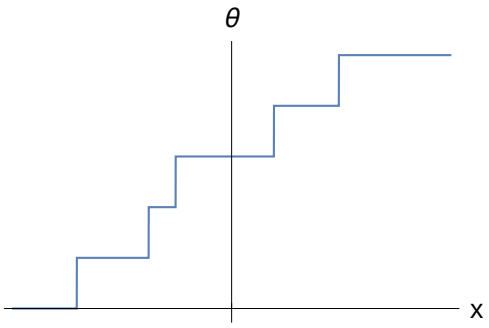

Figure 4.3: Sketch of a standard height field associated with density tracking cumulative particle number. Starting at the left hand end of the system and increasing in steps of unit size until it reaches total particle number.

$$\partial_{t'} h + \frac{\omega^2}{2}(\partial_u h)^2 + (\partial_u^2 h)^{-1} - \sqrt{2}\xi - \frac{u^2}{2} = 0. \tag{4.13}$$

We now assume that h is dominated by quadratic behaviour with small fluctuations. In fact this must be the case as the hodograph transformed height field corresponds to the integral of the momentum distribution and must therefore be start from zero, be maximum at the origin and then return to zero, see (Fig. 4.4). The transformation will introduce the pseudo-potential that will cancel with the u^2 term.

$$h(u, t') = \frac{\eta u^2}{2\omega} + h'(u, t'), \tag{4.14}$$

where we have free choice of $\eta = \pm 1$. Expanding the second derivative term to first order in these fluctuations we find

$$\partial_{t'} h' + \frac{\omega^2}{2}(\partial_u h')^2 + \eta u \omega \partial_u h' - \omega^2 \partial_u^2 h' - \sqrt{2}\xi + \eta\omega = 0. \tag{4.15}$$

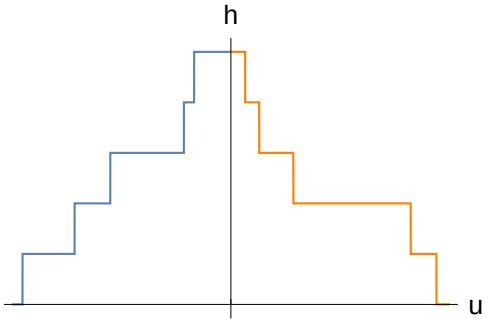

Figure 4.4: Sketch of height field in hodograph transformed description tracking cumulative momentum. It starts at the left hand end of the system in momentum space increasing to maximum at the origin then decreases to zero at the right hand end of the system in momentum space.

It is possible to shift to a moving frame, as discussed by Spohn [51], that removes the single derivative in h' by $t' = \tau - \eta\frac{\ln|u|}{\omega}$. This takes us from (u, t') to (u, τ) where the equation is

$$\partial_\tau h' + \frac{\omega^2}{2}(\partial_u h')^2 - \omega^2\partial_u^2 h' - \sqrt{2}\xi + \eta\omega = 0. \tag{4.16}$$

We note that this method will only work in the harmonic trap, as both the cancellations due to the pseudo-potential and the hodograph transform only achieve the desired effect in this case. To have some idea of how expect the height field to behave we consider the case of an equilibrium semi circle. Note this is only equilibrium without the dissipation and noise terms so our scaling to remove N is not present.

$$p = \omega\sqrt{x^2 - R^2}, \tag{4.17}$$

where $R = \sqrt{\frac{2N}{\omega}}$. Therefore the initial condition on g is

$$g = \frac{1}{\omega}\sqrt{u^2 - R^2\omega^2}, \tag{4.18}$$

which is a semi circle with radius $\omega\sqrt{N}$

$$\pm\, h = \frac{1}{2}u\sqrt{\frac{u^2}{w^2} - 2N} - Nw\log\left(w\sqrt{\frac{u^2}{w^2} - 2N} + u\right), \tag{4.19}$$

the sign depends on the branch we need to take. At this point we return to our system, and reinstate our scaling to remove N, with noise and consider some crucial features that we need

1. At $t = -\infty$ we have $N = 0$ and no noise.
2. Choosing $\eta = -1$ gives $h(u, \tau(u, -\infty)) = -\frac{u^2}{2\omega}$ with the sign choice given by physical considerations. This also allows us to see that $\omega g = u$ or kinetic energy equals potential energy ($p^2/2 = \omega^2 x^2/2$).
3. The Cole-Hopf transformed initial condition $Z(u, \tau(u, -\infty)) = e^{-\frac{1}{2}h'(u,\tau(u,-\infty))}$ is defined up to a multiplicative constant this allows us to normalize it and get $Z \approx \delta(u)$ as particle number goes to zero.

By comparing with the known solution from [9] we see that the form we have obtained is

$$h'(u, \tau) = \frac{u^2}{2\omega^2\tau} - \frac{\tau}{96\omega^2} - \eta\omega\tau - 4\ln(-2\omega) - 2\left(\frac{\tau}{16\omega^2}\right)^{\frac{1}{3}}\xi_\tau, \tag{4.20}$$

the differences are the fact we are still in imaginary time and the additional term linear in τ that exists in order to remove the constant term from (4.16). Finally we will check the Tracy-Widom scaling, reversing our transformations to bring the N dependence back we see that solving for the points of intersection of the height function without noise $h' = 0$ will give show us that u and τ have the same scaling in particle number. Comparing with the expected radius of the semi circle we find $\tau \approx \sqrt{N}$. Furthermore this gives us that the noise from KPZ scales like $\tau^{\frac{1}{3}} \approx N^{\frac{1}{6}}$. We see that near $u \to 0$ the interval $t \in (-\infty, 0]$ corresponds to $\tau \in [0, \infty)$. In the thermodynamic limit $N, \tau \to \infty$ we look at the fluctuations near $u \to 0$ giving $t \to 0$. ξ_τ follows the Tracy-Widom distribution as shown in [9]. The above procedure would not have worked without the hodograph transform as the height function would have been monotonic.

4.2 Complex Contour

Here we will begin to examine other ways of writing the action. Considering a complex approach we will see how a phase space representation can be recovered and that the density shift employed in the previous section is equivalent to a choice of gauge. We begin with the action in the thermodynamic limit

$$S = \int_0^1 dt \int dx \left(\phi \partial_t \rho + \frac{\rho}{2} \left(\frac{\pi^2}{3} \rho^2 + (\omega x)^2 - (\partial_x \phi)^2 \right) \right), \tag{4.21}$$

writing in terms of the complex variables $p = v + i\pi\rho$ we find

$$S = \frac{1}{2\pi i} \int_0^1 dt \int dx \left(\frac{1}{2}(\chi + \bar{\chi})(\partial_t p - \partial_t \bar{p}) + \frac{\bar{p}^3}{6} - \frac{p^3}{6} + \frac{\omega^2 x^2}{2}(p - \bar{p}) \right), \tag{4.22}$$

where $\partial_x \chi = p$. The full time derivative terms can be removed leaving only the cross terms with a time derivative

$$S = \frac{1}{2\pi i} \int_0^1 dt \int dx \left(\frac{1}{2}(\chi \partial_t \bar{p} - \bar{\chi} \partial_t p) + \frac{\bar{p}^3}{6} - \frac{p^3}{6} + \frac{\omega^2 x^2}{2}(p - \bar{p}) \right). \tag{4.23}$$

The first term can be evaluated purely as boundary terms, $\bar{\chi} p|_t = 0$ and $\chi \partial_t \bar{\chi}|_x = 0$, using integration by parts. To write this as a contour integral in the complex plane we define $z_\pm = \omega x \pm p$ where p or its conjugate is chosen if the contour is above or below the real axis.

$$H = \frac{i}{8\pi\omega} \oint \left[\frac{1}{12}(z_-^3 - z_+^3) + \frac{1}{4}(z_-^2 z_+ - z_+^2 z_-) \right] (dz_+ + dz_-). \tag{4.24}$$

The application of Stokes theorem allows us to simplify the integral to one over the interior of the contour in the complex plane

$$H = \frac{i}{8\pi\omega} \int dz_+ dz_- z_+ z_-. \tag{4.25}$$

This is analogous to integrating over the classical harmonic oscillator in phase space, in fact it is only a factor of 2π out in the equivalent real time variables $z = \omega x + ik$ same variables

$$\int dx dk \left(\frac{\omega^2 x^2}{2} + \frac{k^2}{2} \right) = \frac{i}{4\omega} \int dz d\bar{z} |z|^2. \tag{4.26}$$

As there are many contour integrals that would have given this under Stokes theorem we can use this gauge freedom to simplify out contour integral. We are allowed anything of the form

$$\oint \left(a(z_+, z_-)dz_+ + b(z_+, z_-)dz_-\right), \tag{4.27}$$

where

$$\frac{\partial a}{\partial z_-} - \frac{\partial b}{\partial z_+} = z_+ z_-. \tag{4.28}$$

Our original integral had the choice

$$a = b = \frac{1}{12}(z_-^3 - z_+^3) + \frac{1}{4}(z_-^2 z_+ - z_+^2 z_-), \tag{4.29}$$

but under the gauge transform

$$a \to a - \frac{z_+^3}{12} + \frac{z_-^3}{12} - \frac{z_+^2 z_-}{4} - \frac{z_+ z_-^2}{4}, \tag{4.30}$$

$$b \to b - \frac{z_+^3}{12} + \frac{z_-^3}{12} - \frac{z_+^2 z_-}{4} + \frac{z_+ z_-^2}{4}, \tag{4.31}$$

our integral becomes

$$H = \frac{i}{8\pi\omega} \oint \frac{z_+ z_-^2}{2} dz_+, \tag{4.32}$$

which is much simpler. We note that using our gauge freedom we can add in a term

$$\oint (z_+ - z_-)^2 (dz_+ + dz_-). \tag{4.33}$$

This does not change the integral and has the same effect as the shift in density performed in the last section $\rho \to \rho + c$ as it adds terms quadratic in density and velocity.

4.3 Dynamic Emptiness and Algebraic Curves

In this section we will address the second question that arose from the previous chapter, that of time dependent solutions. We will show that more information can be obtained

from the time dependent hydrodynamic action using the example of emptiness formation probability for harmonically trapped fermions. The stationary calculation has been done by Dean and Majumdar [12] using the one dimensional log gas, covered in section 3.1, where they calculate the critical density of a trapped gas with an emptiness on one side. Showing that the equilibrium density of the Wigner semi circle (1.5) can be recovered at zero emptiness, they go on to derive asymptotics of the Tracy-Widom distribution [8] from their results. Therefore showing that a third order phase transition is present. An alternative time dependent calculation has been considered by people like Matysin [40] and Abanov [32] but only in homogenous systems, see section 3.4 for the inclusion of a trap. Here we will seek to study the third order phase transition from the dynamic perspective with an external harmonic trap. After some general theory we will examine the action along the zero energy, so called separatrix condition (see section 3.2.1). Examining how this action relates to its initial configuration will lead us to the structure of emptiness in the complex space of a Riemann surface and how this structure evolves over time. In doing so we will see how the emptiness region heals along the separatrix trajectory and provide interesting links to algebraic curves.

4.3.1 Methodology

In this section we will consider a specific case, in particular the case of emptiness formation. Having already calculated the ground state in the previous section 3.2.1 we now wish to explore the temporal properties that the large deviations of emptiness formation have. Continuing to look at the Tracy-Widom distribution and its asymptotics; from the separatrix condition (3.47) we note that our velocity and density are related by a Hilbert transform, this suggests that they can be thought of as real and imaginary parts of a complex function. Hence we transform the equations of motion (3.44,3.45) into a more symmetric form

by changing from the real density and velocity fields (ρ, v) to the analytic complex field $p = v + i\pi\rho$

$$\partial_t p + p\partial_x p = \omega^2 x, \tag{4.34}$$

$$\partial_t \bar{p} + \bar{p}\partial_x \bar{p} = \omega^2 x, \tag{4.35}$$

where $\bar{p}$ is the complex conjugate of p on the real axis. The equations are now in the form of Riemann invariants. (4.34) can be solved using the method of characteristics to give the time evolution as

$$x_0 = x\cosh\omega t - p\frac{\sinh\omega t}{\omega}, \tag{4.36}$$

$$p_0 = p\cosh\omega t - x\omega\sinh\omega t. \tag{4.37}$$

So as long as we have the initial condition we can substitute in (4.36,4.37) in order to find the behaviour at later times. In fact we wish to describe our system using algebraic curves, as will be seen in the next section, our initial condition will be given by a polynomial $F(p_0, x_0) = 0$. The way to proceed from this method is now clear. We begin with defined initial density or velocity field. As we wish to evolve our state in time along the separatrix condition we can use the relation (3.47) in order to calculate the corresponding field not given in the initial condition. This allows us to form a complex field p which is a combination of the density and velocity. Finally this can be evolved in time simply by applying (4.36,4.37).

The transformation to complex fields will also change the separatrix condition, in fact we find that we have moved from our original description in terms of the density and velocity fields to one in terms of the complex fields p and $\bar{p}$ that are analytic in the upper and lower half plane respectively.

$$p(z,t) = \omega z \pm \int_{-\infty}^{\infty} \frac{\rho(y,t)}{z-y} dy\,. \tag{4.38}$$

Here we must consider the structure of p in the complex plane. The density $\rho(y,t)$ will be zero on some intervals in the real line due to the confining potential. This allows p and $\bar{p}$

to be two branches of the same analytic function, which could not happen if ρ was non zero everywhere. We will see later that the initial emptiness p is a combination of two branch cuts on the Riemann surface. The first is the equilibrium one that is present due to the harmonic trap, this is present on the Riemann sphere and runs over the support of the density. The second one occurs due to the emptiness condition, running from a point inside the equilibrium configuration to infinity, and hence overlaps with the previous branch cut. This causes the initial Riemann surface to resemble a torus which is topologically distinct from the equilibrium one of a sphere, hence the point where the third order transition takes place. Adding another emptiness region is topologically equivalent to another branch cut appearing on the Riemann surface.

Once we have found our time dependent solution we can substitute it back into the action to find the probability of our solution occurring. So in a similar way we wish to transform the action (3.50) into the complex field variables. This connection is made by using the integral of the separatrix condition (3.47)

$$\phi_0 = \frac{\omega x^2}{2} - \int \rho_0(x') \ln|x - x'| dx'. \tag{4.39}$$

Noting that p is a complex function we will expand our description into the complex plane where $z = x + iy$, with (4.40) being true on the real line. After the action is transformed into a contour integral in the complex plane, with $\partial_x \chi = p$ we have

$$S = \int \phi_0(x)\rho_0(x)dx = \oint dz \bar{\chi} \partial_z \chi = \int d^2 z \partial_{\bar{z}} \bar{\chi} \partial_z \chi. \tag{4.40}$$

With the adjusted boundary conditions that both $\chi^2 - \bar{\chi}^2$ and $|\chi|^2$ must vanish at the boundary of $x = \pm\infty$ and the contour runs along the real axis closing in the upper or lower half plane. By studying time evolution of our solution we will see how the surface changes and plot real slices through the surface for analysis.

4.3.2 Single Emptiness

Here we will consider dynamics of the simplest case, that of a single emptiness region at the edge of the system. Therefore we wish to form the algebraic curve for a single emptiness region. Starting with the equilibrium solution, setting $\omega = 1$, we note that it is unchanged under time evolution by (4.36,4.37), as seen in previous sections. We will add an emptiness region by considering the minimal change to the polynomial that will give non equilibrium behaviour, this is an increase in degree by multiplication by x and subsequent inclusion of all terms that are lower order. This process will preserve the equilibrium solution at large times as the term $x^{-1} \to 0$ exponentially as $t \to \infty$. The only terms we can add must be lower order and constant under time evolution, these are a term proportional to the time invariant $x^2 - p^2$ and an additional constant, all other terms will increase the degree of the polynomial or disrupt the equilibrium at large times.

$$F_0(p, x) = c_2 + (x^2 - p^2)c_1 + xc_0 - x(x^2 - p^2) = 0, \tag{4.41}$$

To fix the constants we will examine the physical properties of our disturbed polynomial. If we rearrange for p we have the square root of a cubic over a linear term. As the density must have finite support and be simply connected the cubic must have either one real root and two complex ones or one single root and one double. To calculate the roots of (4.41) we will define the zero to be at a and the divergence to be different from this by an emptiness of δ giving the linear term with the root $-a + \delta$. In order to have a positive density our values of δ are restricted to $0 < \delta < 2a$. The other roots r_1, r_2 can be obtained by considering the large x asymptotics of (3.47)

$$p(x, t) = x - \frac{1}{x} \int \rho(y, t) dy + \dots \tag{4.42}$$

This gives us three equations the remaining roots must satisfy. Specifically there must be no constant term in the expansion, hence

$$-2a + \delta - r_1 - r_2 = 0. \tag{4.43}$$

Equating coefficients of the x^{-1} term tells us that

$$4a^2 + 4a(-2\delta + r_1 + r_2) + 3\delta^2 + 2r_1r_2 + 8 = 2\delta(r_1 + r_2) + r_1^2 + r_2^2. \tag{4.44}$$

The third condition is that the density is normalised. Together these conditions give a double root at $r_1 = r_2 = -a + \delta/2$, with the following relation between a and δ

$$4a^2 - \delta^2 = 8. \tag{4.45}$$

Combining this we have the normalised initial condition

$$p(x) = \frac{(x + a - \frac{\delta}{2})\sqrt{x - a}}{\sqrt{x + a - \delta}}. \tag{4.46}$$

This is the density in a harmonic trap where no particles are in a region of size δ. We can see that when no emptiness is required, $\delta = 0$, the semi circle is recovered. It is discussed in [12] and we restate here that this density is not an equilibrium one. Indeed, although it has a square root zero at one end the other end of the gas has a one over square root singularity. This is the most likely density to observe if, when measured, the gas has no particles in a region of size δ. If we wish to recover the most likely configuration already obtained by Dean and Majumdar we simply write our density in terms of location of divergence s and size of support $L(s)$, given by the relations

$$s = -a + \delta, \tag{4.47}$$

$$L(s) = 2a - \delta. \tag{4.48}$$

To get

$$\rho(x) = \frac{(L + 2x)\sqrt{L + s - x}}{2\pi\sqrt{s - x}}, \tag{4.49}$$

where the right hand end is given by the normalisation

$$L = \frac{2}{3}\left(\sqrt{s^2 + 6} - s\right). \tag{4.50}$$

Returning to our algebraic curve we now know it to be

$$F_0(p, x) = a\left(a - \frac{\delta}{2}\right)^2 + (x^2 - p^2)(\delta - a) + 2x - x(x^2 - p^2) = 0, \tag{4.51}$$

to include time in the equations we shift according to the characteristics (4.36,4.37). Now we have a degree three polynomial in both p and x which can be solved to give the density as a function of time. Double checking the infinite time limit we note that combination $x^2 - p^2$ does not change under time evolution as it is the equilibrium state. While the term $x^{-1} \to 0$ exponentially as $t \to \infty$. This allows the equilibrium solution to be recovered at large times. In terms of our Riemann surface discussed earlier we see that the torus does not actually break apart until time goes to infinity, thus giving us the surprising result that the topology of our solution only changes at infinity. This can be clearly seen by examining the order of the polynomial (4.51) and noting that the change in order is also at this point, an equivalent approach is therefore analysis of the algebraic curve. After taking the infinite time limit we are left with a hyperbola, which due to the initial normalisation condition, has semi major axis $\sqrt{2}$. To find the solution at intermediate times we apply full time evolution to (4.51)

$$F_t(p,x) = (y - 2a)\left(y - \frac{\delta}{2}\right)^2 - (p\cosh t - x\sinh t)^2(y - \delta) = 0, \tag{4.52}$$

where $y = a - p\sinh t + x\cosh t$. This will be our algebraic curve that we shall consider later. We can see that the divergence is removed very quickly as the particles that are clumped up near the left edge rush to fill the emptiness region exponentially fast. This time dependent solution (4.52) is a new result as although the initial condition was already known the dynamics are new here. We now wish to find the edge of the gas at a given time, this can either be done by looking for the locations where the velocity diverges $\partial_p x = 0$ or equivalently by finding the double roots (Fig. 4.6) of this polynomial in p. The edges of the gas, given by points of infinite gradient, are initially at the zero of the hyperbola on the right and the divergence on the left. As time passes the cusp, initially on the left, outside the support of the gas, moves along the hyperbola as the diverging line asymptotes to $y = x$ and will formally vanish at $t \to \infty$. Examining the general case of a cusp we see that it is defined by the square root divergence so

$$p = \frac{C}{\sqrt{\Delta x}}, \tag{4.53}$$

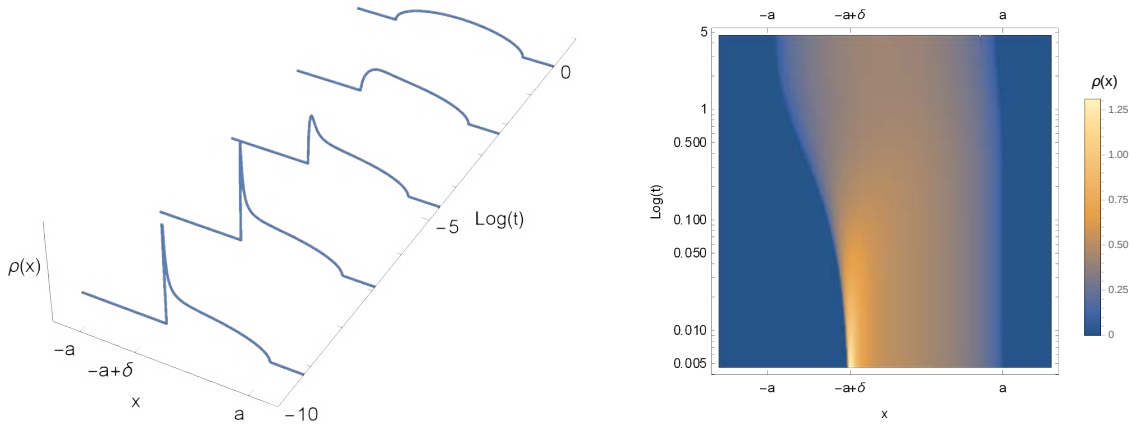

Figure 4.5: Density plots for $\delta = 1$ in logarithmic time with initial divergence at edge of emptiness region healing back to the equilibrium semi circle.

where C is a constant coming from evaluation of the numerator near the square root divergence. To reconnect with our example we see that $\Delta x = x + a - \delta$, as this is linear in x our results for small time evolution $x \to x - pt$ still apply. Rearranging for Δx and applying small time evolution we find

$$\Delta x = \frac{C^2}{p^2} + pt. \tag{4.54}$$

Now we use the condition for double root $\partial_p x = 0$ to find the turning point $p^* = \left(\frac{2C^2}{t}\right)^{\frac{1}{3}}$. Substituting in we finally get the cusp behaviour around the edge at small times as

$$\Delta x(t) = C' t^{\frac{2}{3}}. \tag{4.55}$$

This is the general expected behaviour for a square root singularity and indeed what we find in our specific case. Therefore the most natural variable to use in the vicinity of the edge is the length rescaled by $t^{2/3}$. This power provides a tantalising hint to the connection with the KPZ equation. An interesting topic in itself as the KPZ equation originates from non equilibrium stochastic processes but the Tracy-Widom distribution is found as the probability

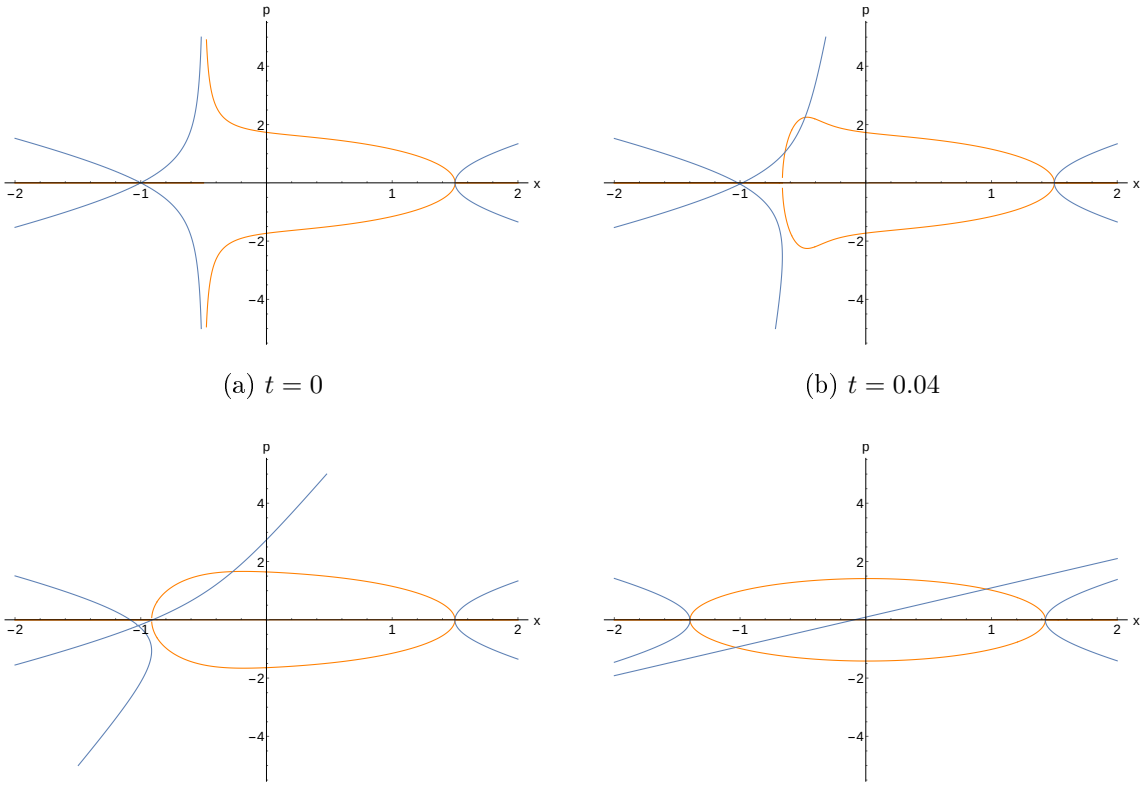

(a) $t = 0$ (b) $t = 0.04$

(c) $t = 0.2$ (d) $t = 3$

Figure 4.6: Contour plots of the polynomial (4.52), with the real part corresponding to velocity in blue and the imaginary part corresponding to density in orange plotted in the (x, p) plane for $\delta = 1$. The density heals to equilibrium and the point of multiplicity in velocity moves towards infinity over time.

distribution of the last particle in a harmonically trapped gas in equilibrium. We can see from the plot that although initially the edge behaves like an astroid it quickly transitions into exponential decay to the long time value of $-\sqrt{2}$.

Here we will discuss another result of this dynamic approach, the classification of the topology on the projective plane. The projective plane is way of visualising the real plane on the surface of a sphere. It is constricted by placing a sphere above the origin of a plane then drawing a line from every point in the plane through the centre of the sphere, in this way

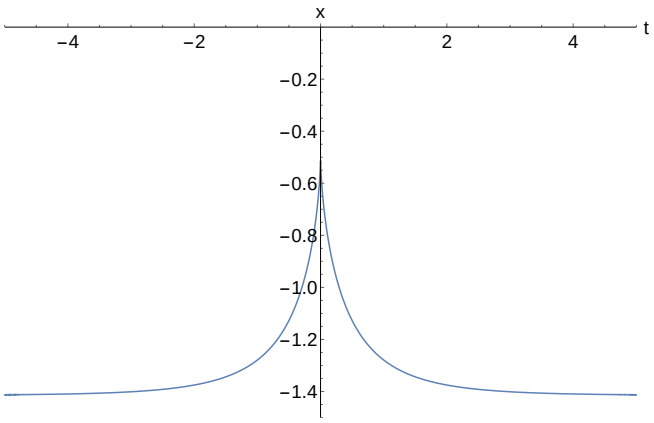

Figure 4.7: Position of edge closest to emptiness region over time for $\delta = 1$ with cusp at initial time.

every point in the plane is mapped to two points on the sphere one in each hemisphere. This process maps infinity onto the equator of the sphere where the two hemispheres join, this allows us to see how the algebraic curves behave at infinity and there associated topology. This is equivalent to the Riemann surface view discussed earlier but in terms of the algebraic curve. The topology of algebraic curve (4.52) can be seen clearly in the projective plane (Fig. 4.8). We can see that initially there is one loop in the projective plane and as time evolves this transitions to the equilibrium hyperbola joined by a line at a point that gets closer and closer to infinity as time progresses. Classification of the initial curve is traditionally done via two numbers. The degree of the polynomial, in our case 3 is related to the genus by Riemann–Hurwitz formula giving a genus of 1, and the multiplicity of the points in the plane. We can see that the cusp/crossing feature will only appear if the two branches of p meet at a point; mathematically this is $(x - r_1)(x - r_2)(x - r_3) = 0$. In our case two of the roots are the same real root (multiplicity 2) and the other is real but distinct. These correspond to the crossing feature in figure 4.6 and the square root zero respectively. To see what this means in terms of our polynomial $F(p, x)$ we consider the discriminant of F_0 with respect to p given by $\text{dis}(F_0, p) = 4(x - c_0)(x - r_1)(x - r_2)(x - r_3)$. As we know that two of these roots are the same if the crossing feature exists then $\text{dis}(\text{dis}(F_0, p), x) = 0$ is the condition for a

crossing point of multiplicity greater than one in the projective plane. As can be seen from figure 4.8 the crossing persists at all finite times and after tedious algebra it can be shown that $\mathrm{dis}(\mathrm{dis}(F_t, p), x) = 0$. It is only in the $t \to \infty$ limit that the joining line is removed, this condition breaks and the change in topology occurs.

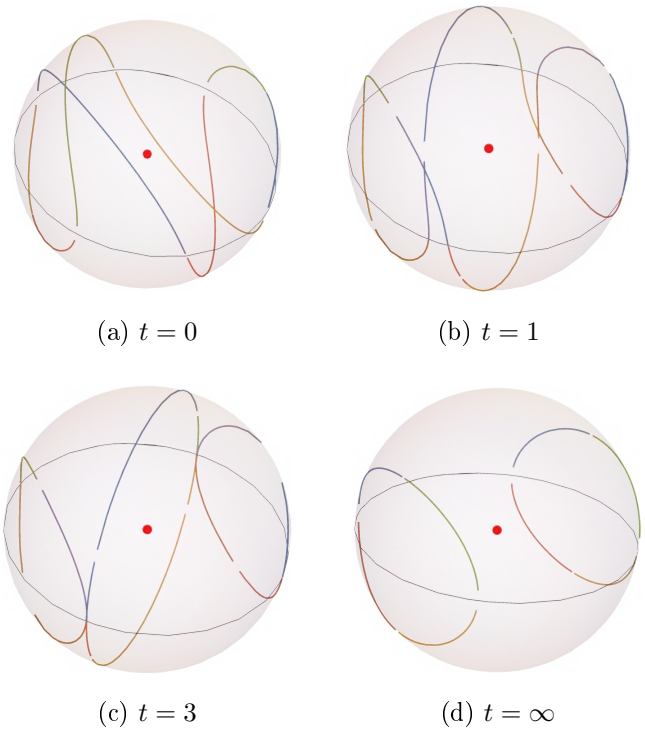

(a) $t = 0$ (b) $t = 1$

(c) $t = 3$ (d) $t = \infty$

Figure 4.8: Real part of algebraic curve (4.52) corresponding to velocity plotted in the projective plane for $\delta = 1$, with movement of the crossing point towards infinity and the different branches shown in different colours.

The final part of the analysis of a dynamic single emptiness configuration is to recover the left tail asymptotics of the Tracy-Widom distribution. To do this we evaluate the action on the solution to the equations of motion. There are several methods to do this; the first is to perform the calculation in real space and the second is to take inspiration from our complex contour formulations and perform the calculation in the complex plane. A third method from [32] is to consider the area of the Space-Time disturbance which we will cover

later. For the first method we start with the action

$$S = N^2 \int dt \int dx \left(\phi \partial_t \rho + \frac{\rho}{2} \left(\frac{\pi^2}{3} \rho^2 + (\omega x)^2 - (\partial_x \phi)^2 \right) \right). \tag{4.56}$$

As we will be considering the limit of small emptiness ($\delta \to 0$) we follow ideas by Abanov [32] and differentiate the action with respect to δ.

$$\frac{\partial S}{\partial \delta} = N^2 \int dt \int dx \left(\frac{\partial \rho}{\partial \delta} \left(-\partial_t \phi - \frac{(\partial_x \phi)^2}{2} + \frac{\pi^2 \rho^2}{2} + \frac{\omega^2 x^2}{2} \right) + \frac{\partial \phi}{\partial \delta} \left(\partial_t \rho + \partial_x (\rho v) \right) \right) - \int dt \frac{\partial \phi}{\partial \delta} \partial_x \phi \rho |_{x=-\infty}^{x=\infty} - \int dx \frac{\partial \rho}{\partial \delta} \phi |_{t=-\infty}^{t=0}. \tag{4.57}$$

Appling the equations of motion only the boundary terms from integration by parts remain. One of these evaluates the density at $x = \pm\infty$ which due to the finite support of the density is also zero. Therefore we are left with

$$\frac{\partial S}{\partial \delta} = - \int dx \frac{\partial \rho}{\partial \delta} \phi |_{t=-\infty}^{t=0}. \tag{4.58}$$

As the density at $t = -\infty$ is the Wigner semi circle only one limit depends on δ. Integrating the Hilbert transform identity we can write ϕ in terms of ρ

$$\phi = \frac{\omega^2 x^2}{2} - \int \rho(x') \ln |x - x'| dx'. \tag{4.59}$$

therefore the action is

$$\frac{\partial S}{\partial \delta} = \int \frac{\omega^2 x^2}{2} \frac{\partial \rho(x)}{\partial \delta} dx - \int \rho(x') \frac{\partial \rho(x)}{\partial \delta} \ln |x - x'| dx dx', \tag{4.60}$$

the same as Dean and Majumdar's action [12]. If we separate the contribution from the potential form our effective velocity we find

$$S = \int \frac{x^2}{2} \rho(x) dx - \int \phi \rho dx, \tag{4.61}$$

We now observe that on the support of the density the field ϕ is a constant and as ρ is normalized all we need is the value of that constant, given by the integral of the velocity between $-\infty$ and $-a+\delta$. This integral does not converge but luckily we are only interested in

the derivative with respect to δ and so can remove divergences that contain no δ dependence, we find

$$\frac{\partial}{\partial\delta}\int_{-\infty}^{-a+\delta}\left(v-x+\frac{1}{x}\right)dx-\frac{\partial(-a+\delta)}{\partial\delta}\left(-x+\frac{1}{x}\right)|_{-a+\delta}=\frac{\partial}{\partial\delta}\int_{-\infty}^{-a+\delta}vdx, \tag{4.62}$$

where the integrals can now be evaluated in Mathematica to get

$$\frac{\partial S}{\partial\delta}\approx\frac{\delta^2}{\sqrt{2}} \tag{4.63}$$

The second method is to express the action in terms of complex fields to show the close relation to the algebraic curves discussed above. In these complex fields $p=v+i\pi\rho$ and $\partial_x\chi=p$ we have the action previously calculated (4.40) where Stokes theorem has been used to obtain the area integral. The Dean and Majumdar action corresponds to the integrand on the real axis. In accordance with the electrostatic analogy in section 3.5.

$$S=\int dx\,\frac{x^2}{2}\rho_0(x)+\int d^2z\partial_{\bar{z}}\bar{\chi}\partial_z\chi=\int dx\,\frac{x^2}{2}\rho_0(x)+\oint dz\bar{\chi}\partial_z\chi. \tag{4.64}$$

We apply integration by parts requiring that the boundary term vanishes as in previous sections. The potential term is easy to evaluate and on the solution gives.

$$\int dx\,\frac{x^2}{2}\rho_0(x)=\frac{1}{32}\left(-3\delta^4+3\delta^3\sqrt{\delta^2+8}-8\delta^2+8\right). \tag{4.65}$$

For the other term we may then deform the contour out to ∞ and expand there, using the fact that the complex integral of z^n around the origin is only non zero for $n=-1$ we get the contribution

$$\oint dz\bar{\chi}\partial_z\chi=\frac{1}{8}\left(2\delta^2-\delta\sqrt{\delta^2+8}-8\ln\left(\sqrt{\delta^2+8}-\delta\right)+4\right). \tag{4.66}$$

Adding together and expanding for small δ we find that the action on our solution is given by

$$S\approx\frac{3}{4}-\frac{3\ln(2)}{2}+\frac{\delta^3}{3\sqrt{2}}. \tag{4.67}$$

As in Dean and Majumdar's paper for the GUE [12] this is proof of the third order phase transition.

4.3.3 Double Emptiness

Previously we have considered the case of a single emptiness region by allowing the minimal disturbance to our equilibrium algebraic curve. Therefore, in order to consider more complex situations we will look at the next order adjustments which come from multiplying our equilibrium solution by x^2 and including all lower order terms such that $t \to \infty$ returns us to equilibrium.

$$F_0(x,p) = x^2(x^2-p^2) + x^2c_0 + xc_1 + c_2 + x(x^2-p^2)c_3 + (x^2-p^2)c_4 = 0, \tag{4.68}$$

When rearranged this will give us a density squared with a quartic term over a quadratic term, so in total we have six roots to find. This opens up many possible solutions. The one we will consider here is that of an emptiness region on each side of the gas, called double emptiness. This gives us the starting conditions of the quadratic roots at $-a+\delta_1$ and $a-\delta_2$ enforcing an emptiness region of size δ_1 on the left of the gas and an emptiness region of size δ_2 on the right of the gas. The condition $0 < \delta_1, \delta_2 < a$ must hold to ensure the density does not become negative. Additionally we need that the gas has simply connected finite support, in order for this to happen the quartic cannot change sign so two sets of double roots are required. Complex roots would also have this property but would generate extra regions of density that we don't want. To find the double roots r_1, r_2 we follow the same procedure as the single emptiness case and enforce that the large x asymptomatics are as follows

$$p(x,t) = x - \frac{1}{x}\int \rho(y,t)dy + \dots. \tag{4.69}$$

By equating the constant term we get the condition

$$\delta_1 - \delta_2 - 2r_1 - 2r_2 = 0, \tag{4.70}$$

and from the x^{-1} term

$$4a^2 + 3\delta_1^2 + 3\delta_2^2 + 4\delta_2 r_1 + 4\delta_2 r_2 + 8r_1 r_2 = 4a(\delta_1+\delta_2) + 2\delta_1(\delta_2 + 2(r_1+r_2)) + 8. \tag{4.71}$$

From these the double roots can be found to be

$$r_{1,2} = \frac{1}{4}\left(\delta_1 - \delta_2 \pm \sqrt{8a^2 - 8a\delta_1 - 8a\delta_2 + 3\delta_1^2 + 2\delta_1\delta_2 + 3\delta_2^2 + 16}\right). \tag{4.72}$$

With this and some algebra our double emptiness is given by

$$p(x) = \frac{-2(\delta_1 - a)(a - \delta_2) + (\delta_1 - a)^2 + (a - \delta_2)^2 + 4x(\delta_1 - \delta_2) - 8x^2 + 8}{8\sqrt{(a - \delta_1 + x)(-a + \delta_2 + x)}}. \tag{4.73}$$

When $\delta_1 = \delta_2 = 0$ the semi circle should be obtained, to achieve this we must fix $a = \sqrt{2}$. The lack of choice in a stems from the fact that the gas in completely confined by the two emptiness regions and has nowhere to move too. Setting this value for a also ensures that the initial density is normalised as long as the condition $0 < \delta_1, \delta_2 < a$ is respected. As before this density is the critical density for an emptiness on either side of the gas, this was shown in [12]. To see what we have here is equivalent it is enough to change variables from the size of the emptiness to its location, given by the relations

$$s_1 = -a + \delta_1, \tag{4.74}$$

$$s_2 = a - \delta_2. \tag{4.75}$$

This recovers

$$\rho(x) = \frac{4x(s_2 - s_1) - 8x(x - s_1) + (s_2 - s_1)^2 + 8}{8\pi\sqrt{(x - s_1)(s_2 - x)}}. \tag{4.76}$$

Unlike in [12] we can now investigate the dynamics of our solution via the time evolution according to the equations of motion.

$$x \to x\cosh\omega t - p\frac{\sinh\omega t}{\omega}, \tag{4.77}$$

$$p \to p\cosh\omega t - x\omega\sinh\omega t. \tag{4.78}$$

With $\omega = 1$ we see from figure 4.9 that the behaviour is very similar to that of a single emptiness region but on both sides of the gas. The divergences at the start of the emptiness region quickly smooth over as the gas rushes to fill the emptiness, this happens very fast so is plotted on logarithmic time. We can see that as before the crossing point of multiplicity 2 in

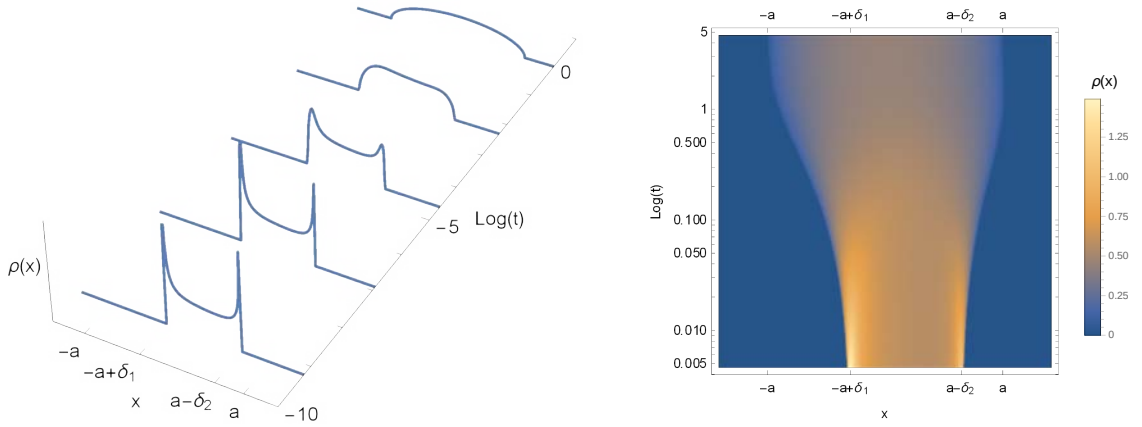

Figure 4.9: Density plots of double emptiness configuration for $a = \sqrt{2}, \delta_1 = 1, \delta_2 = 0.5$ in logarithmic time with initial divergence at both edges of the gas healing back to the equilibrium semi circle.

the velocity curve moves towards infinity along the negative velocity branch on the left hand side (Fig. 4.10). The corresponding multiplicity point on the right hand side moves towards the same infinity in the positive velocity branch. The fact that this is indeed the same infinity can be seen better in the projective plane plots (Fig. 4.12). To find the behaviour at long times we rearrange (4.73) to get

$$\begin{aligned} x^2 - p^2 + \frac{(\delta_2 - \delta_1)(x^2 - p^2)}{x} + \frac{p^2}{x^2}(a - \delta_1)(a - \delta_2) \\ = -\frac{(4a^2 - 4a(\delta_1 + \delta_2) + \delta_1^2 + 2\delta_1\delta_2 + \delta_2^2 + 8)^2}{64x^2} \\ - \frac{(\delta_1 - \delta_2)^2}{4} - \frac{4a^2 - 4a(\delta_1 + \delta_2) + \delta_1^2 + 2\delta_1\delta_2 + \delta_2^2 + 8}{8x}(\delta_1 - \delta_2) \\ + \frac{4a^2 - 4a(\delta_1 + \delta_2) + \delta_1^2 + 2\delta_1\delta_2 + \delta_2^2 + 8}{4}. \end{aligned} \tag{4.79}$$

In the limit $t \to \infty$ the combination $x^2 - p^2$ is unchanged and the combinations $x^{-1}, x^{-2} \to 0$ and $p^2 x^{-2} \to 1$ gives us

$$x^2 - p^2 = 2. \tag{4.80}$$

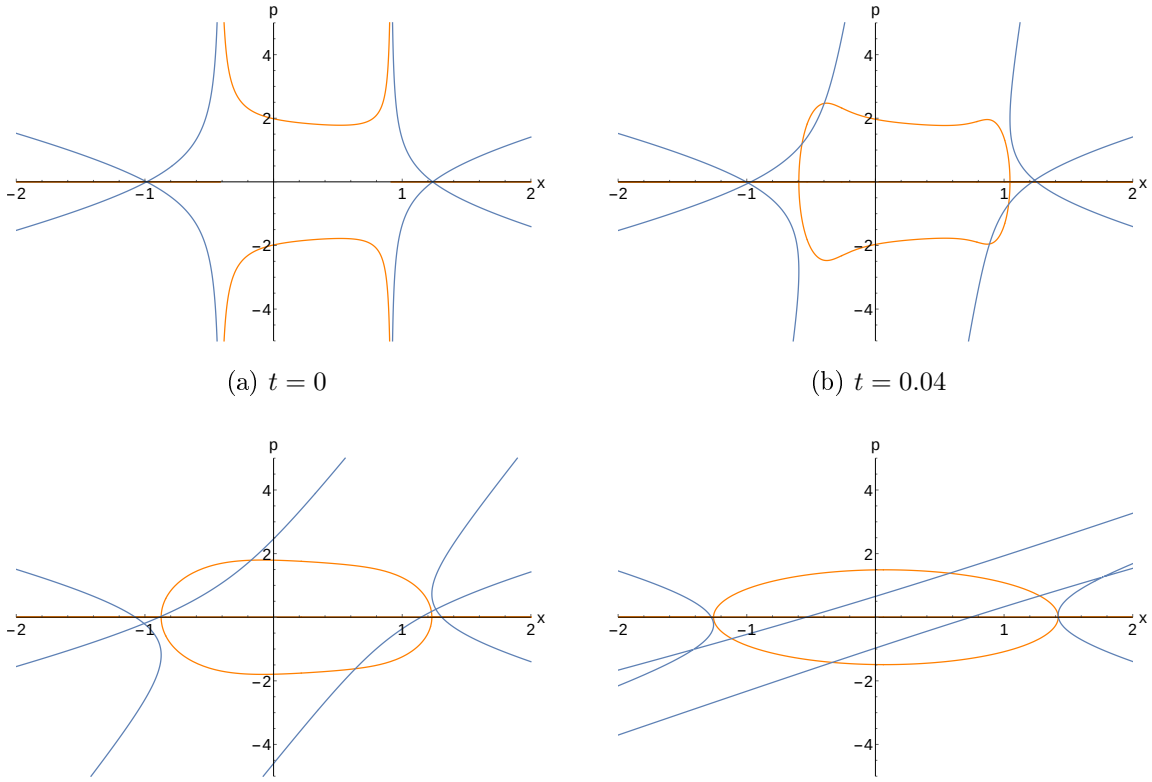

(a) $t = 0$ (b) $t = 0.04$

(c) $t = 0.2$ (d) $t = 0.9$

Figure 4.10: Contour plots of the polynomial (4.73) over time, with the real part corresponding to velocity in blue and the imaginary part corresponding to density in orange plotted in the (x, p) plane for $a = \sqrt{2}, \delta_1 = 1, \delta_2 = 0.5$. The density heals to equilibrium and the points of multiplicity in velocity move towards separate infinities over time.

Which is a hyperbola. The location of the edge point over time also follows a similar path to the single emptiness case. We can see from figure 4.11 that the edge points on both sides will initially move fast and over long time return to the equilibrium hyperbola. The analysis that we performed on the single emptiness to show the presence of KPZ scaling will still hold here due to the divergence still being caused by a one over square root singularity.

Finally, we examine the algebraic curve for a double emptiness configuration in the projective plane (Fig. 4.12). As we now have a polynomial of fourth order by the Rie-

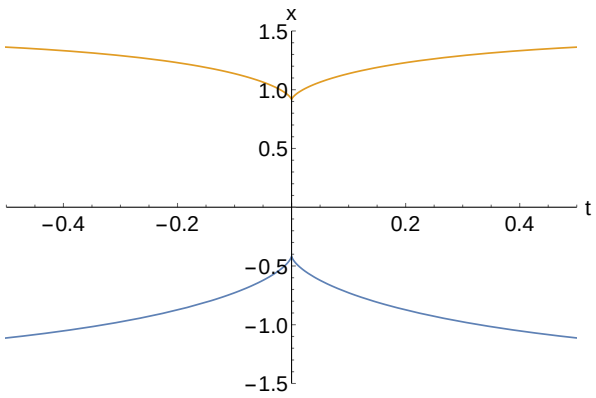

Figure 4.11: Position of right edge in orange and left edge in blue over time for $a = \sqrt{2}, \delta_1 = 1, \delta_2 = 0.5$ both with cusps at initial time.

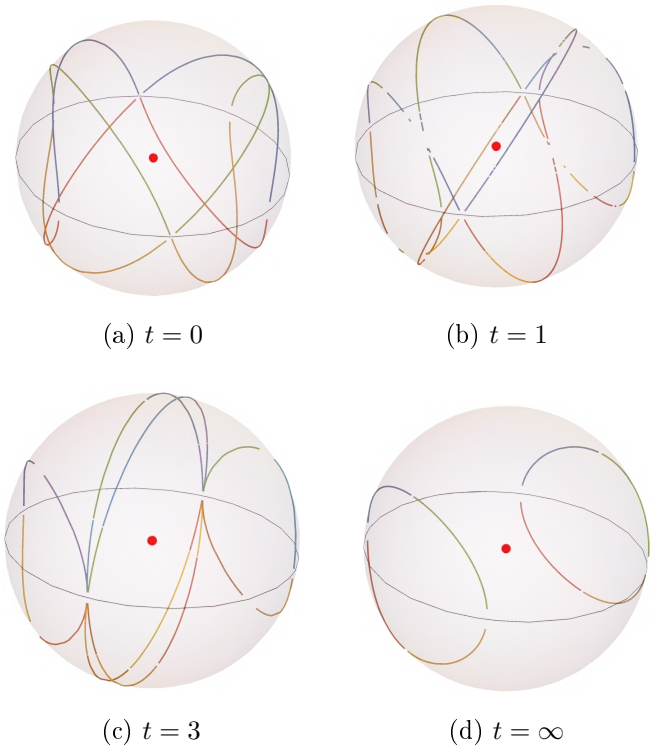

(a) $t = 0$ (b) $t = 1$

(c) $t = 3$ (d) $t = \infty$

Figure 4.12: Real part of algebraic curve (4.73) corresponding to velocity plotted in the projective plane for $a = \sqrt{2}, \delta_1 = 1, \delta_2 = 0.5$, with movement of the crossing points towards infinity and the different branches plotted in different colours.

mann–Hurwitz formula the genus of our curve is 3. We also note the continued existence of points of multiplicity 2. For this configuration we have two of them that persist over time moving towards each other. For any finite time this topology is conserved but at infinite time we see that the points of multiplicity 2 merge and the degree of the polynomial drops back down to equilibrium.

4.3.4 Emptiness Inside

To obtain a double emptiness solution in the last section we used the algebraic curve

$$F_0(x,p) = x^2(x^2-p^2) + x^2c_0 + xc_1 + c_2 + x(x^2-p^2)c_3 + (x^2-p^2)c_4 = 0. \tag{4.81}$$

This gave a squared density of a quartic over a quadratic. The choice was then made to look for double emptiness, but we noted that other solutions were possible. In this section we will consider an alternative solution. This is where the quadratic roots are inside two of the quartic roots. Physically this means that our density is no longer simply connected as it has an emptiness in the middle. In terms of polynomial roots we have the quadratic roots at δ_R and $-\delta_L$ giving an emptiness region of length $\delta_R + \delta_L$ that covers the origin. We then have outside edges of the gas at two of the quartic roots one of which we shall define as a and the other root, r_1, will be left to find. The conditions so far are $0 < \delta_R < a$ and $r_1 < -\delta_L < 0$. Finally in order to not disturb the density we have constructed the remaining two roots from the quartic which will be made a double root r_2. Again the way to find our remaining roots will be asymptotic comparison to

$$p(x,t) = x - \frac{1}{x}\int \rho(y,t)dy + \dots. \tag{4.82}$$

The conditions are very similar to the double emptiness case. From equating the constant term we have

$$-a + \delta_R - \delta_L - 2r_2 - r_1 = 0, \tag{4.83}$$

and the x^{-1} term gives

$$-a^2+2a(-\delta_R+\delta_L+2r_2+r_1)+3\delta_R^2-2\delta_R(\delta_L+2r_2+r_1)+(\delta_L+r_1)(3\delta_L+4r_2-r_1)=8. \quad (4.84)$$

A solution to these conditions is that the single root is $r_1 = -a$ and the double root is $r_2 = (\delta_R - \delta_L)/2$, along with the normalisation condition

$$4a^2 - (\delta_L + \delta_R)^2 = 8. \quad (4.85)$$

Putting all this together gives the form of an initial condition for emptiness inside the gas

$$p(x) = \left(x + \frac{\delta_L - \delta_R}{2}\right)\sqrt{\frac{(x^2 - a^2)}{(x - \delta_R)(\delta_L + x)}}, \quad (4.86)$$

where δ_L, δ_R is the size of the emptiness to the left or right of the origin respectively. Requiring the condition $0 < \delta_L, \delta_R < a$. Squaring both sides we get

$$p^2(x - \delta_R)(\delta_L + x) = \left(x - \frac{\delta_R - \delta_L}{2}\right)^2 (x^2 - a^2). \quad (4.87)$$

We can then evolve in time according to

$$x \to x\cosh\omega t - p\frac{\sinh\omega t}{\omega}, \quad (4.88)$$

$$p \to p\cosh\omega t - x\omega\sinh\omega t. \quad (4.89)$$

With $\omega = 1$ we can again examine the dynamics of the emptiness solution (Fig. 4.13). With an emptiness region inside the gas we see that the divergences are again present but this time inside the gas. This gives the standard square root singularities at the outer edges, although they are shifted outwards from the standard equilibrium position by a small amount dependent on the width of the internal emptiness region. Like the other cases we have considered the gas returns to equilibrium very fast so we have plotted densities in logarithmic time. On plotting the evolution in the (x, p) plane (Fig. 4.14) we see that a point of multiplicity 2 exists in the middle of the emptiness region. Unlike the cases with emptiness near the edge this point does not move over time and remains even after the density has healed. To find the behaviour at long times we rearrange (4.87) to get

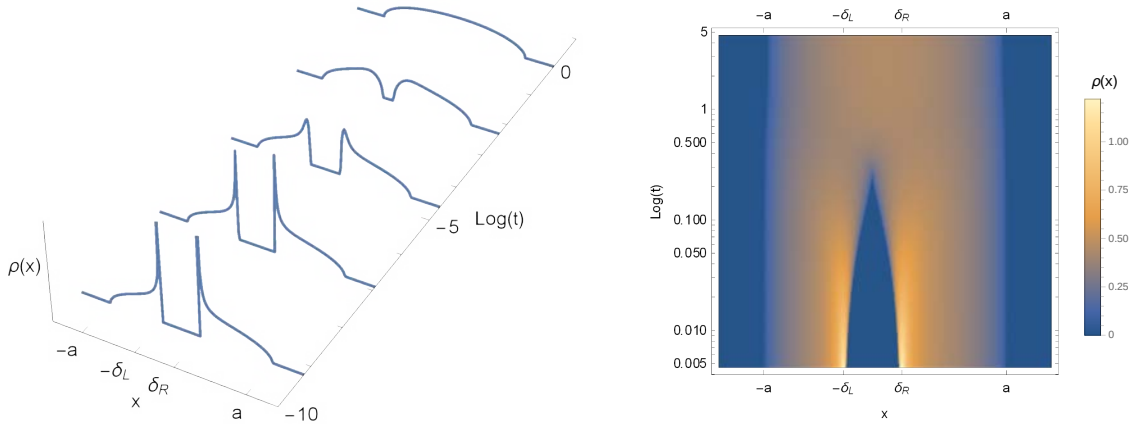

Figure 4.13: Density plots of the emptiness inside configuration for $\delta_L = 0.5, \delta_R = 0.2$ in logarithmic time with initial divergence at both edges of the emptiness region healing back to the equilibrium semi circle.

$$x^2 - p^2 + \frac{(\delta_L - \delta_R)(x^2 - p^2)}{x} = \delta_L \delta_R \left(1 - \frac{p^2}{x^2}\right) - \frac{(\delta_L + \delta_R)^2}{4} + a^2 + \frac{a^2(\delta_L - \delta_R)}{x} + \frac{a^2(\delta_L - \delta_R)^2}{4x^2}. \quad (4.90)$$

In the limit $t \to \infty$ the combination $x^2 - p^2$ is unchanged and the combinations $x^{-1}, x^{-2} \to 0$ and $p^2 x^{-2} \to 1$ gives us

$$x^2 - p^2 = a^2 - \frac{(\delta_L + \delta_R)^2}{4}. \quad (4.91)$$

Which is a hyperbola. Considering the location of the edge of the emptiness region over time we can see the area of disturbance in space-time caused by the emptiness (Fig. 4.15). Again due to the one over square root divergence exhibited near the emptiness the same KPZ scaling that was found in the single emptiness case still holds. We do however see the region shrink and disappear as the gas heals giving a very similar shape to the astroid found by Abanov [32] for the unconfined case. This is understandable as our emptiness is near the centre of the system where the trap is weak and an unconfined system is a good

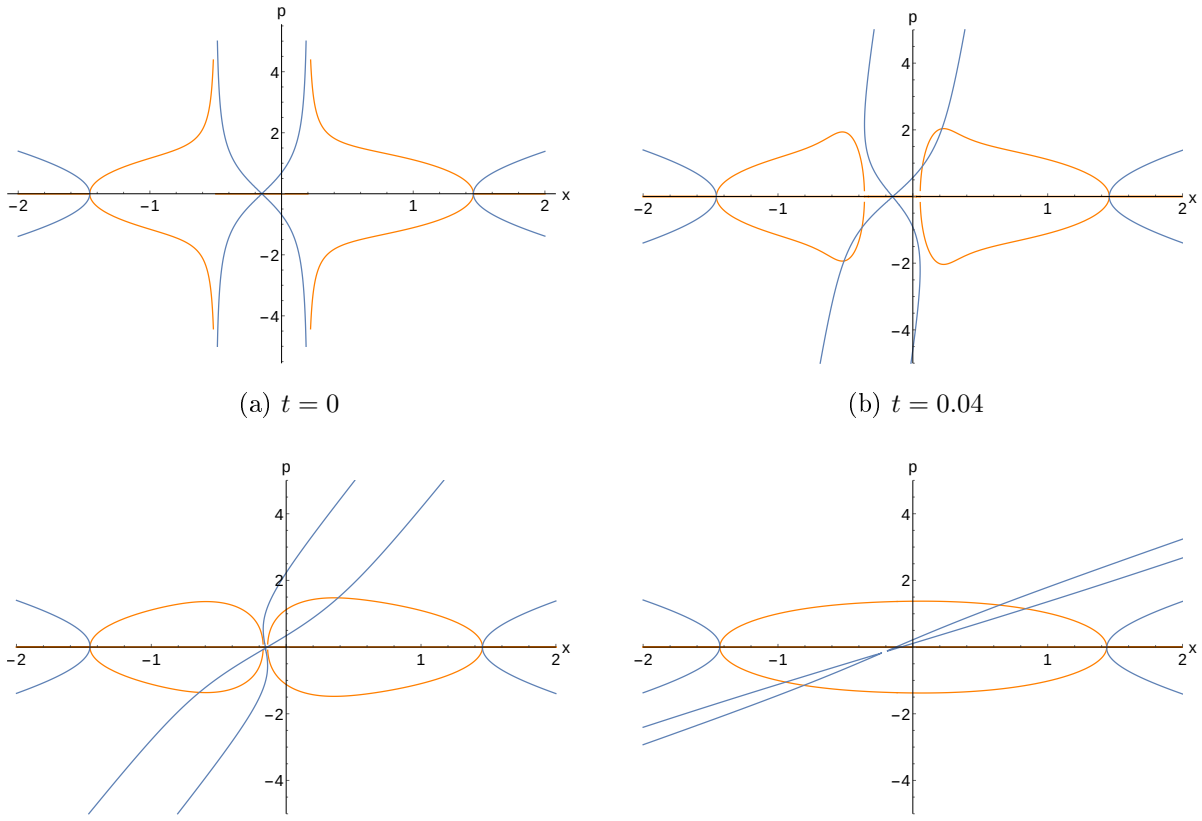

(a) $t = 0$ (b) $t = 0.04$

(c) $t = 0.2$ (d) $t = 0.9$

Figure 4.14: Contour plots of the polynomial (4.87) over time, with the real part corresponding to velocity in blue and the imaginary part corresponding to density in orange plotted in the (x, p) plane for $\delta_L = 0.5, \delta_R = 0.2$. The density heals to equilibrium and the point of multiplicity in velocity remains fixed at its initial location.

approximation.

Finally we can consider the topology in the projective plane (Fig. 4.16). Like the double emptiness case we have a polynomial of degree four giving a genus of 3. Only one point of multiplicity greater than one exists and as discussed before is at the midpoint of the emptiness region. In contrast to the previous two cases the projective plane shows a slightly distorted equilibrium configuration of the hyperbola with a disconnected double band round the middle corresponding to the emptiness. We might expect the band in the

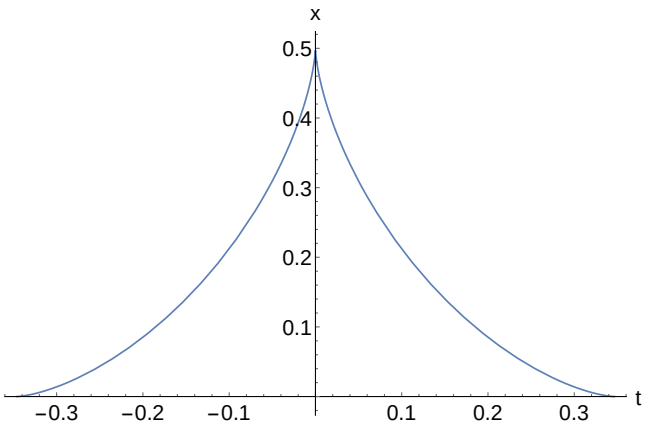

Figure 4.15: Position of right side of emptiness for emptiness inside configuration over time for $\delta_L = \delta_R = 0.5$ with removal of emptiness region over time and initial cusp.

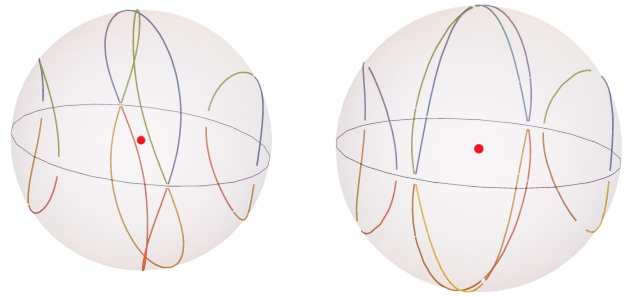

(a) $t = 0$

(b) $t = 1$

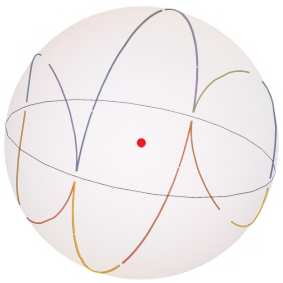

(c) $t = 3$

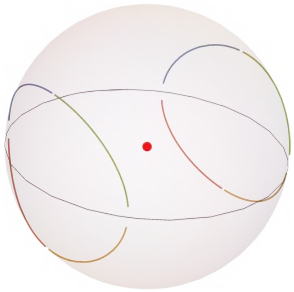

(d) $t = \infty$

Figure 4.16: Real part of algebraic curve (4.87) corresponding to velocity plotted in the projective plane for $\delta_L = 0.5, \delta_R = 0.2$, the crossing point remains stationary and the different branches are plotted in different colours.

middle to shrink and disappear in the infinite time limit as the previous two cases did. This does happen but the middle band also moves to connect the equilibrium hyperbola, showing much more similarity to the other cases than expected.

4.3.5 Space-Time Disturbance

It has been argued in a paper by Abanov [32] that the area of space time disturbed is proportional to the logarithm of the probability of observing that state in the first place. As in our case the equilibrium condition is a line at $x = -\sqrt{2}$ we can look at the area enclosed by (Fig. 4.7) and that line. The other adjustment necessary can be seen from an assumption used in [32] "the extra cost in action of having [emptiness] is constant per unit space–time area." This was true in the case of the XXZ spin chain but grossly violated in our harmonically trapped system. Therefore, we must find the extra cost in action of our emptiness occurring at different points in space-time. It can easily be argued that time will not effect this as all of our calculations can be translated in time without any change to the solutions. The space dependence is much more significant since creating an emptiness region outside the support of the equilibrium configuration has no energy cost at all but an emptiness region at the centre of the trap has high cost. On the equations of motion the action becomes

$$S = \int d\tau \int dx \frac{\pi^2}{3} \rho_c(x,t)^3. \tag{4.92}$$

We can see from this that we must weight our space time area by the equilibrium density cubed. Here we will consider this method of calculation for the space-time disturbance caused by a single emptiness region (Fig. 4.7). Although an analytical expression for $x(t)$ exists for all t it is far to large to fit on a page and resists integration attempts, we therefore present a numerical calculation of the weighted area along with a fitting to the function $c(a-\delta+\sqrt{2})^3$ of the same form as the expected result from [12] where c is a fitting parameter

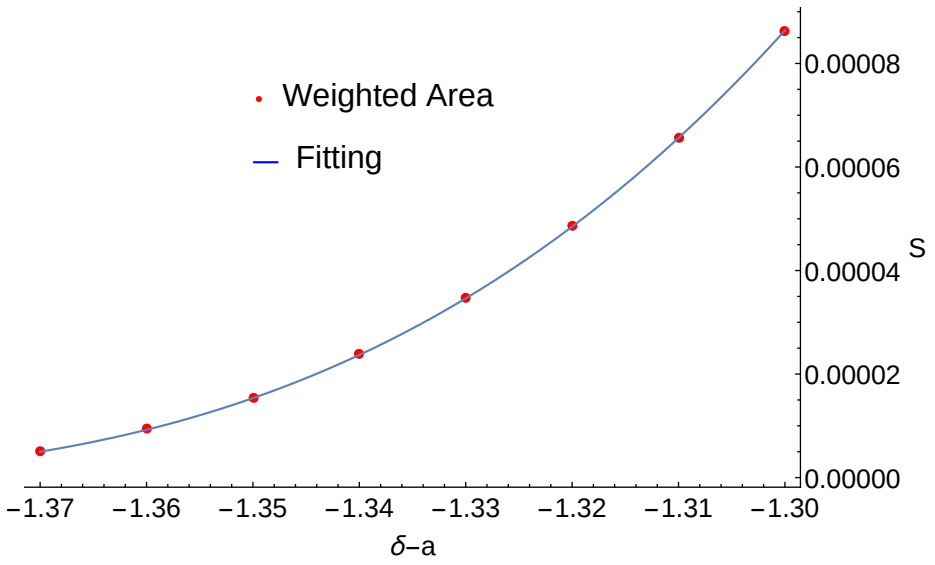

Figure 4.17: Weighted area in space-time from numerical calculations with good agreement to expected form of Tracy-Widom asymptotic behaviour as a function of the hard wall location.

4.3.6 Dynamic Emptiness Summary

In conclusion we have shown how to analyse the third order phase transition from the GUE eigenvalues using a hydrodynamic method. We showed how, on the separatrix condition, the complex plane could be used to both form an appropriate description of emptiness but also to evaluate the action. From this we have seen how single, double and emptiness inside configurations can be constructed from the algebraic curves as well as subsequent time evolution. This provides new incites into the dynamics of the density with emptiness initial conditions. From the area of space time disturbed hints at a connection with KPZ hierarchy were provided. Plots of these curves in the projective plane gave an interpretation of the transition using the topology of algebraic curves. We note that following our method algebraic curves can be used to find other more complicated emptiness configurations. Looking to future work, it would be interesting to see whether other orders of phase transitions can be classified using the same algebraic curve method that we have presented here. We also stopped slightly short of a topological classification of emptiness configurations which

it would be nice to complete. Finally it would be interesting to see if the two main parts of this chapter can be combined, specifically to see if a KPZ like surface can grow into an emptiness configuration and with what probability.

Conclusion

In this thesis we have examined emptiness formation probability in a one dimensional harmonically trapped gas. In doing so new and interesting questions have been discovered and possible solutions discussed. Many techniques have been used both those that are traditional in this field of research as well as novel uses of lesser known approaches.

In the first chapter we covered the background techniques that underpin this area of theory, although well known it is both interesting and allows the thesis to be a more complete presentation. First we covered the Lieb-Liniger model, starting in the homogenous case we added a confining harmonic potential and showed how to calculate ground state quantities in the limits of strong and weak interaction strength. Further, we then covered how to use Bethe ansatz to examine the region of arbitrary interaction showing the equations that can be solved to obtain relevant quantities in this regime. The experimental viability of this model was also covered and some brief discussion of the techniques used in practice. Then we moved onto random matrix theory, initially an unconnected topic, we showed how it can be used as an equivalent description of free fermions. Moving onto show how observable quantities are calculated in this formalism we compared the densities obtained from the random matrix theory and Lieb-Liniger approach. It was then clear that for all its machinery random matrix theory could not be used to describe any other interaction regime of Lieb-Liniger other than that of free fermions. For the final part of the background

chapter we covered hydrodynamics, how it can be used in the weakly interacting regime and how, when combined with the Bethe ansatz from earlier in the chapter, it could be used for arbitrary interaction.

The second chapter began with the original motivation behind this project, the question of last particle distributions. We showed the original way of calculating this distribution in the fermionic case by using random matrix theory. The solution being that of the Tracy-Widom distribution and, combining techniques from the section on hydrodynamics, we showed a lesser known distribution of Tracy-Widom after a trap quench. The question of how interaction strength would effect the edge distribution was then formulated. To tackle this a hydrodynamic approach was used giving the first new result in this thesis of the edge distribution of a weakly interacting gas, in the appropriate scaled variables. From this result we saw that the asymptotics of the left tail from the edge distribution are highly dependent on interaction but the right tail is to first order only affected by the confining potential. As an alternative to analytics we showed some numerical methods for calculating the Tracy-Widom distribution. In particular we looked at numerical random matrix theory calculations and DMRG, showing that both can be used to find the edge distribution in this case. To end the chapter we again discussed the difficultly of the arbitrary interaction case suggesting that a hydrodynamic action for our system would give us the best chance of success.

Motivated by the previous chapter we proceed to reformulate our system as a one dimensional log gas. What followed was probably the most important calculation in the thesis. We showed that the log gas action is the boundary term for a time dependent hydrodynamic action evaluated on the separatrix condition, furthermore this was shown by using a stochastic approach and averaging out the noise. Several important points were then noted about this description. First we had achieved the desired result from the last chapter, a hydrodynamic action that when combined with the Bethe ansatz and some good numerics could, in principle, be used to describe emptiness for arbitrary interaction. Second, in this

new formalism we had time dependence so dynamic solutions were now able to be studied. Finally we found a glimpse of a connection between the equilibrium fermionic system in which Tracy-Widom is known to be found and the non-equilibrium stochastic systems where it also appears. These last two points would be the focus for our final chapter. But first we explored other interesting links that existed between this new description and other areas of physics. We considered the interpretation of our system as charges and showed how the harmonic trap could be thought of as a specific distribution of extra charges. Additionally emptiness on a circular system was considered and we showed its links to the CUE and angular variables. We also showed how another one dimensional system, Calogaro Sutherland, was more applicable to random matrix theory than Lieb-Liniger and we used the hydrodynamic action to write an action for any beta in the random matrix ensemble.

Entering the final chapter we now had the techniques we needed and some new questions to answer. Firstly we were inspired by the noise averaging to get hydrodynamics from the previous chapter so employed this in reverse with the aim of making contact with the KPZ equation. This we achieved using a density shift and a hodograph transform, which gave the rather nice connection to the non linear Luttinger liquid. With this result an analytical path can be traced right from the initial random matrix distribution to the KPZ equation and associated hierarchy. Therefore answering the question of why the Tracy-Widom distribution shows up in these two vastly different areas. As a nice aside we showed how our action could be written in the complex plane and the aforementioned density shift was just a gauge transform, this proved to be important for the final part of the chapter. The second and final question to be addressed from the previous chapter was that of dynamic emptiness. This initially seemed simple as our hydrodynamic action and corresponding equations of motion could easily be used to calculate dynamics. However when we looked deeper with our ideas of a complex contour action from before led us to find a new description of the dynamics using complex algebraic curves. This in turn gave descriptions of these dynamics

by using the topology of the Riemann surface. We used this fruitful description to examine some cases of emptiness.

We end this thesis with a discussion of future directions for work in this area. This is a combination of work that we attempted but could not get reasonable results from, work that we did not get time to do and new ideas we have from looking back on the work presented in this thesis. From our hydrodynamic action and Bethe ansatz we have presented a procedure to find dynamics of emptiness and asymptomatics of the last particle distribution left tail. The first piece of future work would be to carry out this procedure, it would not be a trivial task, but it would answer the question of how last particle distributions behave under a change in interaction strength. With the extreme limits already calculated in this thesis an interesting question would be how the distribution changes between the two, is it a smooth change or does it exhibit a sharp transition somewhere? A possible way to do this would be using the hodograph transform from the last chapter but it may be a problem that is only numerically tractable.

Another direction of work would be to consider the effect of dimensionality on the edge distribution. For example particles in two dimensions with a spherically symmetric trapping potential. In random matrix theory there is a mapping between the Ginebre unitary ensemble and fermions in two dimensions [52], there also exists work on describing two dimensional surface growth using interior and exterior harmonic moments [53] that we expect to be linked. It would be interesting to see what effect dimensionality has upon the last particle distribution. The work on stochastic surfaces was only done for the specific case of the Gaussian unitary ensemble while the hydrodynamic action is available for a wider range of ensembles so it would be interesting to explore the technique we showed in a wider range of cases. Finally it more can defiantly be done in the realm of emptiness dynamics where a topological classification of emptiness configurations could be investigated as well as the harder challenge of combining with stochastic growth to consider the probability of these

configurations arising in that formalism.

Appendix A

Chapter One Appendix

A.1 Thomas Fermi Approximation

To justify the Thomas Fermi approximation we look at relative sizes of the kinetic and potential energy density's from the second quantised version of the Lieb-Liniger Hamiltonian (1.8). On substituting in our ground state density (1.5) we have

$$E_{kin} = \frac{\mu}{2mg}\left[\frac{1}{R^2} + \frac{x^2}{R^4\sqrt{1-\frac{x^2}{R^2}}}\right],$$
$$E_{pot} = \frac{\mu^2}{g}\left(1-\frac{x^2}{R^2}\right)^2.$$

When $x^2 << R^2$ (i.e near the middle of the potential) we see that the ratio

$$\frac{E_{kin}}{E_{pot}} = \frac{1}{\mu m}\frac{1}{2R^2} = \left(\frac{\xi(0)}{\sqrt{2}R}\right)^2. \tag{A.1}$$

This is negligible in the thermodynamic limit, so the approximation is valid. When $x^2 \approx R^2$ near the Thomas Fermi radius the fraction $\frac{E_{kin}}{E_{pot}}$ becomes very large and the approximation is not valid.

A.2 Bethe Ansatz Boundary Condition

Here we will show that the ansatz in section 1.1.3 satisfy the boundary conditions of the Lieb-Liniger model. To do this we will show how the eigenfunction can be split into symmetric and antisymmetric parts, therefore enforcing zero value in the required limit. As a reminder our eigenfunction was claimed to be

$$\chi = \text{const} \left[\prod_{1 \leq l < i \leq N} \left(\frac{\partial}{\partial x_j} - \frac{\partial}{\partial x_l} + c \right) \right] \det \left(e^{i k_j x_l} \right). \tag{A.2}$$

We extract a factor to write it as

$$\chi = \left(\frac{\partial}{\partial x_2} - \frac{\partial}{\partial x_1} + c \right) \tilde{\chi}, \tag{A.3}$$

where the new modified eigenfunction is

$$\chi = \text{const} \prod_{j=3}^{N} \left(\frac{\partial}{\partial x_j} - \frac{\partial}{\partial x_1} + c \right) \left(\frac{\partial}{\partial x_j} - \frac{\partial}{\partial x_2} + c \right) \left[\prod_{3 \leq l < i \leq N} \left(\frac{\partial}{\partial x_j} - \frac{\partial}{\partial x_l} + c \right) \right] \det \left(e^{i k_j x_l} \right). \tag{A.4}$$

This allows us to write the boundary condition for our modified eigenfunction as

$$\left[\left(\frac{\partial}{\partial x_2} - \frac{\partial}{\partial x_1} \right)^2 - c^2 \right] \tilde{\chi} = 0, \qquad x_2 \to x_1. \tag{A.5}$$

From our definition we can see that $\tilde{\chi}$ is antisymmetric in x_1, x_2 and the coefficient of derivatives is symmetric meaning that the expression holds in the limit. This can be similarly shown for all other x_j to show that the boundary condition is indeed satisfied by the ansatz.

A.3 Determinant Integration Formula

In this section we will prove a formula that is useful for evaluating the various correlation functions in random matrix theory as it allows us to integrate a determinant over one of our

variables. To prove this we will be following the work of [25]. We start by considering

$$\mathrm{Det}\left(K_N(x_i,x_j)_{1\leq i,j\leq k+1}\right)=\begin{vmatrix} K_N(x_1,x_1) & \dots & K_N(x_1,x_{k+1}) \\ \vdots & & \vdots \\ K_N(x_{k+1},x_1) & \dots & K_N(x_{k+1},x_{k+1}) \end{vmatrix}. \tag{A.6}$$

We evaluate by expanding along the bottom row

$$\begin{aligned}\mathrm{Det}\left(K_N(x_i,x_j)_{1\leq i,j\leq k+1}\right) &= K_N(x_{k+1},x_{k+1})\mathrm{Det}\left(K_N(x_i,x_j)_{1\leq i,j\leq k}\right) \\ &+\sum_{l}^{k}(-1)^{k+1-l}K_N(x_{k+1},x_l)\mathrm{Det}\left(K_N(x_i,x_j)_{1\leq i,j\leq k+1,j\neq k}\right).\end{aligned} \tag{A.7}$$

Now we must integrate over x_{k+1}. The first term has all the x_{k+1} dependence outside the determinant and as the $K_N(x,x)$ is normalised gives a factor of N. for the other term the x_{k+1} dependence in inside the determinant so we consider

$$\mathrm{Det}\left(K_N(x_i,x_j)_{1\leq i,j\leq k+1,j\neq k}\right)=\begin{vmatrix} K_N(x_1,x_1) & \dots & \dots & K_N(x_1,x_{k+1}) \\ \vdots & & & \vdots \\ K_N(x_k,x_1) & \dots & \dots & K_N(x_k,x_{k+1}) \end{vmatrix}. \tag{A.8}$$

Which has the $j=l$ column missing. We can multiply in the factor of $K_N(x_{k+1},x_l)$ into the final column so all x_{k+1} dependence is in the final column. Then performing the integration can be done with the help of the reproducing kernel identity

$$K_N(x_l,x_j)=\int K_N(x_l,x_{k+1})K_N(x_{k+1},x_j)dx_{k+1}. \tag{A.9}$$

The new row can be moved to fill the gap in the determinant by gaining factors of (-1). This can be achieved for all k terms in the sum to finally show that

$$\int \mathrm{Det}\left(K_N(x_i,x_j)_{1\leq i,j\leq k+1}\right)dx_{k+1}=(N-k)\mathrm{Det}\left(K_N(x_i,x_j)_{1\leq i,j\leq k}\right). \tag{A.10}$$

Appendix B

Chapter Two Appendix

B.1 Integration Under Determinant

It is not clear that the operation of moving the integral inside the determinant in equation (2.7) is trivial and indeed it is not. In this section we will prove that this is possible. We will prove the so called Cauchy-Binet formula

$$\int d^N x \mathrm{Det}(p_i(x_j))\mathrm{Det}(p_l(x_m)) = \mathrm{Det}\left(\int p_i(x)p_j(x)dx\right), \tag{B.1}$$

where in our case $p_i(x_j)$ are some polynomials. It is worth noting that this formula will only hold for exactly two determinants. We begin by writing the determinant using the Leibniz formula

$$\int d^N x \mathrm{Det}(p_i(x_j))\mathrm{Det}(p_l(x_m)) = \int d^N x \sum_{P,P'} (-1)^P (-1)^{P'} \prod_{i=1}^{N} p_i(x_{P_i}) \prod_{j=1}^{N} p_j(x_{P'_j}), \tag{B.2}$$

where the P's are permutations of the set of integers up to N. We will now perform a change of variables to $y_1 = x_{P_1}$ which gives $x = y_{1P_1^{-1}}$, under this change of variables we have

$$\int d^N x \mathrm{Det}(p_i(x_j))\mathrm{Det}(p_l(x_m)) = \int d^N y \sum_{P,P'} (-1)^P (-1)^{P'} \prod_{i=1}^{N} p_i(y_i) \prod_{j=1}^{N} p_j(y_{1P_j^{-1}P'_j}). \tag{B.3}$$

A new permutation can now be defined $PP' = P''$, then interchanging the new permutation with its index, equivalent to transposing the matrix, we can apply one integral to each y_i

$$\int d^N x \mathrm{Det}(p_i(x_j))\mathrm{Det}(p_l(x_m)) = \sum_{P''}(-1)^{P''}\prod_{i=1}^{N}\int dy p_i(y)p_{P_i''}(y). \tag{B.4}$$

Finally inverting the Leibniz formula we get our required result

$$\int d^N x \mathrm{Det}(p_i(x_j))\mathrm{Det}(p_l(x_m)) = \mathrm{Det}\left(\int p_i(x)p_j(x)dx\right). \tag{B.5}$$

B.2 Christoffel Darboux

The Christoffel Darboux formula is incredibly useful for evaluating sums over polynomials of the form (2.13), using a telescoping sum idea to remove most of the terms. To prove this we begin with some definitions

$$\int_a^b w(x)p_m(x)p_n(x)dx = h_n\delta_{n,m}. \tag{B.6}$$

The polynomials $p_i(x)$ are integrated over the appropriate integral, with the weight $w(x)$. We define the inner product as

$$\langle f, g\rangle := \int_a^b w(x)f(x)g(x)dx, \tag{B.7}$$

if $h_n = 1$ for all n then the polynomials would be orthonormal. Additionally if the polynomials $p_n = k_n x^n + O(x^{n-1})$ have $k_n = 1$ for all n then the polynomial is monic. First we must prove the theorem

$$p_{n+1}(x) = (xA_n + B_n)\,p_n(x) + C_n p_{n-1}(x), \tag{B.8}$$

where $A_n = k_{n+1}/k_n$and $C_n = -A - nh_n/(A_{n-1}h_{n-1})$. We begin with the quantity $p_{n+1} - A_n x p_n(x)$ is a polynomial of degree less than or equal to n and can therefore be written as the sum of polynomials in the following way

$$p_{n+1} - A_n x p_n(x) = \sum_{m=0}^{n} c_m p_m(x). \tag{B.9}$$

Applying the inner product with a one of the polynomials from the sum gives us

$$c_k h_k = \langle p_{n+1}(x), p_k(x) \rangle - A_n \langle x p_n(x), p_k(x) \rangle . \tag{B.10}$$

As $k \leq n$ the first inner product is zero. For $k < n-1$ the polynomial $xp_k(x)$ has degree less than n which would also set the second inner produce to zero. This gives the only non zero c_k the ones where $k = n, n-1$. Therefore the sum only has two terms

$$p_{n+1} - A_n x p_n(x) = c_n p_n(x) + c_{n-1} p_{n-1}(x). \tag{B.11}$$

Examining the case where $k = n-1$ specifically

$$h_{n-1} c_{n-1} = -A_n \langle x p_n(x), p_{n-1}(x) \rangle = -A_n h_n \frac{k_{n-1}}{k_n} \tag{B.12}$$

Giving $c_{n-1} = C_N$ and $c_n = B_n$ to complete the proof.

Now we move onto the Christoffel Darboux formula

$$\sum_{k=0}^{n} \frac{p_k(x) p_k(y)}{h_k} = \frac{k_n}{h_n k_{n+1}} \frac{p_{n-1}(x) p_n(y) - p_{n+1}(y) p_n(x)}{x - y}. \tag{B.13}$$

to prove this theorem we start by multiplying our the first formula we proved in this section by $p_n(y)$

$$p_{n+1}(x) p_n(y) = (x A_n + B_n) p_n(x) p_n(y) + C_n p_{n-1}(x) p_n(y), \tag{B.14}$$

and the same with $x \leftrightarrow y$

$$p_{n+1}(y) p_n(x) = (y A_n + B_n) p_n(y) p_n(x) + C_n p_{n-1}(y) p_n(x). \tag{B.15}$$

Taking the difference of the above two equations and summing over n we find

$$(x-y) \sum_{k=1}^{n} \frac{p_k(x) p_k(y)}{h_k} = \sum_{k=1}^{n} \frac{p_{k+1}(x) p_k(y) - p_{k+1}(y) p_k(x)}{A_k h_k} - \sum_{k=1}^{n} \frac{p_k(x) p_{k-1}(y) - p_k(y) p_{k-1}(x)}{A_{k-1} h_{k-1}}. \tag{B.16}$$

Most of the terms from the sums on the right hand side of the equation cancel leaving only the n^{th} term of the first sum and the 1^{st} term from the second sum. This term can be incorporated into the sum on the left hand side as the 0^{th} term completing the proof

$$\sum_{k=0}^{n} \frac{p_k(x) p_k(y)}{h_k} = \frac{k_n}{h_n k_{n+1}} \frac{p_{n-1}(x) p_n(y) - p_{n+1}(y) p_n(x)}{x - y}. \tag{B.17}$$

B.3 Airy Kernel

Here we will evaluate the kernel of Hermite polynomials at the edge and perform asymptotic analysis to obtain the Airy kernel, the method shown here is from [54]. We begin with the kernel (2.13)

$$K_N(x,y) = e^{-\frac{1}{4}(x^2+y^2)} \sum_{i=0}^{N-1} \frac{He_n(x)He_n(y)}{n!\sqrt{2\pi}}. \tag{B.18}$$

Evaluating the sum using the Christoffel Darboux formula (see appendix B.2) and rescaling by a factor of $\sqrt{2}$ to swap back to the physicists Hermite polynomials, we have

$$K_N(x,y) = \frac{e^{-\frac{1}{2}(x^2+y^2)}}{2^N(N-1)!\sqrt{\pi}} \frac{H_N(x)H_{N-1}(y) - H_N(y)H_{N-1}(x)}{x-y}. \tag{B.19}$$

As we wish to consider the behaviour of this function near the edge we will rescale

$$\bar{x} = \sqrt{2N} + \frac{x}{\sqrt{2}N^{\frac{1}{6}}}, \tag{B.20}$$

$$\bar{y} = \sqrt{2N} + \frac{y}{\sqrt{2}N^{\frac{1}{6}}}. \tag{B.21}$$

To consider the thermodynamic limit of

$$\frac{1}{\sqrt{2}N^{\frac{1}{6}}} K_N(\bar{x},\bar{y}). \tag{B.22}$$

We will use the large N asymptotic form of the Hermite polynomials found in [27]

$$\lim_{N\to\infty} e^{-\frac{x^2}{2}} H_N(x) \approx \pi^{\frac{1}{4}} 2^{\frac{N}{2}+\frac{1}{4}} N^{-\frac{1}{12}} \sqrt{(N-2)!} \left[\pi Ai\left(\sqrt{2}N^{\frac{1}{6}}(x-\sqrt{2N})\right) + O\left(N^{-\frac{2}{3}}\right)\right]. \tag{B.23}$$

This gives the thermodynamic limit of our kernel as

$$\frac{1}{\sqrt{2}N^{\frac{1}{6}}} K_N(\bar{x},\bar{y}) \approx \frac{f(N)}{x-y} \left[Ai(x)Ai(a(N)y+b(N)) - Ai(y)Ai(a(N)x+b(N))\right], \tag{B.24}$$

where the functions of N are as follows

$$f(N) = \frac{1}{(N-1)!} \pi^2 N^{-\frac{1}{12}} (N-1)^{-\frac{1}{12}} \sqrt{(N-2)!(N-3)!}, \tag{B.25}$$

$$a(N) = \frac{(N-1)^{\frac{1}{6}}}{N^{\frac{1}{6}}}, \tag{B.26}$$

$$b(N) = 2(N-1)^{\frac{1}{6}}(\sqrt{N} - \sqrt{N-1}). \tag{B.27}$$

Next we will expand the Airy functions around a point x_0, y_0 neglecting terms of quadratic order and higher

$$Ai(a(N)x+b(N)) = Ai(a(N)x_0+b(N)) + a(N)(x-x_0)Ai'(a(N)x_0+b(N)) + O((x-x_0)^2). \tag{B.28}$$

This gives us

$$\begin{aligned}\frac{1}{\sqrt{2}N^{\frac{1}{6}}}K_N(\bar{x},\bar{y}) = \frac{f(N)}{x-y}[&Ai(x)(Ai(a(N)y_0+b(N)) + a(N)(y-y_0)Ai'(a(N)y_0+b(N))) \\ &-Ai(y)(Ai(a(N)x_0+b(N)) + a(N)(x-x_0)Ai'(a(N)x_0+b(N)))].\end{aligned} \tag{B.29}$$

We now have free choice of the parameters x_0, y_0 so chose them to be

$$x_0 = x - f(N)^{-1}, \tag{B.30}$$

$$y_0 = y - f(N)^{-1}. \tag{B.31}$$

Finally applying the thermodynamic limit to our functions that depend on N, $f(N \to \infty)^{-1} \to 0, \quad a(N \to \infty) \to 1, \quad b(N \to \infty) \to 0$ we get

$$\frac{1}{\sqrt{2}N^{\frac{1}{6}}}K_N(\bar{x},\bar{y}) = \frac{Ai(x)Ai'(y) - Ai'(x)Ai(y)}{x-y} \equiv \mathcal{A}_{(s,\infty)}, \tag{B.32}$$

as expected.

B.4 Painleve II

The Painleve II transcendent $q(x)$ is defined as the solution to the following equation

$$\partial_x^2 q(x) - xq(x) - 2q^3(x) = 0. \tag{B.33}$$

This equation can be interpreted classically as a particle of unit mass in an effective potential

$$v_{eff} = -\frac{1}{2}\left(xq^2 + q^4\right). \tag{B.34}$$

If we make the identification $q(x) \longrightarrow x(t)$ we can see that this can be viewed as a potential that changes in time. It starts of as a negative quartic with only one maxima at the origin. As time becomes negative it inverts to a quartic with local minima at the origin and maxima at $\pm\sqrt{-t/2}$. It has been shown numerically and analytically [55] that if you demand that

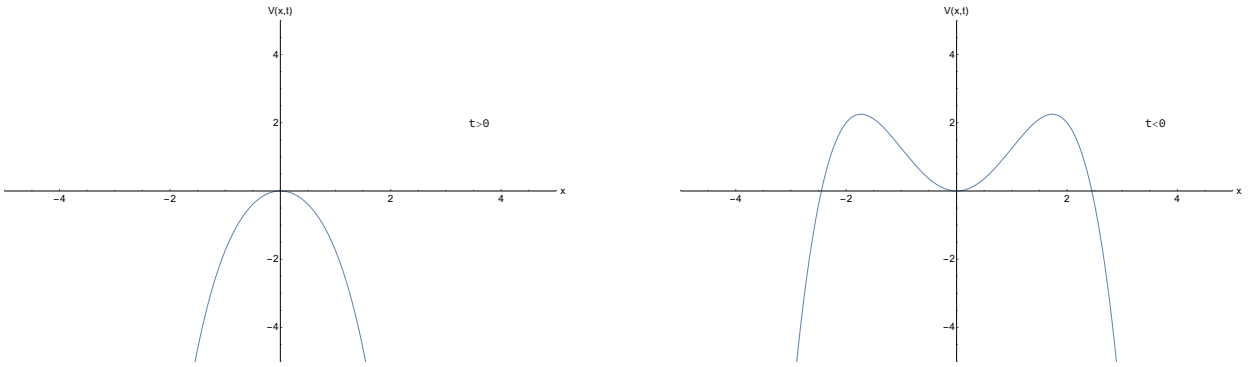

(a) $t > 0$ (b) $t < 0$

Figure B.1: The potential before and after the critical time with a change in behaviour from unstable point to stable point at the origin.

the Painleve II transcendent behaves like $kAi(x)$ as $x \to \infty$ and $\sqrt{-x/2}$ as $x \longrightarrow -\infty$ then equation (B.33) can be used to propagate the solution backwards to find that the only possible value of k that is allowed is $k = 1$, this is known as the Hastings McLeod solution. The classical mechanics analogy is very useful here as this solution corresponds to a particle that is initially just off the origin and as time moves backward and the region around the origin becomes locally stable the particle has exactly enough energy to climb up the potential barrier to $\sqrt{-t/2}$. It is easy to see from this why $k = 1$ is the only solution, as if the value of k is slightly smaller than 1 then the particle will not manage to climb the potential and at finite time decay to the origin hence the solution would also decay at a finite value. If the value of k is slightly higher than 1 then the particle will move over the maxima at $\sqrt{-t/2}$ and move off to infinity, correspondingly the solution blows up to infinity. This instability makes the Hastings McLeod solution hard to find numerically.

Appendix C

Chapter Three Appendix

C.1 Hilbert Transform

We have used the Hilbert transform liberally throughout this thesis, in this section we will discuss it in more detail with a particular focus on its properties in the complex plane. The Cauchy integral formula states that

$$f(x) = -\frac{1}{\pi i} \oint_c \frac{f(z')}{x - z'} dz'. \tag{C.1}$$

for a function $f(z')$ with no poles in the upper half plane. As long as $f(z')$ decays fast enough at infinity the integral may be written as a real one along the real line

$$f_R(x) + i f_I(x) = -\frac{1}{\pi i} \int_{-\infty}^{\infty} \frac{f_R(x') + i f_I(x')}{x - x'} dx', \tag{C.2}$$

where the function has been split into real and imaginary parts. Equating real and imaginary parts we get

$$f_R(x) = -\frac{1}{\pi} \int_{-\infty}^{\infty} \frac{f_I(x')}{x - x'} dx', \tag{C.3}$$

$$f_I(x) = \frac{1}{\pi} \int_{-\infty}^{\infty} \frac{f_R(x')}{x - x'} dx'. \tag{C.4}$$

As we can see the Hilbert transform can be used to relate the real and imaginary parts of a complex function that is analytic in the upper half plane. We also note that the Hilbert transform applied twice will act as an inverse up to a minus sign.

Appendix D

Chapter Four Appendix

D.1 Luttinger Liquid

An important theory in one dimensional physics is Luttinger liquid theory, in this section we will see how the action of interacting particles in one dimension can be re-formulated as a non-linear Luttinger liquid. This will allow us to compare to our hydrodynamic action in the main text and accurately perform the shift in density field required. The action we begin with is the Lieb-Liniger one

$$S = -\int dtdx \left(\bar{\Psi}\partial_t \Psi - \frac{1}{2m}\partial_x \bar{\Psi}\partial_x \Psi + (V(x) - \mu)\bar{\Psi}\Psi + \frac{g}{2}\bar{\Psi}\bar{\Psi}\Psi\Psi \right). \tag{D.1}$$

The first step is to split the fields into an amplitude and phase description $\Psi = \sqrt{n_0 + \rho(x,t)}e^{i\psi(x,t)}$ on substituting into the action we get

$$S = -\int dtdx \left(i\rho\partial_t\psi - \frac{1}{2m}\left((n_0+\rho)(\partial_x\psi)^2 + \frac{(\partial_x\rho)^2}{4(n_0+\rho)} \right) + (V(x)-\mu)(n_0+\rho) + \frac{g}{2}(n_0+\rho)^2 \right). \tag{D.2}$$

During this process boundary terms are created that are full time derivatives of the density and the field ψ as the density is normalised the further integral over space sets this term to zero. The condition on ψ gives the boundary condition $\int dxdt\partial_t\psi = 0$. We will now set the

value of the background density to $n_0 = \mu/g$, this choice removes all terms linear in ρ. At the same time we will introduce a potential field for density $\rho = \partial_x\theta/\pi$, this gives us

$$S = -\int dtdx \left(\frac{i}{\pi}\partial_x\theta\partial_t\psi - \frac{1}{2m}\left((n_0 + \frac{1}{\pi}\partial_x\theta)(\partial_x\psi)^2 + \frac{(\partial_x^2\theta)^2}{4\pi^2(n_0 + \frac{1}{\pi}\partial_x\theta)} \right) + \frac{1}{\pi}V(x)\partial_x\theta + \frac{g}{2\pi^2}(\partial_x\theta)^2 \right). \tag{D.3}$$

The additional constant in the action $-\mu n_0 + g n_0^2/2 + \int V(x) n_0$ has been neglected. If we wish to make contact with the hydrodynamic action we have presented in the main text we must take the strong interaction limit $g \to \infty$, this gives the background density as a small quantity that we can expand the higher derivative term in

$$\begin{aligned} S = -\int dtdx \Bigg(\frac{i}{\pi}\partial_x\theta\partial_t\psi - \frac{1}{2m}\left((n_0 + \frac{1}{\pi}\partial_x\theta)(\partial_x\psi)^2 + \frac{(\partial_x^2\theta)^2}{4\pi(\partial_x\theta)} - \frac{n_0(\partial_x^2\theta)^2}{4(\partial_x\theta)^2} \right) \\ + \frac{1}{\pi}V(x)\partial_x\theta + \frac{g}{2\pi^2}(\partial_x\theta)^2 \Bigg). \end{aligned} \tag{D.4}$$

As our action will be functionally integrated over the velocity we can use stationary phase to find the saddle point. At this point we have the condition

$$\partial_x\psi = \frac{im}{\pi n_0}\partial_t\theta. \tag{D.5}$$

On the saddle point we neglect higher terms in the small parameter n_0 and get

$$S = -\int dtdx \left(-\frac{m}{2n_0\pi^2}(\partial_t\theta)^2 - \frac{1}{2m}\left(-\frac{m^2}{\pi^3 n_0^2}\partial_x\theta(\partial_t\theta)^2 + \frac{(\partial_x^2\theta)^2}{4\pi(\partial_x\theta)} \right) + \frac{1}{\pi}V(x)\partial_x\theta + \frac{g}{2\pi^2}(\partial_x\theta)^2 \right). \tag{D.6}$$

Finally by a simple change of variables $y = ct, c = \sqrt{gn_0/m}$ we can see that the non-linear Luttinger liquid action is

$$S = -\int dydx \left(-K^{-1}(\partial_y\theta)^2 + K^{-1}(\partial_x\theta)^2 - \frac{1}{2mc}\left(-\frac{g}{\pi^3 n_0}\partial_x\theta(\partial_y\theta)^2 + \frac{(\partial_x^2\theta)^2}{4\pi(\partial_x\theta)} \right) + \frac{1}{\pi c}V(x)\partial_x\theta \right). \tag{D.7}$$

With the Luttinger parameter K given by the ratio of velocities $\pi c/g$. In this section we have derived the non-linear Luttinger liquid action from a one dimensional gas with contact interactions and in the strong interaction limit we have gone further, formulating the action in a way that can be compared to our hydrodynamic one in the main text.

D.2 Hodograph Transform

The hodograph transform is a technique used to swap the dependent and independent variables in a problem. This can be seen intuitively in performing an integral as instead of finding the area under the curve $y(x)$ it is equivalent to find the area under the inverse function $x(y)$ and then take the difference with the total area. This can help when the inverse function is far easier to deal with. In our case we do not wish to use the hodograph transform for integration we wish to use in on a differential equation, the principle however is the same.

$$p(x,t) = u, \quad t = t', \quad x = g(u,t'). \tag{D.8}$$

Using the chain rule we have

$$dp = \partial_x p dx + \partial_t p dt, \tag{D.9}$$

and

$$dx = \partial_p g dp + \partial_{t'} g dt'. \tag{D.10}$$

Rearranging we find

$$dp = (\partial_p g)^{-1} dx - \partial_{t'} g (\partial_p g)^{-1} dt'. \tag{D.11}$$

Hence by comparison with (D.9) the first partial derivatives transform as

$$\partial_x p = (\partial_u g)^{-1}, \quad \partial_t p = -\partial_{t'} g (\partial_u g)^{-1}. \tag{D.12}$$

To consider higher derivatives we must see how the partial derivatives transform from the original (x,t) variables to the new u, t' ones. This can be done with the chain rule in combination with the definition of the hodograph transform (D.8)

$$\partial_x = \partial_x u \partial_u + \partial_x t' \partial_{t'} = \partial_x p \partial_u, \tag{D.13}$$

$$\partial_t = \partial_t u \partial_u + \partial_t t' \partial_{t'} = \partial_t p \partial_u + \partial_{t'}. \tag{D.14}$$

To convert fully to our new variables we use the transformed first derivatives (D.12)

$$\partial_x = (\partial_u g)^{-1} \partial_u, \tag{D.15}$$

$$\partial_t = -\partial_{t'} g (\partial_u g)^{-1} \partial_u + \partial_{t'}. \tag{D.16}$$

Then simply applying these to (D.12) gets us the hodograph transformed second derivatives

$$\partial_x^2 p = -(\partial_u g)^{-3} \partial_u^2 g, \tag{D.17}$$

$$\partial_t^2 p = -(\partial_u g)^{-3} \left[(\partial_{t'} g)^2 \partial_u^2 g - 2 \partial_u g \partial_{t'} g \partial_{t'} \partial_u g + (\partial_u g)^2 \partial_{t'}^2 g \right], \tag{D.18}$$

$$\partial_x \partial_t p = -(\partial_u g)^{-3} \left[\partial_u g \partial_{t'} \partial_u g - \partial_{t'} g \partial_u^2 g \right]. \tag{D.19}$$

If we required higher derivatives it is just a case of applying the derivatives (D.15,D.16) repeatedly.

Bibliography

[1] Thierry Giamarchi. One-dimensional physics in the 21st century. *Comptes Rendus Physique*, 17(3-4):322–331, 2016.

[2] M. A. Cazalilla, R. Citro, T. Giamarchi, E. Orignac, and M. Rigol. One dimensional bosons: From condensed matter systems to ultracold gases. *Reviews of Modern Physics*, 83(4):1405–1466, 2011.

[3] F. D.M. Haldane. 'Luttinger liquid theory' of one-dimensional quantum fluids. I. Properties of the Luttinger model and their extension to the general 1D interacting spinless fermi gas. *Journal of physics C: Solid State Physics*, 14(19):2585–2609, 1981.

[4] T. Giamarchi. Some experimental tests of Tomonaga-Luttinger liquids. *International Journal of Modern Physics B*, 26(22), 2012.

[5] H. Monien, M. Linn, and N. Elstner. Trapped one-dimensional Bose gas as a Luttinger liquid. *Physical Review A - Atomic, Molecular, and Optical Physics*, 58(5):R3395–R3398, 1998.

[6] S. Alestra, C. Bordry, C. Brand, E. Burnaev, P. Erofeev, A. Papanov, and C. Silveira-Freixo. Rare event anticipation and degradation trending for aircraft predictive maintenance. *11th World Congress on Computational Mechanics, WCCM 2014, 5th European*

Conference on Computational Mechanics, ECCM 2014 and 6th European Conference on Computational Fluid Dynamics, ECFD 2014, (Wccm Xi):6571–6582, 2014.

[7] Evgeny Burnaev. Rare Failure Prediction via Event Matching for Aerospace Applications. *2019 3rd International Conference on Circuits, System and Simulation, ICCSS 2019*, pages 214–220, 2019.

[8] Craig A. Tracy and Harold Widom. Level-spacing distributions and the Airy kernel. *Communications in Mathematical Physics*, 159(1):151–174, 1994.

[9] Tomohiro Sasamoto and Herbert Spohn. One-Dimensional Kardar-Parisi-Zhang equation: An exact solution and its universality. *Physical Review Letters*, 104(23):1–4, 2010.

[10] Jean-Phillipe Bouchaud and Marc Potters. Financial applications of random matrix theory: a short review. *The Oxford Handbook of Random Matrix Theory*, pages 823–850, 2015.

[11] Elliott H. Lieb and Werner Liniger. Exact analysis of an interacting bose gas. I. the general solution and the ground state. *Physical Review*, 130(4):1605–1616, 1963.

[12] David S. Dean and Satya N. Majumdar. Extreme value statistics of eigenvalues of Gaussian random matrices. *Physical Review E - Statistical, Nonlinear, and Soft Matter Physics*, 77(4):1–17, 2008.

[13] Toshiya Kinoshita, Trevor Wenger, and David S. Weiss. Observation of a one-dimensional Tonks-Girardeau gas. *Science*, 305(5687):1125–1128, 2004.

[14] Thibaut Jacqmin, Julien Armijo, Tarik Berrada, Karen V. Kheruntsyan, and Isabelle Bouchoule. Sub-poissonian fluctuations in a 1D bose gas: From the quantum quasicondensate to the strongly interacting regime. *Physical Review Letters*, 106(23):1–4, 2011.

[15] T. C. Dorlas. Orthogonality and completeness of the Bethe Ansatz eigenstates of the nonlinear Schroedinger model. *Communications in Mathematical Physics*, 154(2):347–376, 1993.

[16] Yu Zhu Jiang, Yang Yang Chen, and Xi Wen Guan. Understanding many-body physics in one dimension from the Lieb-Liniger model. *Chinese Physics B*, 24(5):1–18, 2015.

[17] M. Olshanii. Atomic scattering in the presence of an external confinement and a gas of impenetrable bosons. *Physical Review Letters*, 81(5):938–941, 1998.

[18] Eugene P. Wigner. On the statistical distribution of the widths and spacings of nuclear resonance levels. *Mathematical Proceedings of the Cambridge Philosophical Society*, 47(4):790–798, 1951.

[19] David S. Dean, Pierre Le Doussal, Satya N. Majumdar, and Grégory Schehr. Noninteracting fermions at finite temperature in a d -dimensional trap: Universal correlations. *Physical Review A*, 94(6):1–55, 2016.

[20] H. Bethe. On the Theory of Metals. *Zeitschrift für Physik*, (71), 1931.

[21] Mikhail Zvonarev. Notes on Bethe Ansatz. http://cmt.harvard.edu/demler/TEACHING/Physics284/LectureZvonarev.pdf. 2010.

[22] Tim Langen. Non-equilibrium Dynamics of One-Dimensional Bose Gases. *Springer*, 337(6100):1318–22, 2012.

[23] Rudolf Grimm, Matthias Weidemüller, and Yurii B. Ovchinnikov. Optical Dipole Traps for Neutral Atoms. *Advances in Atomic, Molecular and Optical Physics*, 42(C):95–170, 2000.

[24] Madan Lal Mehta. *Random Matrices*. Academic Press, New York, 3rd edition, 2004.

[25] Terry Tao. 254a, notes 6: Gaussian ensembles | what's new. https://terrytao.wordpress.com/2010/02/23/254a-notes-6-gaussian-ensembles/. (Accessed on 02/26/2021).

[26] A. Minguzzi and D. M. Gangardt. Exact coherent states of a harmonically confined tonks-girardeau gas. *Physical Review Letters*, 94(24), 2005.

[27] Milton Abramowitz and Irene A. Stegun. *Handbook of Mathematical Functions with Formulas, Graphs, and Mathematical Tables*. Dover, New York, ninth dover printing, tenth gpo printing edition, 1964.

[28] Viktor Eisler and Zoltán Rácz. Full counting statistics in a propagating quantum front and random matrix spectra. *Physical Review Letters*, 110(6):1–5, 2013.

[29] Celine Nadal and Satya N. Majumdar. A simple derivation of the Tracy-Widom distribution of the maximal eigenvalue of a Gaussian unitary random matrix. *Journal of Statistical Mechanics: Theory and Experiment*, 2011(4), 2011.

[30] Gernot Akemann and Max R. Atkin. Higher order analogues of Tracy-Widom distributions via the Lax method. *Journal of Physics A: Mathematical and Theoretical*, 46(1), 2013.

[31] Yu Kagan, E. L. Surkov, and G. V. Shlyapnikov. Evolution of a Bose-condensed gas under variations of the confining potential. *Physical Review A - Atomic, Molecular, and Optical Physics*, 54(3):R1753–R1756, 1996.

[32] Alexander G Abanov. HYDRODYNAMICS OF CORRELATED SYSTEMS Emptiness Formation Probability and Random Matrices 1 Hydrodynamics of correlated systems. *ArXiv e-prints*, page 0504307, 2005.

[33] GSL Project Contributors. GSL - GNU scientific library - GNU project - free software foundation (FSF). http://www.gnu.org/software/gsl/, 2010.

[34] Jean-Marie Stéphan. Free fermions at the edge of interacting systems. *SciPost Phys.*, 6:57, 2019.

[35] James R. Garrison and Ryan V. Mishmash. Sophisticated dmrg. https://github.com/simple-dmrg/sophisticated-dmrg. 2014.

[36] David J. Gross and Edward Witten. Possible third-order phase transition in the large-N lattice gauge theory. *Physical Review D*, 21(2):446–453, 1980.

[37] J. Bun, J. P. Bouchaud, S. N. Majumdar, and M. Potters. Instanton Approach to Large N Harish-Chandra-Itzykson-Zuber Integrals. *Phys. Rev. Lett.*, 113:070201, Aug 2014.

[38] S Dean David. Langevin equation for the density of a system of interacting Langevin processes. *Journal of Physics A: Mathematical and General*, 29(24):L613, 1996.

[39] Alex Kamenev. *Field Theory of Non-Equilibrium Systems*. Cambridge University Press, 2011.

[40] A. Matytsin. On the large-N limit of the Itzykson-Zuber integral. *Nuclear Physics, Section B*, 411(2-3):805–820, 1994.

[41] Hsiu-Chung Yeh and Alex Kamenev. Emptiness formation probability in one-dimensional bose liquids. *Phys. Rev. A*, 101:023623, Feb 2020.

[42] Mark J. Ablowitz, David J. Kaup, Alan C. Newell, and Harvey Segur. The Inverse Scattering Transform-Fourier Analysis for Nonlinear Problems. *Studies in Applied Mathematics*, 53(4):249–315, 1974.

[43] Fu Mei Yin, Ye Peng Sun, Fu Qing Cai, and Deng Yuan Chen. Solving the AKNS hierarchy by its bilinear form: Generalized double Wronskian solutions. *Communications in Theoretical Physics*, 49(2):401–408, 2008.

[44] J. A.C. Weideman and B. M. Herbst. Finite difference methods for an AKNS eigenproblem. *Mathematics and Computers in Simulation*, 43(1):77–88, 1997.

[45] Michael Stone, Inaki Anduaga, and Lei Xing. The classical hydrodynamics of the Calogero-Sutherland model. *Journal of Physics A: Mathematical and Theoretical*, 41(27):1–23, 2008.

[46] Philippe Di Francesco, Pierre Mathieu, and David Sénéchal. *Conformal field theory*. Graduate texts in contemporary physics. Springer, New York, NY, 1997.

[47] Alexander G Abanov and Vladimir E Korepin. On the probability of ferromagnetic strings in antiferromagnetic spin chains. *Nuclear Physics B*, 647:565–580, 2002.

[48] Olivier Golinelli and Kirone Mallick. The asymmetric simple exclusion process: An integrable model for non-equilibrium statistical mechanics. *Journal of Physics A: Mathematical and General*, 39(41):12679–12705, 2006.

[49] Mehran Kardar, Giorgio Parisi, and Yi Cheng Zhang. Dynamic scaling of growing interfaces. *Physical Review Letters*, 56(9):889–892, 1986.

[50] Adilet Imambekov, Thomas L. Schmidt, and Leonid I. Glazman. One-dimensional quantum liquids: Beyond the Luttinger liquid paradigm. *Reviews of Modern Physics*, 84(3):1253–1306, 2012.

[51] Herbert Spohn. Fluctuating hydrodynamics approach to equilibrium time correlations for anharmonic chains. *Lecture Notes in Physics*, 921:107–158, 2016.

[52] Bertrand Lacroix-A-Chez-Toine, Satya N. Majumdar, and Grégory Schehr. Rotating trapped fermions in two dimensions and the complex Ginibre ensemble: Exact results for the entanglement entropy and number variance. *Physical Review A*, 99(2):021602, 2019.

[53] A Marshakov. Matrix Models, Complex Geometry and Integrable Systems. I. *Theor.Math.Phys.*, 147(2):583–636, 2006.

[54] matrices - Obtaining the Airy kernel from the Christoffel-Darboux formula with asymptotic Hermite polynomials - Mathematics Stack Exchange. https://math.stackexchange.com/questions/565951/obtaining-the-airy-kernel-from-the-christoffel-darboux-formula-with-asymptotic-h. (Accessed on 03/01/2021).

[55] Peter A Clarkson. Asymptotics of the Painleve Equations. https://carma.newcastle.edu.au/resources/jon/Preprints/Books/MbyE/Second-Ed/Material/panleve.pdf. 2008.

[56] V. E. Zakharov and E. A. Kuznetsov. A quasi-classical theory for a three-dimensional wave collapse. *Zhurnal Eksperimentalnoi i Teoreticheskoi Fiziki*, 91:1310–1324, October 1986.

[57] Ca Tracy and Harold Widom. The distributions of random matrix theory and their applications. *New Trends in Mathematical Physics*, pages 1–13, 2009.

[58] Craig A. Tracy and Harold Widom. Introduction to random matrices. In G. F. Helminck, editor, *Geometric and Quantum Aspects of Integrable Systems*, pages 103–130, Berlin, Heidelberg, 1993. Springer Berlin Heidelberg.

[59] Manas Kulkarni, Gautam Mandal, and Takeshi Morita. Quantum quench and thermalization of one-dimensional fermi gas via phase-space hydrodynamics. *Phys. Rev. A*, 98:043610, Oct 2018.

[60] B Paredes, a Widera, V Murg, O Mandel, S Foelling, I Cirac, G V Shlyapnikov, T W Hansch, and I Bloch. Tonks-Girardeau gas of ultracold atoms in an optical lattice. *Nature*, 429(6989):277–281, 2004.

[61] David Simpson. *One Dimensional Transport of Ultracold Bosons*. PhD thesis, University of Birmingham, 2014.

[62] F.G. Tricomi. *Integral Equations*. Dover Publications, New York, 1985.

[63] T. Giamarchi. *Quantum Physics in One Dimension*. International Series of Monographs on Physics. Clarendon Press, 2003.

[64] Eberhard Hopf. Statistical Hydromechanics and Functional Calculus. *Journal of Rational Mechanics and Analysis*, 1:87–123, jul 1952.